Co-Design of Planing Craft and Active Control Systems

by

Esteban L. Castro-Feliciano

A dissertation submitted in partial fulfillment
of the requirements for the degree of
Doctor of Philosophy
(Naval Architecture and Marine Engineering)
in the University of Michigan
2016

Doctoral Committee:

Professor Jing Sun, Co-Chair
Professor Armin W. Troesch, Co-Chair
Assistant Professor Shai Revzen
Assistant Professor David J. Singer

To my family, here and there.

ACKNOWLEDGEMENTS

Initial thanks go to the staff of the Department of Naval Architecture and Marine Engineering, specially Ms. Nathalie Fiveland, which made navigating through the University and program much more manageable.

Professors Shai Revzen and David J. Singer are to be commended for taking the time to serve on the dissertation committee and provide ideas to make this work compelling.

Now, I would like to express my sincere gratitude to my advisors, Professors Jing Sun and Armin Troesch. Professor Jing Sun presented the stimulating idea of investigating active control systems in planing craft while I was a prospective student versed only in traditional naval engineering. Then Professor Armin Troesch provided the planing craft hydrodynamic insight to fully deliberate this idea's potential. Without my advisors' immense knowledge, motivation, and patience this work would have not been possible. Their insights into approaching research problems will forever influence the way I work toward solutions.

I am also appreciative of the significant help provided by Mr. Richard Akers at Main Marine Composites in assisting with POWERSEA simulations, of Professor Joaquim R. R. A. Martins for his direction and teachings on multidisciplinary optimization, and of Professor Mathew Collete for his guidance on the case study investigation.

My sincere thanks also goes to my colleagues in Professor Sun's research group (RACELab) for their feedback on papers and presentations, and general support:

Richard B. Choroszucha, Jun Hou, Zhenzhong Jia, Hyeongjun Park, Zeng (Connie) Qiu, David M. Reed, Hao Wang, Caihao Weng, Kai (Kevin) Wu, and all the visiting students. I also thank my colleagues in Professor Troesch's research group for their feedback and support on my last semester: Julio Cesar Fernandez Polo, Oscar Tascon Muoz, and Harleigh Seyffert.

This work was supported in part by the Naval Engineering Education Consortium (NEEC), by ONR (N00014-11-1-0831 and N00014-11-1-0832, Program Director: Ms. Kelly Cooper), and by the SMART scholarship.

TABLE OF CONTENTS

LIST OF FIGURES

Figure

LIST OF TABLES

Table

LIST OF APPENDICES

Appendix

LIST OF NOMENCLATURES

C_Δ	load coefficient $= \Delta/(\gamma b^3)$
C_v	speed coefficient $= V/\sqrt{gb}$
D_z	acceleration dose from ISO 2631-5
F_1	ACS's body-fixed vertical force at the stern
F_2	ACS's body-fixed vertical force $2b$ forward from the stern
F_z	lift, total vertical force
$H_{1/3}$	significant wave height
L/b	length-to-beam ratio
L/D	lift-to-drag ratio
L_C	chine wetted length
L_K	keel wetted length
R_T^C	calm water drag, total horizontal calm water resistance
R_T^S	seaway drag, total horizontal seaway resistance
R_g	radius of gyration
S_{ed}	daily equivalent static compression dose from ISO 2631-5
V	forward speed of vessel
Δ	displacement
β	deadrise
η_3	vertical displacement of the center of gravity relative to z_{wl}
η_5	rotation of the body relative to the calm water τ

γ	specific weight of water, 10.06 kN/m^3
τ	trim angle
b	beam
g	gravitational acceleration, 9.807 m/s^2
lcg	longitudinal distance of center of gravity from transom
vcg	vertical distance of center of gravity from keel
z_{wl}	vertical distance of center of gravity to the calm water line
ACS	active control system
ARES	adaptive ride enhancement system
AWS	adaptive weighted sum method
CFD	computational fluid dynamics
BMt	transverse metacentric radius
DLL	dynamic-link library
FP	forward perpendicular
GMt	transverse metacentric height
ISSC	International Ship and Offshore Structures Congress
LOA	length overall
LQR	linear-quadratic regulator
MAWS	modified adaptive weighted sum method
MOO	multiobjective optimization
OLU	open-loop unstable
OLS	open-loop stable
RHIB	rigid-hulled inflatable boat
RMS	root mean square
SEAL	Sea, Air and Land Forces
SPAWAR	Space and Naval Warfare Systems Command
SS	sea state

SWCC	Special Warfare Combatant-Craft Crewman
USCG	United States Coast Guard
USV	unmanned surface vehicle

ABSTRACT

Co-Design of Planing Craft and Active Control Systems

by

Esteban L. Castro-Feliciano

Chairs: Jing Sun, Armin W. Troesch

The available planing craft design tools and guidelines were not envisioned to be used with vessels that have Active Control Systems (ACS). Consequently, vessels with ACS are conventionally designed in a sequential manner: first, the geometry of the vessel is designed using traditional guidelines, and then the ACS is implemented. However, sequential design is not always optimal for systems whose dynamics are coupled. This work establishes a co-design framework for a planing craft and its ACS, combines tools in the disciplines of naval architecture, control systems, and optimization in a novel way to perform co-design studies, and compares them with the sequential design. The study was limited to numerical studies based on reduced order models and the strip-theory time-domain planing craft simulation program POWERSEA. The planing crafts studied are prismatic and have a 12 m length and 10.2 tonne displacement. The ACS is modeled as body forces and the controller investigated is a linear-quadratic regulator (LQR); this work did not look into the design or optimization of the ACS's hardware. The calm-water performance was measured with a semi-empirical reduced order model and with POWERSEA. The seakeeping and seaway drag were estimated in sea states (SS) 2 and 3 and the Pareto front was esti-

mated from an exhaustive search that varied the vessel's longitudinal center of gravity (lcg), deadrise (β) and pitch velocity gain for the LQR estimation. Afterwards the Pareto estimation technique Adaptive Weighted Sum (AWS) was modified to better suit the Pareto estimation performed in this study, resulting in the Modified Adaptive Weighted Sum (MAWS). MAWS was applied to the case where the vessel's beam (b), lcg, β and the LQR's pitch and heave velocity gains are optimized for SS 3. Finally, the real-world feasibility of designing the sequential and co-design vessels, obtained from the MAWS, was investigated with a case-study. Co-designing shows potential to significantly reduce calm-water and seaway drag (10% in some cases), and improve seakeeping (20% in some cases). Thus, the co-design framework offers an opportunity for designing planing craft that are more efficient and have better seakeeping than any planing craft ever built before.

CHAPTER I

Introduction

1.1 Overview

Planing vessels are the de facto watercraft for applications that require speed and agility. Therefore, they are in widespread use in many marine applications, specifically in ones that *need* speed such as rescue, military and law-enforcement applications. However, personnel in these areas suffer from high rates of injuries; and this has sparked a recent research interest in improving the safety of planing craft. Looking for ways to improve upon the performance of planing boats, researchers have explored implementing active control system (ACS) to the vessels.

Past research has shown that the seakeeping of the vessel can be significantly improved with an ACS. These studies have ranged from numerical investigations (Wang, 1985; Engle et al., 2011; Rijkens, 2013), model tests (Wang, 1985; Savitsky, 2003), and full-scale tests (Shimozono and Kays, 2011); all showing potential for ACS in planing craft. But in the history of planing craft design and research, the interaction between an ACS and the planing craft geometry has not been investigated during the design stages. This has resulted in designers only looking at planing craft with an ACS which has been designed sequentially; in other words, the planing boat geometry is first selected, and then an ACS is implemented (as shown in Fig. 1.1a). Because both the ACS and vessel geometry affect the performance, sequentially designing

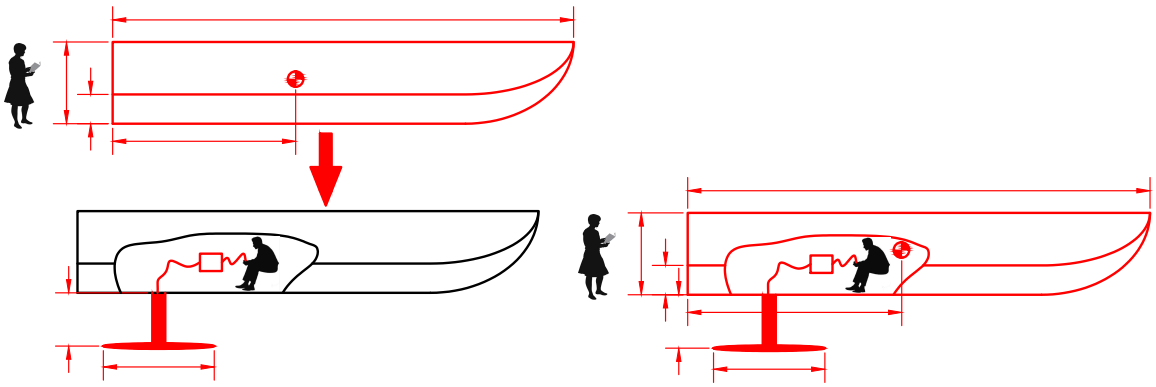

(a) Sequential (b) Co-Design/Simultaneous

Figure 1.1: Investigated optimization methods for coupled systems.

them does not allow to explore the synergy between the two design spaces and might not lead to an optimal vessel.

The co-design of coupled systems guarantees that the true optimal design(s) are in the feasible space. In this dissertation, co-design refers to the simultaneous multidisciplinary optimization approach, as illustrated in Fig. 1.1b. Designers follow a sequential design because the available planing craft design guidelines do not take into account an ACS's influence on the planing craft's geometry, and to the best of the author's knowledge, there has been no report in the open literature on the co-design of a planing craft and its ACS. As a result, it is likely that a designer is selecting a planing craft geometry which unnecessarily inhibits the synergy between the planing craft and its ACS; and this defines the fundamental research question of this work: should the co-design of a planing craft with its ACS be recommended over the conventional (i.e., sequential) design method?

This work establishes a co-design framework for a planing craft and its ACS, combines tools in the disciplines of naval architecture, control systems, and optimization in a novel way to perform co-design studies, and compares them with the sequential design.

This work is organized as followed. In the following sections of Chapter I, Section

1.2 to 1.4, a more comprehensive background on planing craft and their design is presented along with a more articulate motivation for the co-design of planing craft and a preliminary study. In Chapter II, the calm-water propulsion efficiency is explored for vessels that are forced to be open-loop stable (as it is conventionally done in a sequential design) and for vessels that are required to be only closed-loop stable (as it would be done in a co-design). Next, Chapter III performs an exhaustive search in the coupled design space of vessel's longitudinal center of gravity (lcg) and dead-rise (β), and one ACS's linear-quadratic regulator (LQR) tuning parameter using a time-domain simulation program in sea states (SS) 2 and 3. The pareto results are found for when the seakeeping and drag are the objective functions. Afterwards, Chapter IV presents a novel optimization based method to find pareto results, and it is used to find the pareto results with vessel geometry variables lcg, β and beam (b), and two ACS's LQR tuning parameters. Following these results, Chapter V presents a case study and comments on the feasibility of the co-design results. Lastly, Chapter VI summarizes the conclusions and recommends future work.

To the best of the author's knowledge, co-designing a planing craft and its ACS has not been performed in practice — thus the proposed framework offers an opportunity of designing planing craft which are more efficient and have better seakeeping than any planing craft ever built before.

1.2 Background

This research entails three research areas: combined plant and control optimization, planing boat simulation, and ACS in planing craft. Firstly, Section 1.2.1 offers an introduction to planing boats. Next, Section 1.2.2 presents the motivation for investigating co-design in planing craft with ACS. Then Section 1.2.3 presents a short discussion of the "artifact/plant" and "controller" co-design literature. Afterwards in Section 1.2.4, there is an overview of what is the state-of-the-art for high-speed

(a) Fishing/recreational planing boat Tiara 4300 Open (tiarayachts.com)

(b) Offshore racing planing boats (photobucket.com)

Figure 1.2: Examples of civilian planing craft applications.

vessel simulations. The investigation – which involves a wide range of planing vessel and control configurations – will be primarily simulation based, a virtual test bed that is computationally fast is desirable; consequently, computationally expensive computational fluid dynamics (CFD) modeling is not feasible and therefore excluded from the discussion. Lastly, in Section 1.2.5 there is a short discussion of what is the state-of-the-art in applying control systems to planing boats.

1.2.1 Planing Craft Introduction

Planing vessels are used anywhere that speed and simplicity of design are desired, since they represent the simplest watercraft in which "high-speeds" are achievable. Moreover, their hull design is considered mature (Savitsky, 1985). Because of this, their use is widespread in the boating industry — both in civilian and government applications.

In the civilian area, planing boats are commonly used for recreational (e.g., 'cruising'), sport (e.g., sport fishing and racing), and transportation (e.g., water taxi) purposes; some examples are shown in Fig. 1.2. Their speed capabilities are either for entertainment value, or due to the nature of the sport or business.

But in government applications, both in law-enforcement and the military, planing boat use is more necessity-based. In the military, planing boats are frequently used in navies and coast guards. In the U.S., the USCG uses planing boats for rescue and

(a) SWCC's Special Operations Riverine Craft (navy.mil)

(b) USCG's Medium Response Boat (uscg.mil)

(c) SPAWAR Systems Center Pacific USV (navy.mil)

Figure 1.3: Examples of government planing craft applications.

pursuit operations; and the Navy has the Special Warfare Combatant-Craft Crewman (SWCC), where among other things they specialize on inserting and extracting Navy SEALs with planing crafts. Moreover, planing craft use is common in police and wildlife departments – since just like a police car should be capable of pursuing most street cars, a police boat should be fast enough to pursue most civilian planing crafts. A more recent use of planing crafts is in unmanned surface vehicles (USVs), where they can be used to perform laborious or dangerous jobs such as surveying and surveillance. Some examples are shown in Fig. 1.3.

Planing crafts distinguish themselves from traditional displacement vessels once they get up to design speeds, where a significant part of the planing craft's lift force arise from dynamic lift and not from water displacement — sharing many similarities to an airfoil. The exact speed for which a planing vessel is considered to be planing per se, is not clear-cut (Faltinsen, 2005); but a planing boat operating at a speed coefficient of $C_v = V/\sqrt{gb} > 1.5$ is generally considered to be in the planing regime (Savitsky and Brown, 1976), where V is forward speed, b the vessel's beam, and g the gravitational acceleration.

Some basic planing hull terminology are: keel, chine, b, and β. The keel is the longitudinal line across the centerline of the hull as marked in Fig. 1.4. A chine is a sharp angle in the surfaces of the hull, as it is labeled in Fig. 1.4, and also clearly

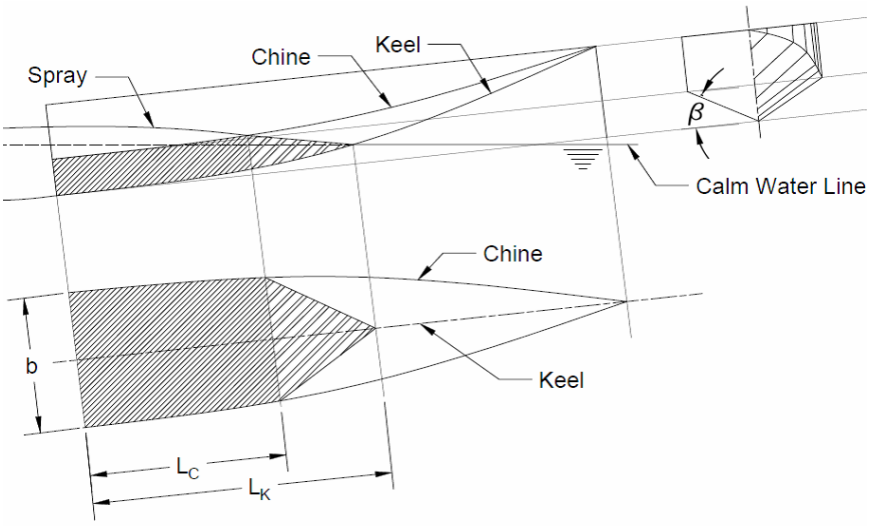

Figure 1.4: Generic planing craft.

seen in Fig. 1.3a. The beam refers to the width of the vessel, but if the location is not specific, it usually refers to the largest width (see Fig. 1.4). And deadrise is the angle between the hull surface and a horizontal line at the keel (see Fig. 1.5 and 1.4).

A traditional planing hull design contains one hard chine, a beam distribution that decreases or stays the same moving forward along the vessel's length, and a positive deadrise distribution that increases or stays the same, also moving forward along its length (see Fig. 1.4). The reason for the decreasing and increasing constraints is such that there are no surfaces that create 'suction'; since these kinds of surfaces lend themselves to instabilities (Faltinsen, 2005).

Nevertheless, to simplify the vessel's hydrodynamics (and thus the modeling), the investigated planing vessels in this research are prismatic in shape; in other words, the beam and deadrise distributions are constant throughout the vessel's length as illustrated in Fig. 1.5.

The planing surface has two main planing regions: a region with "dry" chines, and a region with "wet" chines. As illustrated in Fig. 1.4, the "wet" chines region corresponds to the region encompassed by L_C, and the "dry" chines region by $L_K - L_C$.

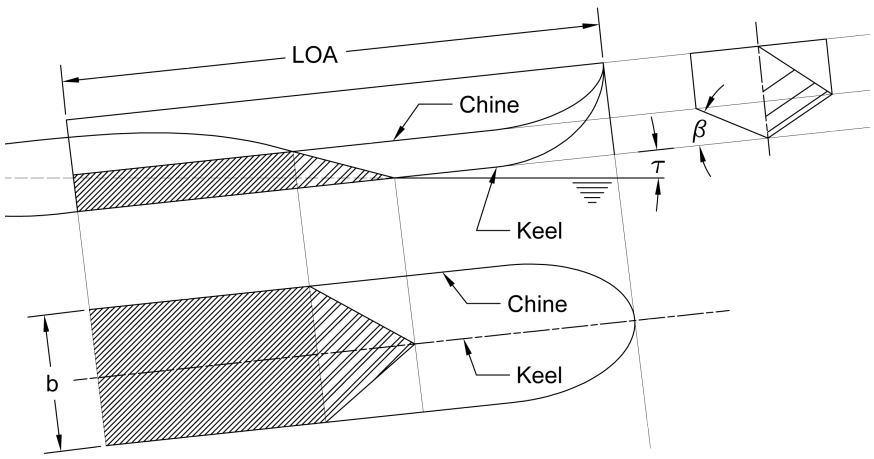

Figure 1.5: Prismatic planing craft.

It could be argued that in reality there may be an additional planing region caused by when the chine-separated water collapses back into the vessel (Savitsky and Brown, 1976); however, it is assumed that this region is non-dominant on the dynamics and statics of the vessel and thus ignored in this research.

For additional introductory information about planing boats, the reader is referred to Savitsky (1985).

1.2.2 Traditional Planing Craft Design, and the Motivation for Co-Design

Planing craft geometry design was mostly based on experience and rule of thumb up until the 1960's, where research in high-speed craft became a popular research subject throughout the 60's and early 70's. The most common planing craft concept design tools used today come from this period of research — where the use of ACSs was essentially nonexistent. These design usually rely on empirical tools to estimate the vessel performance, which does not allow a designer to consider the ACS's effect on vessel performance.

The performance of a vessel is usually measured with three criteria: transport efficiency, seakeeping, and maneuverability. In this research, only transport efficiency and seakeeping are investigated. An improvement in transport efficiency allows the

vessel to travel farther and/or faster with less fuel, providing benefits ranging from making boats more environmentally friendly to reducing operational costs and/or acquisition costs. Improvements to vessel seakeeping can make planing boats safer by reducing the risk of operator injury, increase the range of sea conditions the vessel can safely operate, and potentially improve the transport efficiency when operating in a seaway.

One of the popular calm-water powering prediction methods for planing vessels is Savitsky (1964)'s semi-empirical method. For seakeeping guidance, Savitsky and Brown (1976)'s empirical equations based on model tests by Fridsma (1971) have been used extensively. A summary of the research from this period can be found in Savitsky (1985); Doctors (1985). With these two relatively simple methods, a designer can have a rough concept design of a planing craft and its estimated calm-water and seaway performance; the end result would be a traditionally sound concept design. However, these methods and guidelines were never envisioned to be used for vessels with ACSs. Therefore, if a vessel will have an ACS, the designer might be starting off with a concept design that unnecessarily inhibits the synergy between the planing craft and its ACS.

Before proceeding, note that throughout this study "stable" refers to at least "locally asymptotically stable", "unstable" refers to at least *not* "locally asymptotically stable", and "open-loop" refers to the dynamics of the craft when it operates without an ACS.

Now take for example the success stories of co-designing a vehicle and its ACS in aerospace. Modern fighter aircraft, such as the F-16, may be inherently unstable (Nguyen et al., 1979) (known as "relaxed static stability" in aircraft design), and they are only capable of stable flight because of their ACS. In other words, if you turned off the ACS of the F-16 mid-flight, the plane would diverge from its path (possibly catastrophically) and not glide steadily. But not imposing open-loop stability allows

the aircraft to be lighter, more efficient, and more maneuverable (AGARD, 1974). If the analogous design method was used from conventional planing craft design with ACSs to fighter aircraft design, an aerospace designer would have never come up with the F-16.

Early in planing craft research, it was documented that planing vessels could suffer from dynamic instabilities (bifurcations) such as bow-drop (a transcritical bifurcation in pitch) and porpoising (a supercritcal Hopf bifurcation in pitch-heave); and the first guidelines to prevent these were empirical (Savitsky, 1964), based on model test results conducted by Day and Haag (1952). An overview of planing craft instabilities can be found in Blount and Condega (1992); Hicks et al. (1995). Because the use of ACSs in planing craft is usually not considered at the design stage, instabilities are generally seen as undesirable; and the approach to correct or prevent any instabilities is to modify the vessel hull geometry, change the running trim angle, and/or restrict the operating speeds.

However, restricting the vessel to be open-loop stable (OLS) might prevent the vessel from operating at the optimal lift-to-drag ratio (Savitsky, 1964). Moreover, while the seakeeping of planing craft has improved significantly since the early designs (Savitsky, 1985), there is still a need for seakeeping improvement for vessels operating in rough sea conditions to protect those onboard — such as those of the Coast Guard, police, and military. The rate of injury for this type of craft is known to be high; a survey of SWCC reported that 65% of them had sustained at least one injury during service — with the harsh craft's motion being the primary cause (Ensign et al., 2000).

Consequently, recent research has explored the use of ACS's in planing craft in order to improve the vessel's seakeeping. This research has shown that a planing craft with an ACS is capable of superior seakeeping compared to those without (Wang, 1985; Savitsky, 2003; Shimozono and Kays, 2011; Engle et al., 2011; Rijkens, 2013). In addition, not only can an ACS improve the seakeeping of a planing craft, it can also

stabilize it so that it can operate at its optimal lift-to-drag trim angle (Xi and Sun, 2006). All these promising results for incorporating ACS into planing craft are with vessels that were designed sequentially, i.e., the vessel geometry was first selected, and then the ACS was incorporated. But because the vessel geometry and ACS are coupled (both affect the vessel's dynamics), even better results might be possible if both are co-designed and the hardware-control couplings are explored (Peters, 2010).

Co-design of vessel geometry and ACS requires effective tools to facilitate optimization, particularly the models that capture the sensitivity of key planing boat performance with respect to both geometry and ACS parameters. Recent research in the hydrodynamic optimization of a planing craft (Ayob et al., 2010, 2009; Smith et al., 2012) estimated the seaway drag and seakeeping performance by using empirical equations (Savitsky and Brown, 1976; Savitsky and J. G. Koelbel, 1993). As previously mentioned, the model tests used (Fridsma, 1971) did not have ACS, and therefore the empirical equations do not incorporate the effects of an ACS. Consequently, a time-domain simulation program is required to estimate the seakeeping performance of a planing craft with an ACS.

More specifically, the problem of designing a planing craft with an ACS is an optimization within multiple disciplines — one discipline is the controls engineering, and the other is the naval architecture/hydrodynamics of the vessel and ACS's hardware. Aerospace is one of the most active fields in this kind of optimization; a summary of some the techniques used in aerospace is documented in Sobieszczanski-Sobieski and Hafka (1997). It is easy to see how this problem could be made as complex as the designer would want. For example, we could also include structure design into the problem definition. Therefore, one of the challenges is choosing parameter spaces that have great influence on the design objectives and define the scope to make the problem tractable with available tools. In this paper we focus on exploring simplified definitions of the ACS and vessel's geometry which are known to be influential in the

seakeeping and lift-to-drag ratio, and consider seakeeping and drag reduction as the primary design objectives.

1.2.3 Optimal Design and Control

The plant and control co-design problem exists in a vast range of engineering, science and math disciplines. For a recollection of works in plant/control optimization, the reader is directed to Peters (2010); Alyaqout (2006); Fathy (2003).

An optimization within multiple disciplines should not be confused with a multiobjective optimization (MOO). While the former frequently implies the latter is required, they are two independent optimization problems. As their names imply, an MOO deals with the optimization problems with multiple objectives (e.g., a designer needs to maximize a structure's strength and minimize weight[1]), while an optimization within multiple disciplines deals with having different disciplines involved (e.g., a designer needs to talk to the structures group and the fluid dynamics group to correctly model his structure for optimization). MOOs are further explained in Section 4.1.1.

To illustrate in a conceptual level the possible downfalls of sequential design, let us consider the following toy example. Assume that we have a beam that we desire to control the position of the far end, x_2, by controlling the angle of the other end, x_1, as shown in Fig. 1.6a. Assume that the dynamic deflections in this beam are non-negligible; yet they can be reduced by increasing the structural stiffness, which causes the structure to be heavier. Assuming that the actuator can rapidly set a specified angle at x_1, we can represent this problem as a simplified mass-spring-damper system as in Fig. 1.6b. Moreover, it is assumed that the corresponding stiffness and damping are described by Eq. (1.1-1.2). Now we can derive the open-loop transfer function (an input/output ratio in Laplace domain) from X_1 to X_2, yielding Eq. (1.3) (and

[1]The structure's weight, not the designer's.

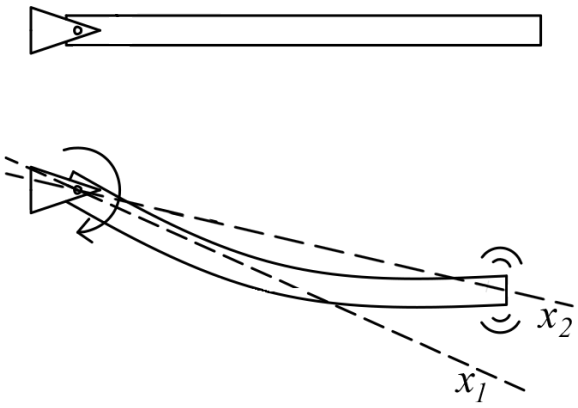

(a) Physical representation of toy example
Top: Beam in static position
Bottom: Beam in motion, i.e., dynamic

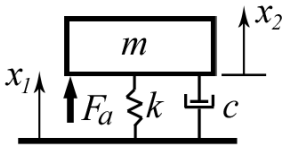

(b) Spring-damper-mass representation of toy example

Figure 1.6: Toy example.

illustrated in Fig. 1.7a).

$$k = m^2\alpha \tag{1.1}$$

$$c = m^2\xi \tag{1.2}$$

$$G(s) = \frac{X_2(s)}{X_1(s)} = \frac{m(\xi s + \alpha)}{s^2 + (m\xi)s + m\alpha} \tag{1.3}$$

where m is the beam's mass, α and ξ are fictional constants for the toy problem's stiffness and damping respectively, and s is the complex variable from the Laplace transform.

Assume that the design goal is to have a settling time of 10 sec, that we have constraints $20 \leq m \leq 60$, and that $\alpha = 0.1$ and $\xi = 0.01$. Exploring the settling time as a function of m, we see from Fig. 1.8a that we first hit the upper m constraint before we reach our settling time goal. We select $m = 60$, and propose that we use a P-controller to reach the desired settling time as shown in Fig. 1.7b. The resulting closed-loop transfer function is Eq. (1.4), and we find out that with a gain $K_p = 0.27$, we satisfy our settling time requirement (see Fig. 1.8b).

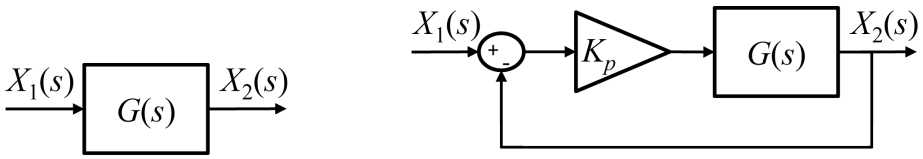

(a) Open-loop (b) Closed-loop with P-controller

Figure 1.7: Block diagrams for toy example transfer functions.

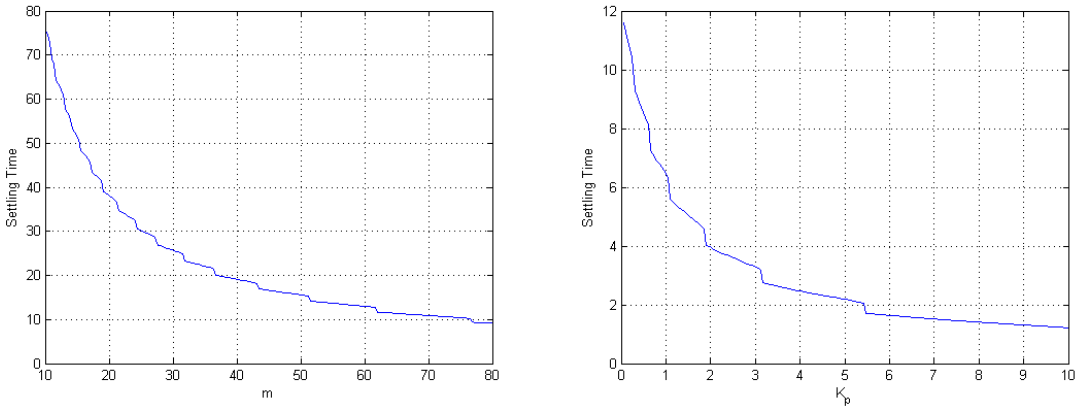

(a) Open-loop settling time (Step 1) (b) Closed-loop settling time for $m = 60$ (Step 2)

Figure 1.8: Toy example sequential design results.

$$\bar{G}(s) = \frac{K_p G(s)}{1 + K_p G(s)} = \frac{m(\xi s + \alpha) K_p}{s^2 + (1 + K_p)(m\xi)s + (1 + K_p)m\alpha} \tag{1.4}$$

Nonetheless, recognizing that both K_p and m are coupled on their influence of the settling time (as it is apparent from Eq. (1.4)), we co-design the physical parameters m and control parameter K_p and we find out that we can in fact go all the way down to the lower bound of $m = 20$ and still meet the settling time requirement by having $K_p = 2.8$, as Fig. 1.9 illustrates. Using the sequential design method, we would have a result that is significantly heavier than the one we obtained by co-designing — and in this example, the co-designed result would likely have a lower acquisition costs and lower operational costs since the beam would have less material, a lower rotational inertia and lower gravitational forces. A more elaborate investigation of the optimal design a flexible structure weight and its control can be seen in Hale et al. (1985).

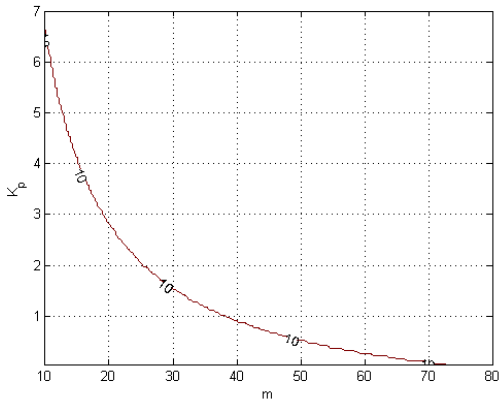

Figure 1.9: Toy example co-design results, closed-loop 10 sec settling time.

1.2.4 Virtual Test Beds

The response of a high-speed planing craft operating in rough seas could be described as highly nonlinear and it is very difficult to model using only first principles. Consequently, there have been many different attempts and approaches to model the behavior of a planing boat in waves. In essence, the modeling of planing boat can fall anywhere in between two simulation philosophies: empirically based or CFD based. In addition, the modeling can be either 3D, 2D, 2.5D or 1D; where the so called 2.5D corresponds to strip theory. Generally speaking, the simulation time increases as one goes from empirically based to CFD based, and from 1D to 3D.

One of the most popular modeling techniques is the 2.5D approach, since it is a good compromise between accuracy and computational expense. Most of the 2.5D approaches are based on strip theory (Zarnick, 1979) using forces estimated by 2D wedge force impacts that are empirically calculated. However, there is research in calculating the 2D impact forces by means of CFD methods; some of these are by boundary element methods for example (Sun and Faltinsen, 2011) and smooth particle methods (e.g., Veen and Gourlay (2012)). The advantage of the CFD approach is that it is less dependent on empirical results than the wedge-force-type models, allowing the modeling of a vessel with cross sections different than simple wedges; nevertheless,

the computational cost is increased with the CFD approach. A modern effort for modeling the planing boat in waves by adding the roll degree-of-freedom (DOF) to the 2.5D, along with an up-to-date list of the existing mathematical models, can be found in Ghadimi et al. (2013). While in the 3D CFD category, the boundary element method based program AEGIR has been successfully used to model high-speed vessels (Rosenthal et al., 2009).

In addition, recent research in USVs has utilized phenomenological models (Bibuli et al., 2012) to describe the motions of the vessel; however these types of models do not provide insight into the controllability or performance of the vessel. Moreover, others have used linear transfer functions found by experimentation (Blank and Bishop, 2008; Naeem and Sutton, 2008); the advantage of linear models is that their analysis is straightforward and can give some insight into the behavior of the vessel, and there are abundant techniques for linear controller design. Nevertheless, linear models fail to represent the real-world dynamics once the vessel reaches planing speeds in a seaway.

In this research, the simulations are performed in the program POWERSEA (Akers, 1999), which is based on the 2.5D approach with empirical wedge force. Since the research will require extensive simulations, the 2.5D approach is adequate since it is computationally fast.

1.2.5 Planing Boat Control Systems

The development and optimization of actively controlled surfaces on high-speed vessels is active research. Some of the control surfaces investigated are hydrofoils/lifting bodies, trim tabs, and interceptors. Engle et al. investigated the use of a bow lifting body to reduce the body motions of a high speed vessel (Engle et al., 2011). Hughes and Weems investigated the control of a high speed catamaran with both a bow lifting body and stern trim tabs (Hughes and Weems, 2011). Moreover, an investigation

into the performance of three different control algorithms controlling both aft and bow lifting bodies on a catamaran was performed by Kays et al. (2009). Navatek has a proprietary system coined adaptive ride enhancement system (ARES), which consists of an aft lifting body (hydrofoil), a microprocessor unit, an inertial measurement unit, GPS, and an interface for the operator. Navatek has stated that in open water tests with a 11 m rigid-hulled inflatable boat (RHIB), ARES reduced the average vertical accelerations at the *lcg* by 28%, the average of the 1/10th highest vertical acceleration at *lcg* by 51%, and the pitch rate root mean square (RMS) by 52% (Shimozono and Kays, 2011). Their control algorithm is based on minimizing a cost function that is evaluated on a pre-set period by changing the gains of the control algorithm. The algorithm to minimize the cost function is set-up as a convex optimization problem, since the cost function is assumed to be well defined and contain only one minimum (Kays et al., 2009). All of the previously mentioned control actuators have been largely based on hydrofoils/lifting bodies. The advantage of lifting bodes over conventional trim tabs (or interceptors) is that lifting bodies have both an added mass and damping in the vertical axis, helping mitigate vertical motions. Disadvantages for the lifting bodies are from an operational viewpoint: they increase the operational draft of the vessel, require additional mechanism if the lifting bodies are retractable, are more susceptible to floating debris, and are more vulnerable to damage when they become airborne.

To the best of the author's knowledge, the first published investigation on the applicability of using actively controlled trim tabs on planing boats to reduce its motions in waves was by Wang (1985). Wang used a proportional controller (P-controller) to control the motion of the trim tab. Wang conducted a series of systematic experiments with regular waves to investigate the effect of actively controlled trim tabs. Because Wang observed that the heave motions were not sensitive to the trim tab excitation, but the pitch motions were, he narrowed down the controller to be a function

of only the pitch motions. Moreover, after further experimentation the best controller resulted to be only a function of pitch rate. Wang's experiments concluded that trim tabs were effective for reducing both the pitching motions and heave motions. The reason why the heave motions are reduced when only the pitch velocity is controlled is due to basic rigid-body-dynamics; for small angles, the motion of a point l-distance away from the motions of the CG is:

$$\dot{\eta}_3' = \dot{\eta}_5 l - \dot{\eta}_3 \tag{1.5}$$

where η_3 and η_5 are the heave and pitch motions respectively, whose positive directions can be seen in Fig. 1.10. Nevertheless, from Eq. (1.5) one can see that the pitch motions of the selected point, $\dot{\eta}_3'$, are only reduced if the reduction in $\dot{\eta}_5' l$ is not outweighed with an increase in η_3.

Savitsky, following Wang's investigation, conducted similar experiments to replicate and expand upon Wang's results; Savitsky used a proportional controller with the pith velocity, and performed tests in regular waves (Savitsky, 2003). Savitsky's results supported Wang's conclusions that actively controlled transom trim tabs reduced both the pitch and heave motions. Savitsky performed a linear analysis and illustrated that actively controlled trim tabs effect is to increase the effective pitch dampening of the vessel.

More recently, Rijkens et al. (2011) performed computer simulations for actively controlled trim tabs on a planing craft. However, in contrast with Wang and Savitsky, Rijkents et al. had simulations in irregular waves. The design of the controller for the trim tabs was based on Wang's proportional controller using the pitch velocity. The results in Rijkens et al. (2011) indicated a decrease in pitch motions, but on the other hand, there were no improvements on the heave motions; a decrease in pitch motions but unchanged heave motions suggest that there was an increase in η_3 which canceled the reduction of $\eta_5 l$ from Eq. (1.5).

1.3 Scope of Study

The study reported in this dissertation is based on numerical studies using reduced order models and strip-theory methods for planing craft simulation. With the exception of the preliminary study in Section 1.4, the planing crafts studied are prismatic and have a 12 m length and 10.2 tonne displacement. The ACS is modeled as body forces and the only controller investigated is an LQR (with the exception of the preliminary study); thus this work did not look into the design or optimization of the ACS's hardware.

Since the optimization results are dependent on all the above assumptions, the reader should have caution on interpreting the results quantitatively. The true significance of this work lies on the qualitative trends observed in the results — therefore any quantitative analysis for vessels not matching the described assumptions (or any vessel that is further along the design cycle) requires additional investigation and should be handled on a case-by-case basis.

While the study focuses on planing craft, the results are of importance to the high-speed crafts design community in general. In particular, the study is important to the design of USVs where the use of an ACS is intrinsic, and to the design of law-enforcement/military vessels where personnel injury is high.

1.4 Preliminary Work

For the preliminary work, we conducted a simple case study that explored if the co-design procedure could lead to different design decisions than those derived by the conventional "Sequential" process. The lcg is considered as the design parameter for the physical design, and three possible lcg choices and two control algorithms form the design space. Each design is tested in four different sea conditions, and at three different speeds. The goal for the simple case study was to select the 'optimal' lcg

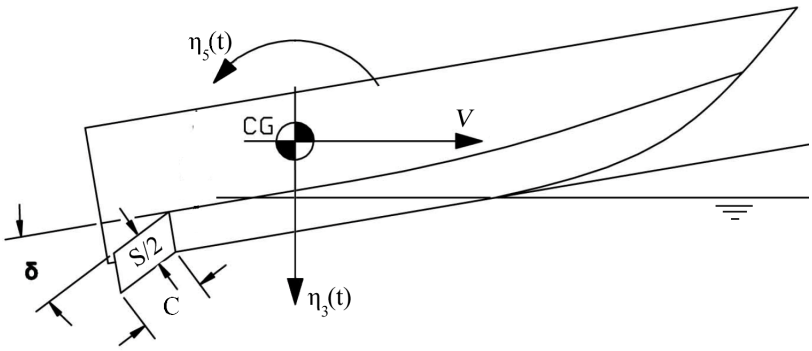

Figure 1.10: Planing vessel with body-fixed coordinate system and trim tabs.

location(s) for when the plant/control is optimized in a sequential, and in a co-design fashion. Because we selected discrete plant/control configurations, the optimization method employed will be the exhaustive search. The test vessel selected for the preliminary research is a small planing craft equipped with trim tabs; the particulars are shown in Tab. 1.1 and an illustration with the body-fixed coordinate system can be seen in Fig. 1.10.

For the case study, the 2.5D modeling with empirical wedge impact forces is used because of the in-house availability of the program POWERSEA Akers (1999). The program POWERSEA allows for the incorporation of user-defined body forces by means of user-defined dynamic-link librarys (DLLs) written in Fortran 77.

1.4.1 Performance Metric

Since one of the main motivations for improving the seakeeping of planing craft is to increase the safety of passengers, the criteria for comparing between plant/control designs will be the vertical accelerations of where a seat would be – thus referred through the paper as the "seat" accelerations (see Fig. 1.11). The acceleration metrics used are the RMS and the vertical acceleration dose, D_z, from the ISO standard 2631-5 (ISO Standard 2631-5, 2004). The advantage of the acceleration dose metric is that it is more sensitive to intermittent large values in the vibration time history – common on vibrations containing shock events. It is important to note that in order to use

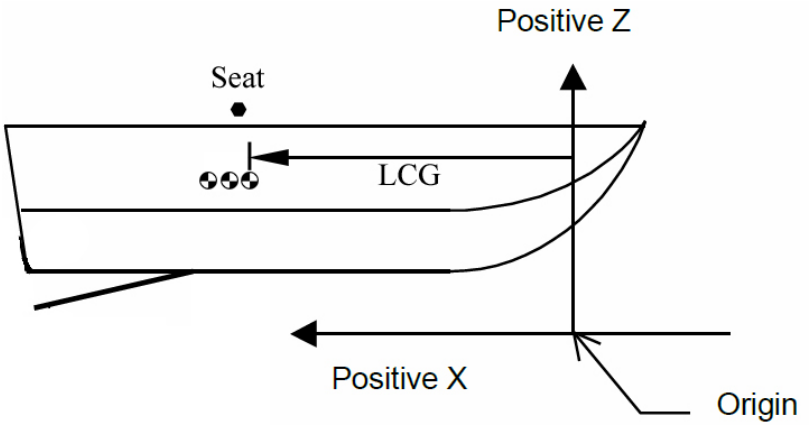

Figure 1.11: Planing vessel with earth-fixed coordinate system and locations of *lcg*.

Table 1.1: Preliminary study's vessel information

LBP (m)	7.0
Beam, b (m)	2.5
Displacement (kN)	31.1

(a) Vessel particulars

Chord Length, C (m)	0.61
Total Span, S (m)	2.13

(b) Preliminary study's trim tab dimensions

Long. Location (m)	Deadrise (deg)
0.37	51
3.92	18
6.70	14

(c) Preliminary study's deadrise at specific locations (aft of FP)

D_z as a metric for comparison, the time series being compared should have the same time length. In the case study results, a fixed time length of 250 sec was used for all sea conditions.

1.4.2 Test Matrix

The test matrix for the case study consists of three *lcg* locations, three constant speeds, and four sea conditions. A summary of the text matrix can be seen in Tab. 1.2. Below follows commentary on the selection of the test cases. The locations of the *lcg* are relative to the forward perpendicular (FP) of the vessel, as it can be seen in

Fig. 1.11.

The *lcg* location of a planing boat is critical so that the vessel's running trim angle is optimal, and also an important component in dictating the dynamic stability of the vessel (Blount and Condega, 1992). The original *lcg* of the vessel, 4.12 m, corresponds to the *lcg* that makes the vessel operate with a 4 degree trim angle at its design speed of 25 knots. For comparison, two other *lcg* locations are selected, corresponding to $\pm 5\%$ the original *lcg*, i.e., $lcg \in \{4.33, 4.12, 3.91\}$ m. As one can suspect, changing the *lcg* locations of the vessel will create a change in the running trim angle of the vessel when maintaining the vessel speed constant. Because we want to compare the performance between different *lcg*s and not different trim angles, the vessels' trim tab is actuated in order to maintain an equivalent average trim angle across the different configurations; this is done by using a Proportional and Integral (PI) controller that causes slow trim dynamics (15 sec rise time). Because the lower the vessel's trim angle, the lower the vertical accelerations response to waves is (Fridsma, 1971), the vessel tries to maintain a trim angle of 2 degrees for all of the test conditions (active and passive).

Since the simulation program POWERSEA is intended to be used with vessels operating in planing conditions, each tested speed of the vessel, V, is selected so that the vessel is in full-planing condition. Following the guidelines by Savitsky and Brown (1976), the vessel should be in full-planing conditions when $C_v > 1.5$; therefore, the selected speeds for the case study are $C_v \in \{2, 3, 4\}$, which correspond to the dimensional speeds of V $\in \{18.6, 27.9, 37.2\}$ knots, accordingly.

In this research, the vessel was simulated in irregular waves conforming to the Pierson-Moskowitz spectra (Michel, 1999); four sea states (SS) are tested: 0, 1, 2, and 3. Following the sea state definitions of Faltinsen (2005), the significant wave heights ($H_{1/3}$) for SS {0,1,2,3} are {0,0.1,0.5,1.25} m accordingly.

Table 1.2: Preliminary study test matrix

Variable	Range
lcg (m)	{4.33, 4.12, 3.91}
V (knots)	{18.6, 27.9, 37.2}
$H_{1/3}$	{0, 0.1, 0.5, 1.25}
Avg. Trim (deg)	2

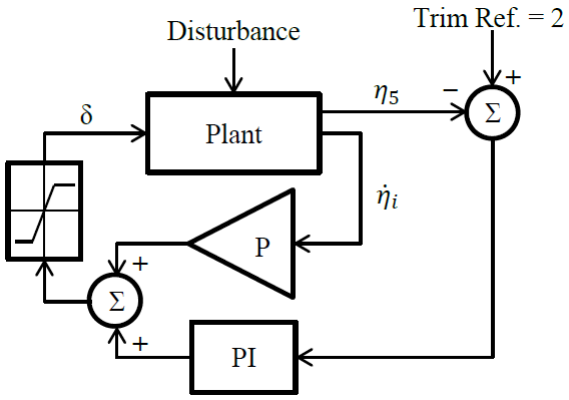

Figure 1.12: P-controller used in preliminary study vessels.

1.4.2.1 Controller Selection

Each case of the test matrix was simulated a total of three times: one being the 'passive' mode, and the other two correspond to the trim tab actively controlled with heave velocity $\dot{\eta}_3$ feedback, or pitch velocity $\dot{\eta}_5$. The trim tab angle (δ) was saturated such that it operated within the bounds on which its modeling is accurate, from 0 deg to 15 deg. An illustration of the P-controller as it was used in the preliminary research can be seen in Fig. 1.12, where $i = \{3, 5\}$. The following paragraphs in this section describe the controller design process used.

Following the results from Savitsky (2003) and Wang (1985), the first approach to controller design was to linearize the system at each operating point and design a proportional controller with pitch velocity feedback. To estimate the structure of the transfer function needed, the linear model presented in Eq. (1.6-1.7) was used (Troesch, 1992).

$$A\ddot{\eta} + B\dot{\eta} + C\eta = F^w + F^t \tag{1.6}$$

$$\eta = \begin{bmatrix} \eta_3 \\ \eta_5 \end{bmatrix}, \; F^w = \begin{bmatrix} F_3^w \\ F_5^w \end{bmatrix}, \; F^t = \begin{bmatrix} F_3^t \\ F_5^t \end{bmatrix} \tag{1.7}$$

Because the linear model estimation was performed in calm water, F^w was set to zero. Next, with a coordinate transformation of $x = [\eta_3, \eta_5, \dot{\eta}_3, \dot{\eta}_5]$, one can transform the system in Eq. (1.6) to a state space model; and using the state space model, a transfer function from the trim tab angle, δ, to the pitch velocity – or heave velocity – is found, Eq. (1.8).

$$G(s) = \frac{b_3 s^3 + b_2 s^2 + b_1 s}{s^4 + a_3 s^3 + a_2 s^2 + a_1 s + a_0} \tag{1.8}$$

The parameters in Eq. (1.8) are estimated by using the following parameter estimation techniques: gradient with instantaneous cost, gradient with integral cost, least-squares with covariance resetting, and least-squares with forgetting factor; from the identification results, the one that yielded the lowest error for each of the operating conditions was the one used for analysis. In most of the cases, the least-squares with forgetting factor technique was the one that resulted with the parameters with the lowest errors between the linear model and the nonlinear simulation results.

Because of the specified coordinate system, a positive deflection of the trim tab will create a negative pitching moment. Since we would like to increase the dampening of the system (Savitsky, 2003), when there is a positive pitch velocity, the trim tab should deflect on the positive direction; this implies that the system should have positive feedback.

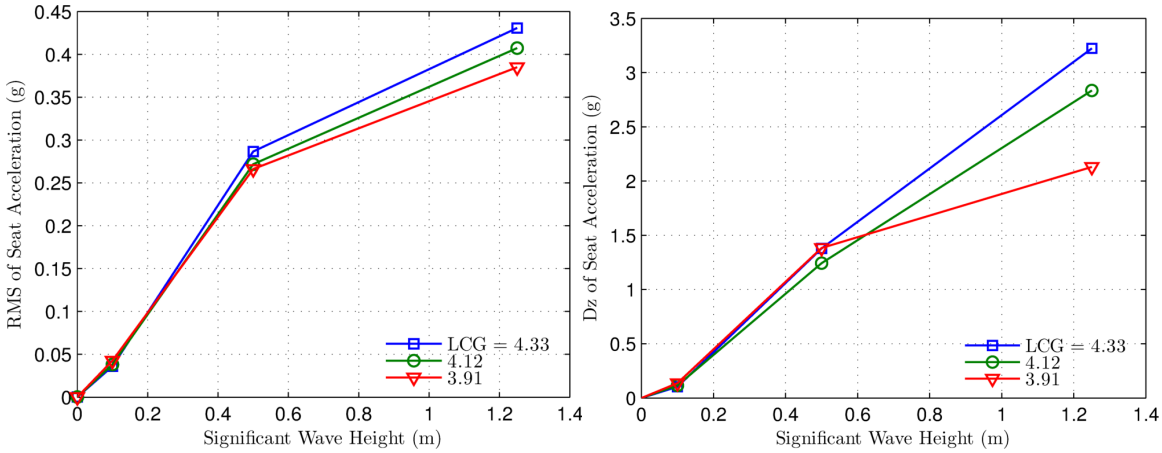

(a) Passive (b) Passive

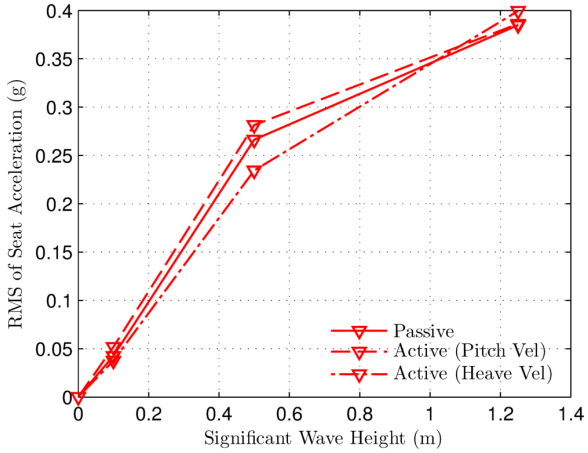

(c) Passive compared with active at $lcg = 3.91$ m

Figure 1.13: Typical results for the passive trim tab simulations, $C_v = 2$.

1.4.3 Discussion of Preliminary Study Results

When following the sequential design process, the overall winner was the vessel with the *lcg* most forward (3.91 m) and the trim tabs controlled with the heave velocity feedback, see Fig. 1.13 for typical results. However, when considering all the results from the exhaustive search we can conclude that when the trim tabs are controlled with the heave velocity feedback, both the *lcg* most forward and original (3.91 m and 4.12 m) are equally good performers, see Fig. 1.14 for typical results.

Furthermore, there were unexpected results from this case study. The results from the preliminary research suggests that reducing the pitch motions does not always

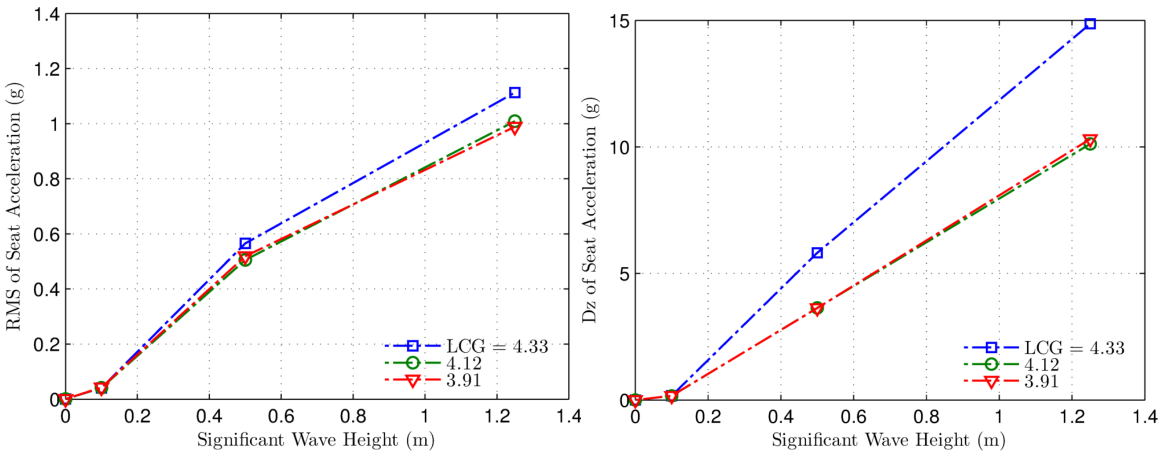

Figure 1.14: Typical results showing equal performance between $lcg = 3.91$ m and 4.12 m, $C_v = 4$ and active control (heave velocity).

reduce the heave accelerations of a planing boat in irregular waves (see Fig. 1.15); however, a control strategy that focuses on the heave velocities can indeed reduce the heave accelerations. From Fig. 1.15, it is clear that the boat behavior is different with the two presented control strategies; to the best of the author's knowledge, the behavior of the craft when controlled with the heave velocity feedback has been neither explored nor tangibly observed in past research. In addition, the results are in contrast with previous research (Savitsky, 2003; Wang, 1985) since this research suggests that a P-controller on the pitch rate is not an adequate control system for reducing heave accelerations, but instead a P-controller on the heave velocity is more effective.

From the preliminary results, it is evident that there are 'optimal' plant/control configurations that are not found if a sequential design approach is taken. Moreover, a planing craft with ACSs has nonlinear behaviors which might change the conventional planing craft design methodology.

Nonetheless, the seakeeping benefits from co-design are unclear in these preliminary results. Consequently, these results motivated a more generalized exploration, and as a first step the calm-water drag was investigated.

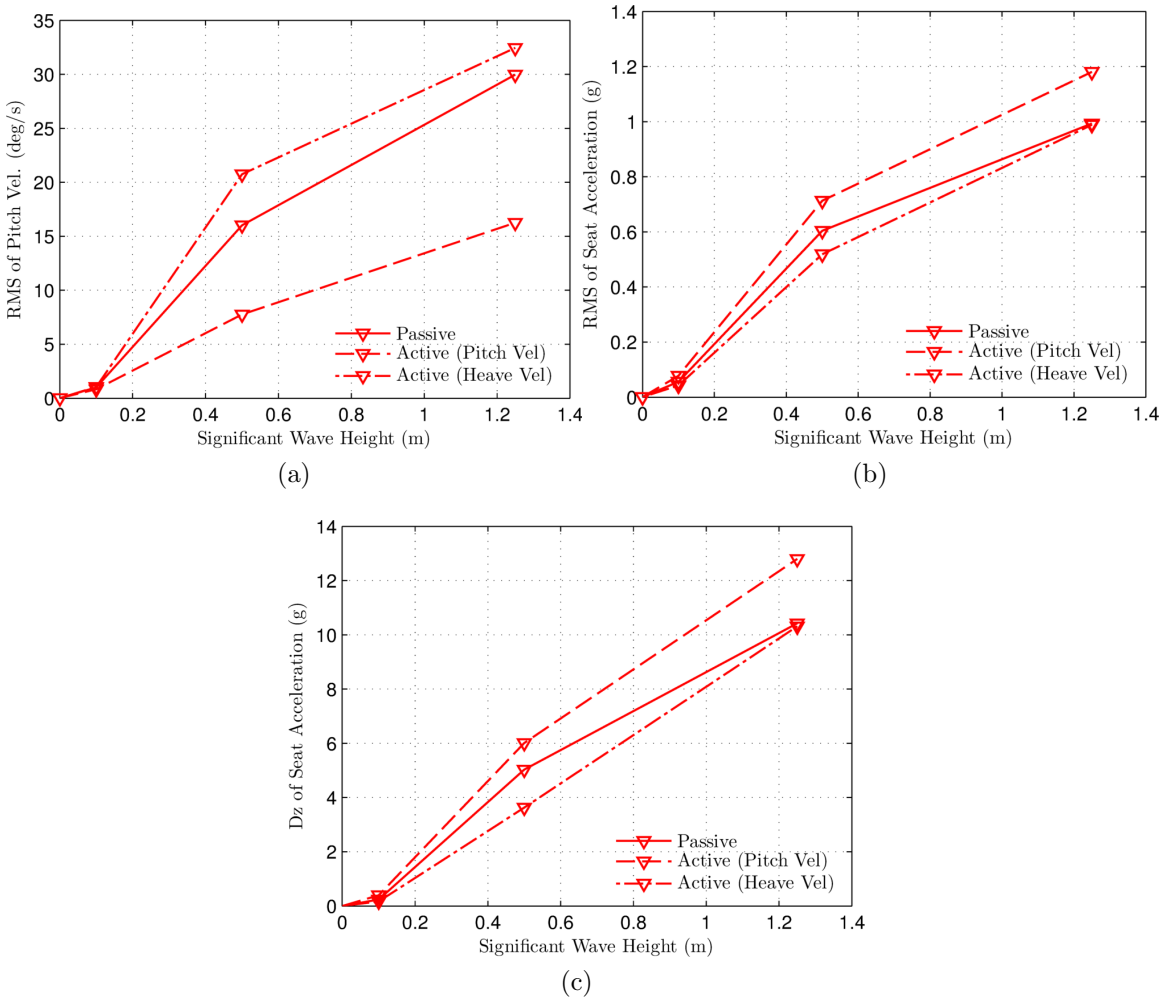

Figure 1.15: Typical results showing reduced pitch velocity but increased vertical accelerations, $C_v = 4$ and $lcg = 3.91$ m.

CHAPTER II

Calm Water Case

2.1 Overview

The discussion in Chapter I and the results of Section 1.4 strongly indicate that the design space is not completely explored when a designer performs a sequential design. Typically, the first metric that a designer evaluates is the calm-water drag — the metric of focus on the early works in planing surfaces. Therefore, the objective of this chapter is to compare the calm water performance of a planing craft with ACS where the *lcg* of the vessel and ACS are designed sequentially (traditional approach), with the calm water performance of a vessel in which the *lcg* and ACS are co-designed.

Two different methods are used to perform this investigation, one is a reduced order model approach (presented in Section 2.2.1) and the other a time-domain approach (presented in Section 2.2.2). Both methods agree with each other closely, with the results suggesting that drag savings up to 20% are possible if the vessel is co-designed.

2.2 Design Methodology

To simplify the vessel's hydrodynamics (and thus the modeling), the vessels investigated are prismatic in shape, i.e., the beam and deadrise distributions are constant

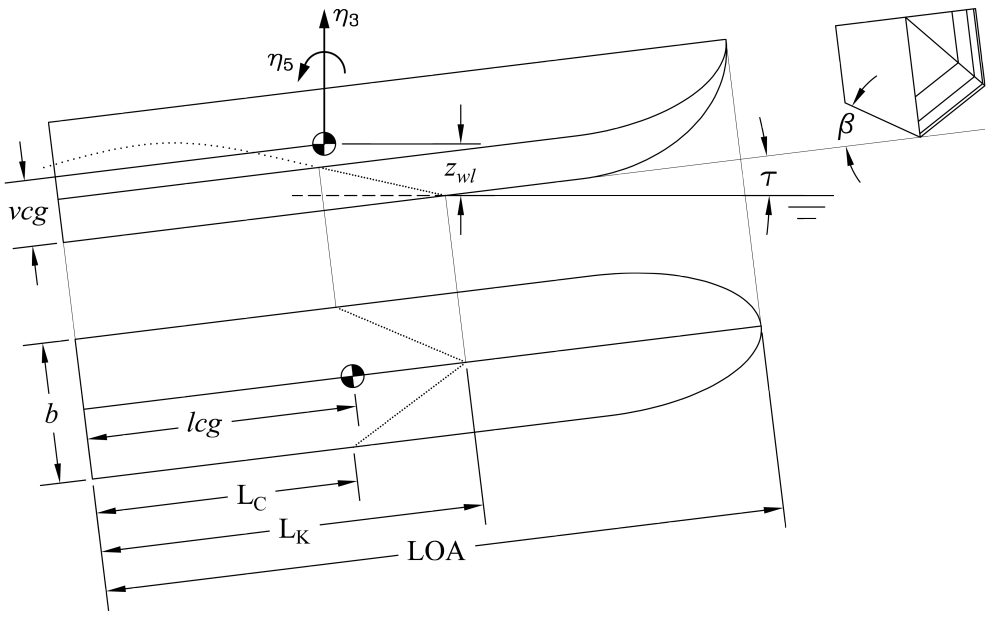

Figure 2.1: Prismatic planing craft.

Table 2.1: Fixed vessel particulars

Fixed Variable	Value
beam, b (m)	4.27
LOA/b	5
vcg/b	0.294
R_g/b	1.25
C_Δ	0.607

throughout the length of the vessel as shown in Fig. 2.1. The vessel shape follows that from the models tested by Fridsma (1969), and the used dimensions and specifications can be seen in Tab. 2.1.

In this investigation, we focus on optimizing the vessel's calm water L/D by changing the lcg — which in turn changes the vessel's running trim angle. Note that because the vertical lift (F_z) is equal to the displacement (Δ), optimizing L/D is equivalent to minimizing the total horizontal drag (R_T). As it has been found, for a fixed speed and hull geometry, there is a global optimum trim angle (Savitsky, 1964). However, the vessel might also have a lcg location where there is porpoising

inception (Day and Haag, 1952); and depending on the speed and hull geometry, the porpoising inception might be before the vessel reaches its optimal L/D (Savitsky, 1964). Consequently, the vessel's 'optimal' L/D is dependent on whether we want a vessel that is open-loop stable (w/o ACS) or if we allow the vessel to be open-loop unstable and stabilize it with an ACS. In other words, if we would like to have a vessel that is stable w/o ACS, the 'optimal' trim angle would be the one that has the lowest drag but still inside the stable region – this is illustrated in Fig. 2.2.

Making the assumption that the calm water L/D is a non-dynamic value in steady and stable operation, the ACS's primary role in the calm water L/D optimization is to provide stability. As a result, the ACS parameters are not investigated in this study. Instead, to investigate the potential from co-designing a planing craft and its ACS, the following two contrasting investigation procedures are conducted; (1) in one the vessel's design space is explored with the constraint that it has to be stable without an ACS (i.e., open-loop stability at the origin), (2) and in the other that it has to be stable with an ACS (i.e., locally controllable).

The L/D and local stability investigation was conducted with two different methods. (i) One was by following the procedure in Faltinsen (2005), which uses Lyapunov's indirect method (Khalil, 2002) with the nonlinear models described in Faltinsen (2005) – therefore this method will be referred as 'Faltinsen Method'. The model used for 'Faltinsen Method' is presented in Appendix A. (ii) The other procedure, which is akin to one used in Sun and Faltinsen (2011), conducts a porpoising inception bisection search of the *lcg* using the time-domain nonlinear simulation program POWERSEA (Akers, 1999) – thus it will be referred to as 'POWERSEA Method'.

The optimal L/D was calculated for a range of C_v and β. More specifically, the 'optimal' *lcg* location (for both design paths) is found for when the vessel has the specifications from Tab. 2.1 and for a range of values for $C_v \in [2.5, 4.5]$ and $\beta \in [5, 30]$.

2.2.1 Faltinsen Method

For the 'Faltinsen Method', the two design paths can be seen as the optimization problems shown in Tab. 2.2, where $x = \begin{bmatrix} lcg & \tau & z_{wl} \end{bmatrix}^T$, τ is the trim angle, z_{wl} is the vertical distance of the CG to the calm water line, M_{cg} is the total moment about the CG, λ_i are the eigenvalues of the linearized model from Faltinsen (2005), $|W_C|$ is the determinant of the controllability matrix of the linearized model, and ϵ is arbitrarily small constant greater than zero. As previously mentioned, the nonlinear model used for defining R_T, F_z, M_{cg} and the linearization of the system are shown in Appendix A, and the methods used to test for stability and controllability are stated in Appendix A.2. The *fmincon* optimizer from MATLAB was used to solve these optimization problems. Apart from the approach taken here, there are multiple ways that one could set up these optimization problems, each with their own advantages and disadvantages. Because the approach taken here leaves a lot of work to the optimizer to gain some efficiency, it is important to give the optimizer as much information as possible so that it does not explore invalid domains. In this case, it is possible to set lower and upper bounds such as $0 < \tau < 15$ and $0 < lcg < 4b$, and also the constraint that the vessel should be in the water, e.g., the keel wetted-length is $L_K > 0$.

2.2.2 POWERSEA Method

For the 'POWERSEA Method', the lcg in which porpoising starts was found by using a bisection method with the program POWERSEA. The vessel is simulated without ACS in calm water for 60 sec, and if the vessel's pitch at the end of the simulation is not oscillating with more than half of a degree of amplitude, the simulated lcg is considered stable and it is reduced by half for the next simulation. However, if the vessel is found to be porpoising, the next simulated lcg is the average of the last unstable lcg and stable lcg. This algorithm is continued until lcg/b converges within

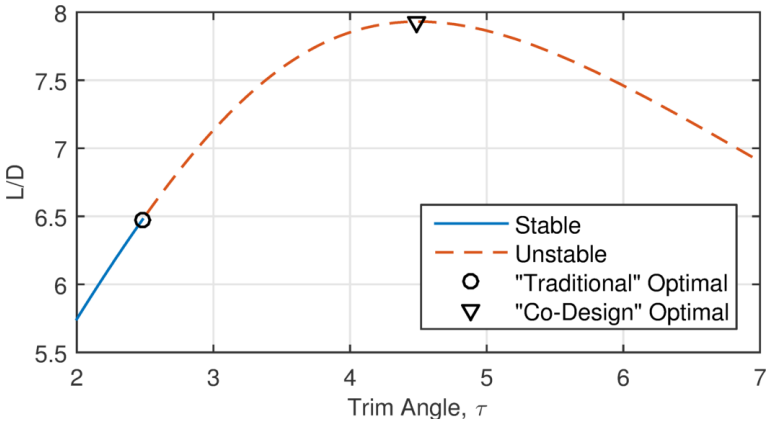

Figure 2.2: Calm water L/D for $C_v = 4.5$ and $\beta = 5°$.

Table 2.2: Calm water drag optimization approaches

Sequential		Co-Design	
$\min_x$	$R_T(x)$	$\min_{lcg}$	$R_T(x)$
s.t.	$F_z(x) - \Delta = 0,$	s.t.	$F_z(x) - \Delta = 0,$
	$M_{cg} = 0,$		$M_{cg} = 0,$
	$\lambda_i(x) < 0,\ i = 1, \ldots, 4$		$\lvert W_C(x) \rvert > \epsilon$

three significant figures.

2.2.3 Calm Water Controllability

Moreover, to compare the calm water controllability between designs, the 'controllability index' c from Friedland (1975) is used as a metric for a measure of controllability between designs. This index is based on the controllability gramian of the vessel's linearized model; and to keep continuity in the controllability gramian values when the system becomes open-loop unstable at the origin, the procedure in Zhou et al. (1999) is used.

2.2.4 Seakeeping Example

To have a sense on how the calm-water L/D translates to when the vessel is operating in a seaway, the vessels found for the two design paths at $C_v = 4.5$ and $\beta = 20°$ are simulated for 2500 sec in POWERSEA with sea states varying from zero to three. The seaways were simulated with the ISSC spectrum with 100 wave components, following the significant wave heights and periods specified for the Atlantic Ocean in Faltinsen (2005).

For the simulations, the vessel's ACS is modeled as two point forces on the vessel, one at the stern and the other at the bow. The ACS controller is a Linear Quadratic Regulator (LQR) designed using the same linearized model used to investigate the stability of the vessel; the model is linearized about the calm-water operating trim and heave estimated by Savitsky method (Savitsky, 1964). A shortcoming of the controller used is that it requires all states of the vessel to be measured during operation: heave, pitch, heave velocity and pitch rate.

From the seakeeping simulations, the average L/D and the acceleration metric D_z from ISO Standard 2631-5 (2004) are computed. It is important to note that to use D_z as a metric for comparison, the time series being compared should have the same time length. The advantage of using D_z as a metric is that its application is simple and it is more sensitive to isolated shocks than the root mean square. Example calculations of the D_z metric can be seen in Appendix B.

2.3 Results and Discussion

2.3.1 Faltinsen Method

When the vessel is required to be open-loop stable, the vessel's optimal efficiency contour is as seen in Fig. 2.3a. As expected, the efficiency reduces with increasing deadrise and speed; this is consistent to what vessel designers are familiar with: if you

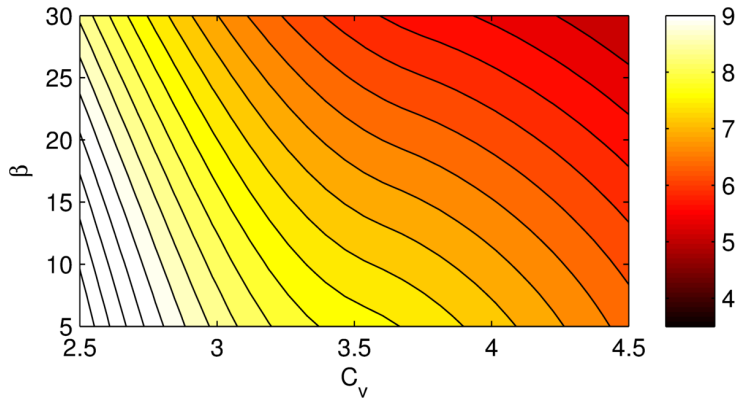

(a) Vessel with stability constraint (Sequential)

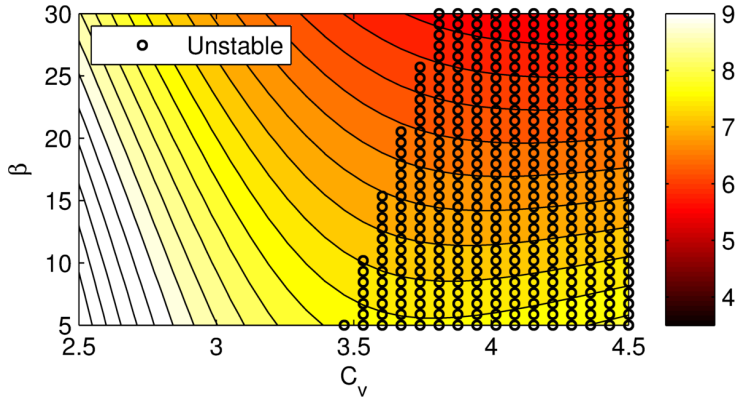

(b) Vessel without stability constraint (Co-Design)

Figure 2.3: Lift-to-drag contour from Faltinsen Method results, with ∘ corresponding to OLU vessels.

want to go somewhere faster, you will need more energy. Therefore, if a designer's only concern was to design a vessel with the highest efficiency inside this domain, then that design point would correspond to $[C_v, \beta] = [2.5, 5°]$.

Nonetheless, when the vessel is allowed to operate at any running attitude as long as it is controllable, the optimal efficiency contour changes as seen in Fig. 2.3b. In this contour, the points that are open-loop unstable are marked with '∘'. In contrast with the previous contour, the efficiency increases when $C_v > 3.5$. Consequently, rather than having only one optimal point as before, there are now two optimal points: one is the same (since it is also open-loop stable), and the other is $[C_v, \beta] = [4.5, 5°]$.

The relative change between the efficiencies when open-loop stability constraint is enforced and relaxed can be seen in Fig. 2.4a, where R'_T and R_T are the co-design

and sequential design vessels drag, accordingly. It is clear that the efficiency gains from allowing the vessel to operate in an open-loop unstable region increases as the speed increases – reaching an impressive 22% L/D increase for the $[C_v, \beta] = [4.5, 5^\circ]$ optimal design point. As a rough estimate, these kinds of efficiency gains translate to reducing fuel related costs (volume, weight and expenses) by 18%.

Nevertheless, there is a difficulty presented if the vessel is required to operate in the new optimal operating point of $[C_v, \beta] = [4.5, 5^\circ]$. As one can see from Fig. 2.4c, the operating trim angle increases as the designs enter the unstable region with the increasing speed. For the required trim angle at $[C_v, \beta] = [4.5, 5^\circ]$, the lcg should be located at 74% of the beam's length (from the transom) – if the lcg is forward of this, there would have to be an external positive trim moment to maintain the vessel at this operating point. However, this challenge merely points to the fact that conventional hull designs would need innovation – opening the door for new and unconventional vessel designs.

While it requires innovative vessel designs to operate at these new optimal operating points, the new designs could actually be more controllable. To compare the "ease of control" in those cases, we compute the relative change in the controllability indexes; the results are shown Fig. 2.4b, where c' and c are the controllability metric of the co-design and sequential design vessel, respectively. According to this metric, when the vessel is required to be open-loop stable at the origin, the system is very close to being uncontrollable (the value ≈ 0); this makes the relative change values to be very large – perhaps misleadingly large. Consequently, to have a sense of the difference in controllability between designs, the nonlinear model from Faltinsen (2005) was simulated when the initial state was perturbed from the origin and controlled by a LQR controller. The LQR controller was tuned so that the vessel responses were as similar as possible; this was attempted by an optimization method with the LQR tuning parameters as the design variables. An example result can be seen in Fig. 2.5,

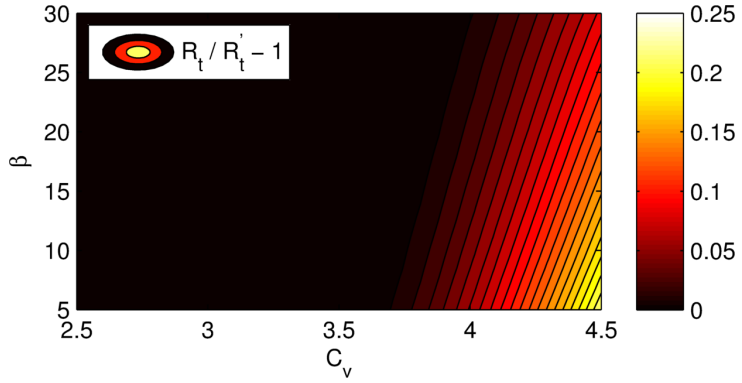

(a) Change in L/D (Sequential to Co-Design)

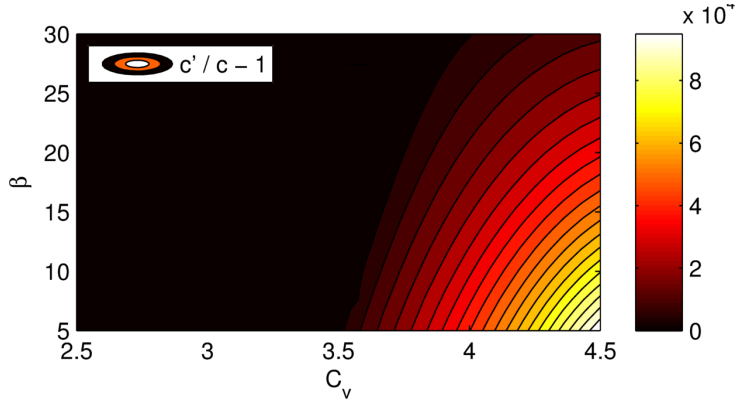

(b) Change in c

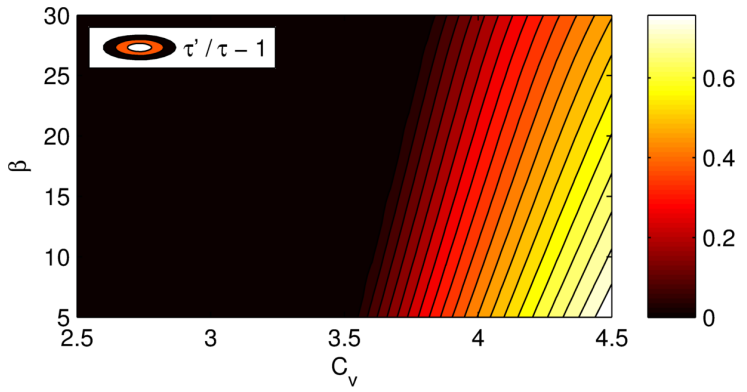

(c) Change in trim angle

Figure 2.4: Relative change in L/D, controllability index (c), and trim from sequential to co-design (Faltinsen Method).

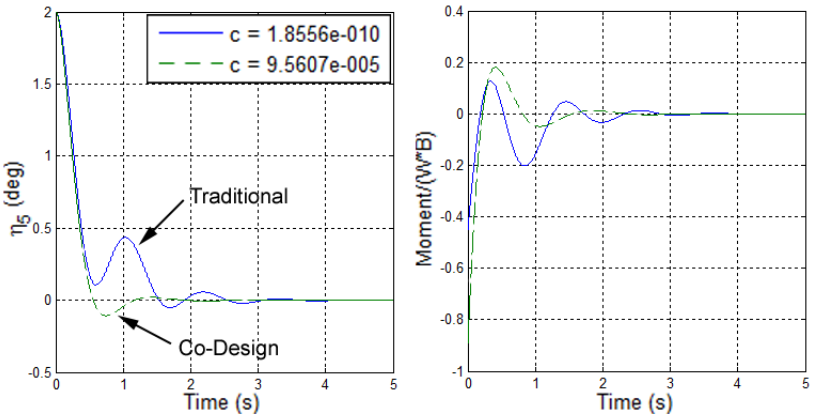

Figure 2.5: Closed-loop nonlinear results for $C_v = 4, \beta = 10°$ (Faltinsen Method).

where the larger controllability index corresponds to the vessel design that required open-loop origin local stability (blue solid line). From these time domain results, it is noticeable that even with increased control effort for the vessel with open-loop stability, it has worse performance than the vessel that is open-loop unstable. Nonetheless, note that these results are for calm water.

2.3.2 POWERSEA Method

This method was used primarily as additional confirmation to the results suggested by using 'Faltinsen Method'. From the optimal lift-to-drag contours shown in Fig. 2.6a and Fig. 2.6b, we can see that the efficiency contours shares some similarities to the ones found with 'Faltinsen Method'. Moreover, comparing Fig. 2.3b and Fig. 2.6b we can observe that 'Faltinsen Method' is more conservative on estimating the domain where the vessels lift-to-drag optimum is open-loop unstable.

Both the 'POWERSEA Method' results and the 'Faltinsen Method' results suggest that the L/D improvement changes with β, with the highest L/D gains at the lower β (see Fig.2.4a and Fig. 2.6c). The improvements in L/D agree with those found by 'Faltinsen Method', reaching an impressive 25% L/D increase for the $[C_v, \beta] = [4.5, 5°]$ optimal design point.

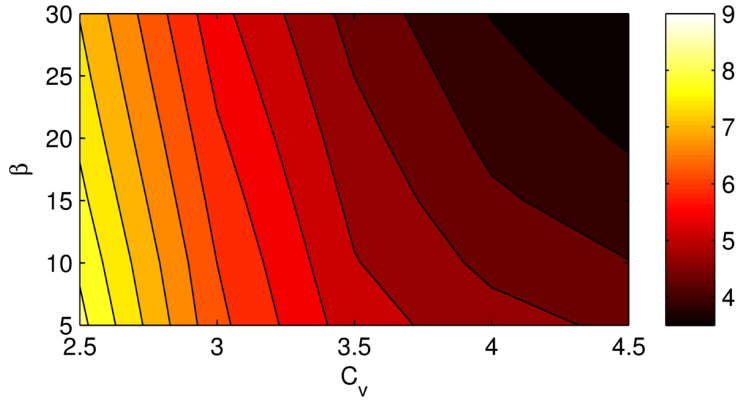

(a) Vessel with stability constraint (Sequential)

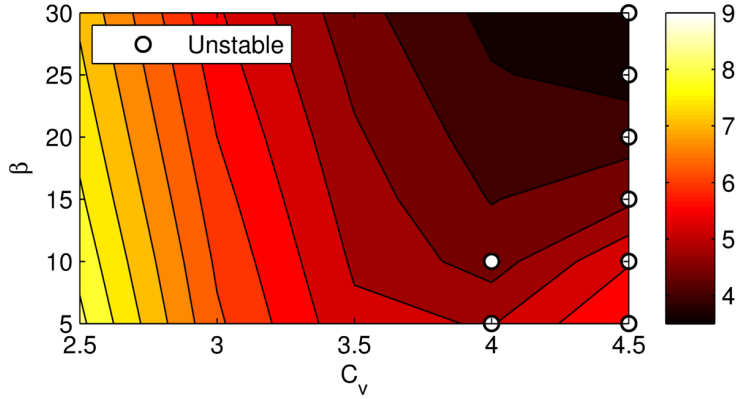

(b) Vessel without stability constraint (Co-Design)

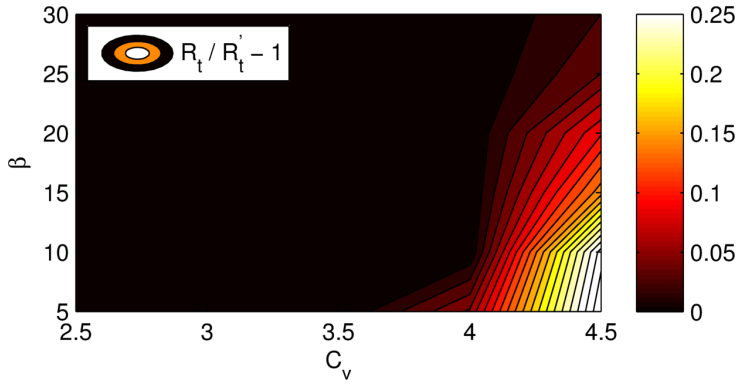

(c) Change in L/D (Sequential to Co-Design)

Figure 2.6: L/D contour from POWERSEA Method results and L/D relative change.

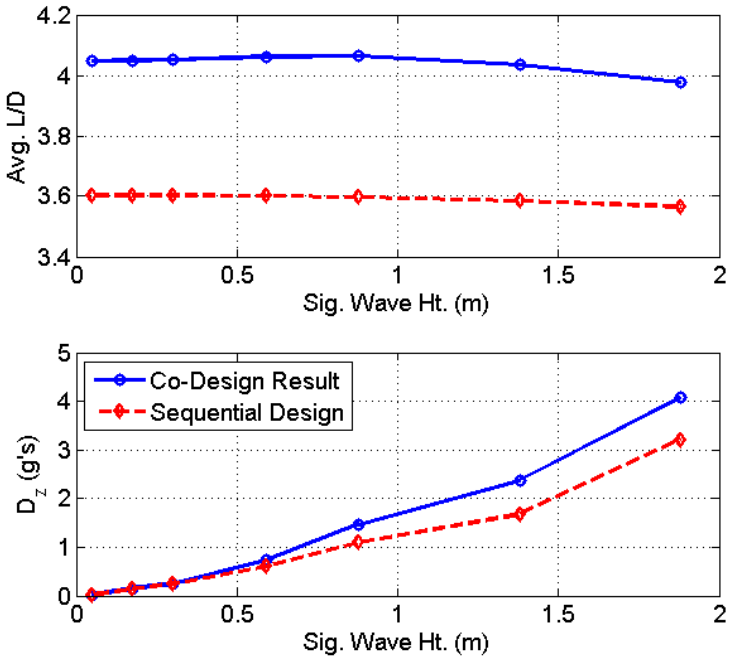

Figure 2.7: Seakeeping POWERSEA results.

2.3.3 Seakeeping Example

The seakeeping results can be seen plotted in Fig. 2.7. From the L/D results, it can be observed that the L/D gains are maintained in a seaway. However, the seakeeping performance was considerably worsened at sea states higher than SS 1 - increasing the vertical acceleration doses by approximately 25%.

2.4 Conclusion

When the vessel and ACS are co-designed, any designs that would be otherwise discarded because they have open-loop instabilities are now viable candidates because the ACS can stabilize the system. Vessels can now be designed to operate on much more efficient running attitudes. Moreover, the calm water controllability investigation shows that the unstable vessels resulting from the co-design approach are actually more controllable (in calm water) than the vessels from the traditional

approach, with this result increasing in strength with higher speeds – a result which indicates a "win-win" situation between calm water controllability and calm water L/D optimization.

The results suggest that co-designed vessels provide designs that are of greater performance, for the metric considered, than traditional vessels. The improvement in transport efficiency but worsening in seakeeping at the higher sea states suggest that there might be a trade-off between the two; therefore future research will investigate techniques to include seakeeping as a design metric in the co-design method. Moreover, the maneuverability of the vessel is an additional design metric that would be affected by the ACS; as a result, if the maneuverability of the vessel is important, this metric should be also incorporated into the co-design study.

Nonetheless, these first results investigating the co-design of a planing craft and its ACS indicate that the traditional design approach does not fully exploit the synergy between a planing craft and its ACS; and as a first step, the stability constraints should be relaxed in the design exploration.

CHAPTER III

Pareto Fronts

3.1 Overview

In this chapter, we build from our previous calm-water co-design results in Chapter II, which showed that the calm-water and seaway drag could be improved if the vessel was allowed to be open-loop unstable (OLU) and be stabilized by an ACS. Here, we explore the seakeeping and seaway drag behavior to further understand and characterize the differences in the sequential design and co-design approaches when applied to a planing craft and its ACS. We accomplish this by performing an exhaustive search in the vessel geometry and control parameter spaces using POWERSEA (Akers, 1999), a strip-theory planing boat simulation program.

The results of this chapter suggest the following:

- Co-designed vessels surpassed the sequentially designed vessels both in seakeeping and transport efficiency. Results suggest reductions in seaway drag of 30% for SS 2 and 10% in SS 3; and reductions in the seakeeping metric D_z (an ISO definition to be discussed in Section 3.2.2) of 20% in SS 2 and 50% in SS 3.

- For the two metrics considered, namely average seaway drag R_T^S and D_z, co-designed optimal vessels at the Pareto front are in general not the same as those resulting from the Pareto front of sequential design.

- ACSs introduce optimal trim angles for seakeeping, i.e., seakeeping does not monotonically improve with lower average trim angles. As a result, they allow the vessel to operate in more efficient trim angles in a seaway without a serious penalty in seakeeping.

3.2 Design Methodology

While the main objective of our research is to explore the optimal vessels obtained by sequential design and co-design, the approach taken is an exploratory one rather than numerical optimization. This approach is taken for the following reasons: (1) It allows us to investigate the seakeeping and drag behavior of the craft as we vary design parameters, and (2) there is a guarantee that we will find the global minimums from the discretized design space. The approach is further explained in Section 3.2.2, and the modeling of the planing craft and ACS is presented in Section 3.2.1.

3.2.1 Modeling

3.2.1.1 Craft Geometry

In order to simplify the vessel's hydrodynamics and isolate the key variables that influence the craft's behavior, the body is designed prismatic and the bow shape follows that from the models tested by Fridsma (1969) which have constant deadrise throughout. The fixed vessel particulars can be seen in Tab. 3.1, and a diagram of the vessel in Fig. 3.1. The vessel's geometry design variables considered in this work are β (deadrise angle) and lcg (longitudinal center of gravity).

3.2.1.2 ACS

The ACS is modeled as two vertical (body-fixed) point forces (F_1 and F_2 in Fig. 3.1), with a horizontal (body-fixed) "drag" penalty proportional to the force

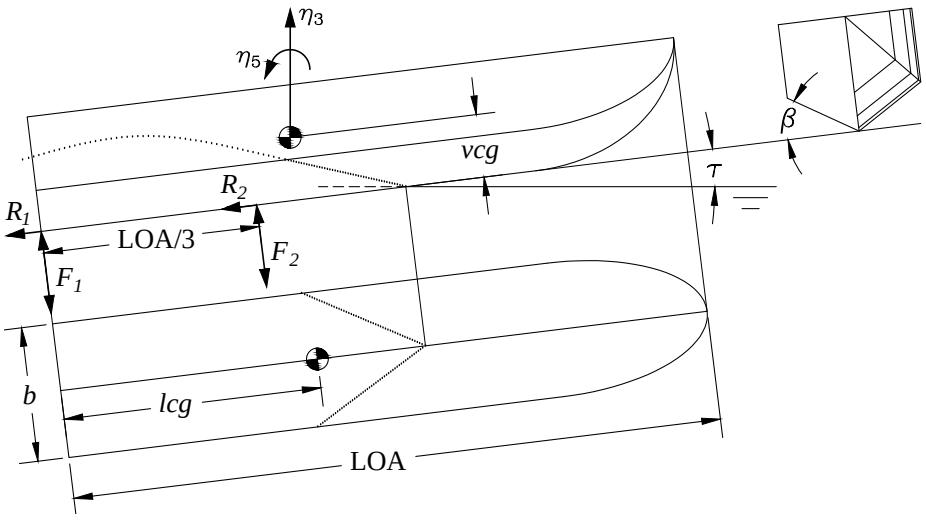

Figure 3.1: Prismatic vessel and definitions.

Table 3.1: Fixed vessel particulars

Fixed Variable	Value
b (m)	2.54
LOA/b	4.72
vcg/b	0.294
R_g/b	1.25
C_Δ	0.607

magnitude (R_1 and R_2 in Fig. 3.1) — a simplistic approach to simulate the ACS's hardware's lift-to-drag ratio (L/D), which is set to $L/D = 10$ (e.g., a hydrofoil). While this approach leaves room for future improvement in terms of ACS's hardware modeling, it more directly captures the "required" forces which could then be in turn analyzed to evaluate appropriate ACS's hardwares. The location of one point force is at the stern, and the other is LOA/3 forward from the stern (illustrated in Fig. 3.1).

The ACS's controller is chosen as the Linear Quadratic Regulator (LQR) designed using the linear model described in Appendix A, with the difference that $\tilde{\boldsymbol{B}}$ (the input matrix) now contains the distance LOA/3 instead of LOA, and $\tilde{\boldsymbol{B}}$ is multiplied by a normalization value of Δ (i.e., $\tilde{\boldsymbol{B}}_{new} = \tilde{\boldsymbol{B}}\Delta$) to bring the optimized variables into proper scales. The controller minimizes the cost function

$$J(\boldsymbol{u}) = \int_0^\infty (\boldsymbol{\eta}^T \mathbf{Q} \boldsymbol{\eta} + \boldsymbol{u}^T \mathbf{R} \boldsymbol{u}) dt \tag{3.1}$$

where the $\mathbf{R}$ matrix is set as an identity matrix (2x2), the state variables' are $\boldsymbol{\eta} = \begin{bmatrix} \eta_3 & \eta_5 & \dot{\eta}_3 & \dot{\eta}_5 \end{bmatrix}^T$, $\mathbf{Q}$ is

$$\mathbf{Q} = \begin{bmatrix} 0 & 0 & 0 & 0 \\ 0 & 0 & 0 & 0 \\ 0 & 0 & 0 & 0 \\ 0 & 0 & 0 & Q_{44} \end{bmatrix} \tag{3.2}$$

where Q_{44} is a design parameter, and $\boldsymbol{u}$ are the ACS's forces. The weight on pitch velocity, Q_{44}, was selected as the design parameter because previous research (Wang, 1985) suggests that seakeeping is sensitive to pitch velocity feedback.

3.2.1.3 Simulated Conditions

In the previous study on co-design of planing craft with ACS presented in Chapter II, the largest drag reduction (the sole optimized objective) of co-designing occurred at

Table 3.2: ISSC spectrum parameters (North Atlantic from Faltinsen (2005))

SS	Mean $H_{1/3}$ (m)	Wave Period (s)
0	calm water	—
1	0.05	6.0*
2	0.3	7.5
3	0.88	7.5

*Extrapolated value

the highest simulated speed of $C_v = 4.5$. However, the co-designed vessel's seakeeping was the worst at this high speed. Since we are focusing on the possibility that the co-designed vessels are significantly better both at seakeeping and drag, the explored speed is $V = 45$ kt ($C_v = 4.6$) — a common high speed for the investigated vessel size.

Two sea conditions are explored: Sea State (SS) 2 and 3. The seaway is assumed to be in the North Atlantic, and is simulated by using the ISSC sea spectrum with 100 wave components. The used ISSC parameters are shown in Tab. 3.2.

Because the seas are stochastic, the objective functions are a function of simulation time which should converge to a value as the simulation time goes to infinity. A naive approach to selecting a simulation length would be to conduct the exploration with a simulation time of one hour as recommended by ITTC (2002) for accurate statistics. But in this chapter, we are interested in "which vessels are better?" instead of "what are the seakeeping statistics within a high-confidence level?". One can see that these two questions have conflicting requirements; in order to find the better vessels, one would want to run as many different configurations as possible — but on the other hand, if we want accurate statistics, we want to run the tests for as long as possible. This kind of problem is known in the machine learning community as the exploration-exploitation tradeoff.

Heuristically speaking, the approach taken in this chapter follows the idea that if the vessels are tested with the same wave-history, there should be a finite simulation

time that when comparing the results, one can select the winner within some certainty. Calculating the confidence interval is non-trivial because, while the seaway has a well-defined stochastic model, the vessel's response is highly nonlinear (Savitsky and Brown, 1976). One approach would be to perform Monte Carlo simulation using random seed numbers for the wave time histories. But in this chapter, we simulated each design for 180 sec with the same seed number, i.e., the wave time histories are identical for all runs. This is akin to treating the results for the 180 sec seaway as a metric, similar to how the controls field uses standard responses to measure performance (e.g., step response and impulse response).

The behaviour of the objective functions with fixed deadrise and varying *lcg* and simulation times are seen in Fig. 3.2; this investigated case suggests that design variables that minimizes the objective space created by a simulation time of 180 sec, are "close" to the design variables that minimize the objective space for extended simulation times. While this approach may not be ideal, it is the most efficient given the available tools and design constraints.

3.2.1.4 Virtual Test Bed

The simulations are performed in the time domain using the program POWERSEA (Akers, 1999), which is based on a strip theory approach with empirical wedge forces (Zarnick, 1979). Consequently, ACS's forces are uncoupled from hull's wave forces. Because the research will require extensive simulations, a strip theory approach is adequate since it is computationally fast. POWERSEA allows for script automation via Component Object Model (COM) interoperability.

The tuning parameters in POWERSEA are empirical, but they have a strong effect on the vessel's stability and operation behavior. However, some tuning parameters are meant to correct for varying deadrise and/or beam (specifically the "geometric" coefficients), which the tested vessels do not have (since they are prismatic).

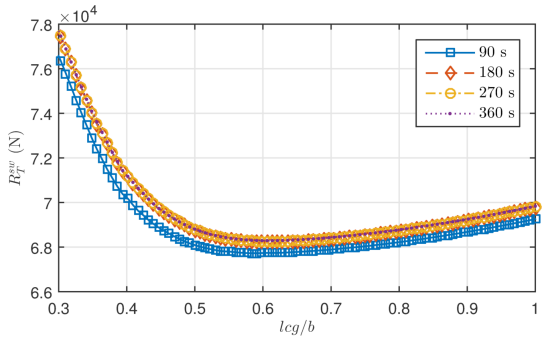

(a) Average seaway drag results

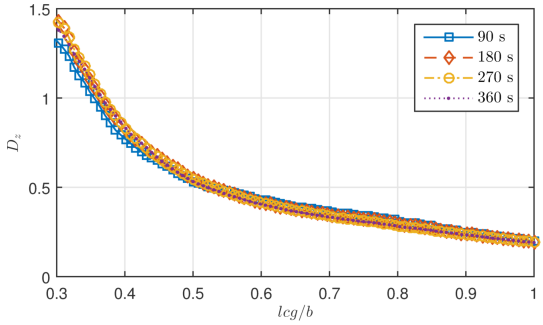

(b) Acceleration dose results

Figure 3.2: Objective functions with varying lcg and simulation time with SS 2, $b = 4.27$ m, $C_v = 4.5$, LOA$/b = 5.0$, $\log Q_{44} = 1$, and $\beta = 20°$.

POWERSEA can automatically adjust these coefficients depending on the operating conditions; but this procedure is itself active research and therefore fixed values were used as it was done in the original program of Zarnick (1979). This chapter's values are shown in Tab. 3.3. The only value that differs from the default POWERSEA and Zarnick (1979) values is the Buoyancy Lift Coefficient. Zarnick (1979) and the POWERSEA documentation have a default of 0.5 for this coefficient. However, this value is originally quoted from Charles L. Shuford (1958), where it indicates that 0.5 is a reasonable value for $\tau \geq 8°$ but larger values are needed for $\tau \approx 4°$. Since we are interested in the optimal drag and seakeeping operating trim angles, and those are known to be around 4° to 5° for drag (Savitsky, 1964) and even lower for seakeeping (Savitsky and Brown, 1976), a value of 0.85 is used following the results in Charles L. Shuford (1958).

Table 3.3: POWERSEA parameters

Fixed Variable	Value
Buoyancy Lift Coefficient	0.85
Buoyancy Moment Coefficient	0.5
Added Mass Correction	0.0
Cross Flow Drag Coefficient	1.333
Geometric Drag Coefficient	0.0
Geometric Lift Coefficient	0.0

3.2.2 Exhaustive Search Approach

In this investigation, we are interested in both the seakeeping performance and drag. Therefore, we have a multi-objective problem. The drag metric is simply the average seaway drag, $J_1 = R_T^S$. The seakeeping metric used is the vertical acceleration dose $D_z = [\sum_i A_{iz}^6]^{1/6}$ presented in ISO Standard 2631-5 (2004), divided by the period in seconds over which D_z was measured to the 1/6 power, $t_m^{1/6}$ (i.e., $J_2 = D_z/t_m^{1/6}$); where A_{iz} is the i^{th} peak of the spine's vertical acceleration response (given by a recurrent neural network model). Example calculations of D_z can be seen in Appendix B. This metric could be interpreted as the D_z normalized to a one second exposure; but it could be extended to include the long-term health effects following the procedure in ISO Standard 2631-5 (2004). A limitation of this metric is that it could over or under-predict the effects of impact accelerations events larger than 4 g's (ISO Standard 2631-5, 2004).

An important note is that while POWERSEA is capable of estimating the seaway accelerations (which are used for calculating D_z) and drag, its accuracy is limited (Akers, 1999). The strength in POWERSEA — or planing boat strip-theory methods in general — lies on capturing the general dynamics of the vessel operating in a seaway in a computationally efficient manner. As a result, POWERSEA allows us to conduct an exhaustive search with the available computational resources. Keep in mind however, that the results in this chapter are more valuable in the relative

Table 3.4: Exhaustive search parameter sweep

Variable	Min	Max	No. Values
lcg/b	0.15	3	21
β (deg)	2	40	21
$\log Q_{44}$	-1	7	21

comparisons and qualitative aspects rather than on the quantitative ones.

The design space consists of $\begin{bmatrix} lcb/b & \beta & \log(Q_{44}) \end{bmatrix}$, where lcg/b and β are physical design parameters and Q_{44} is the control design parameter. Q_{44} is the (4,4) element in the $\boldsymbol{Q}$ matrix (see Section 3.2.1.2), the use of $\log Q_{44}$ instead of Q_{44} is to facilitate the exploration of this metric's influence range — which was found to extend approximately between $-1 < \log Q_{44} < 7$ in preliminary tests. The design space was discretized following Tab. 3.4, and an exhaustive search was performed in POWERSEA. Combinations in which the vessel never reached stable equilibrium in calm water or encountered excessive trim angles during the 180 sec of simulation (e.g., bow-dived or lost stability) were simply classified as "failed" runs and the partial data was unused. The framework used to perform the exhaustive search is further explained in Section 3.2.2.1.

3.2.2.1 Process Framework

The exhaustive search was automated by using POWERSEA's and MATLAB's COM Interop with Visual Basic .NET (VB.NET). The process framework schematic for when the vessel is designed with an ACS and when it is designed without an ACS can be seen in Fig. 3.3 and Fig. 3.4 respectively.

When the vessel is designed with an ACS, the "Exhaustive Search Control" module controls the test design variables, which are passed to the "Vessel Geometry" and "LQR Design" modules. The "Vessel Geometry" module creates the vessel in POWERSEA. Afterwards, the "Stabilizing Velocity-Feedback ACS" module is run, which

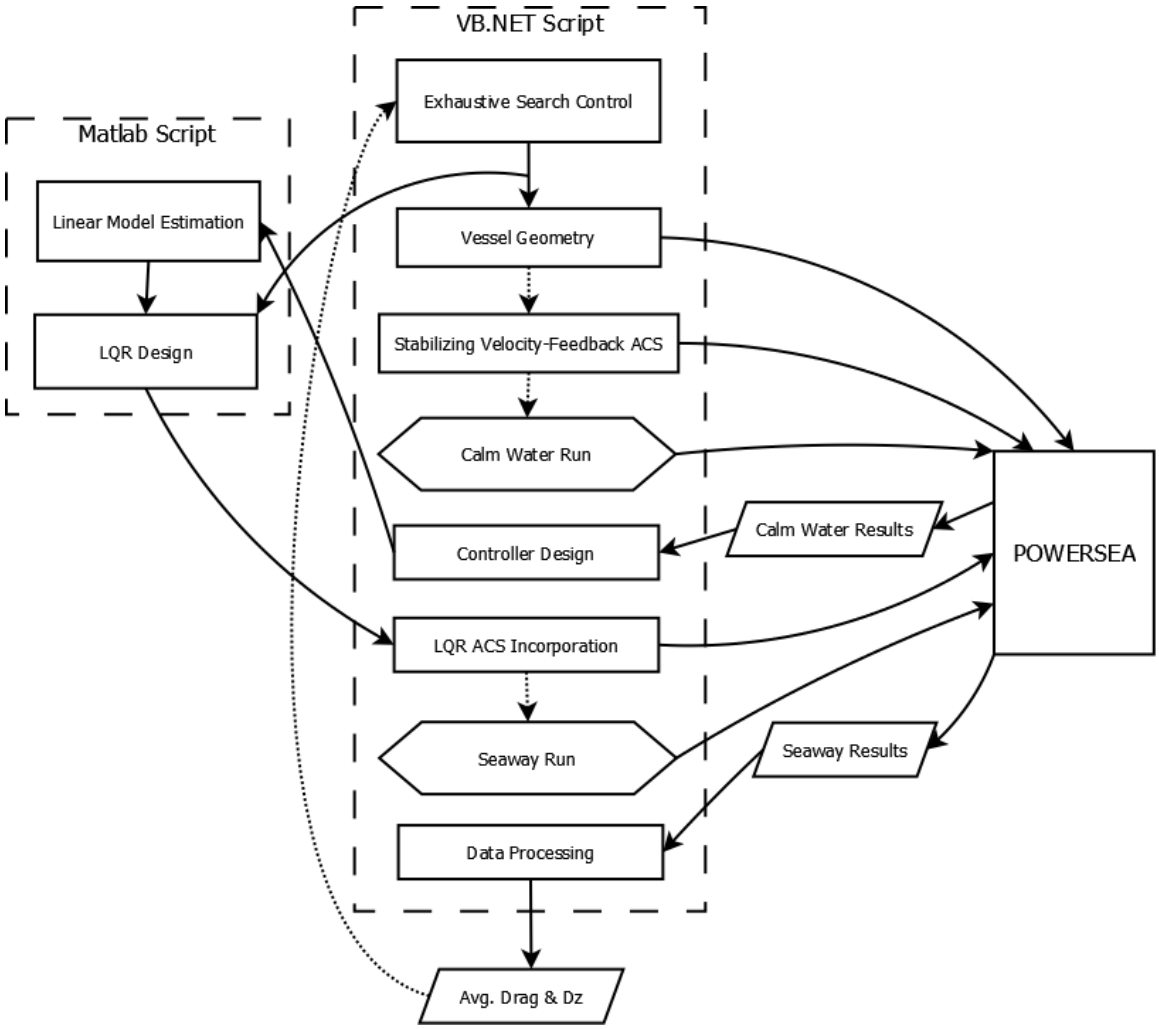

Figure 3.3: Process schematic for vessel designed with ACS, where solid arrow lines represent both data transfer and progression, dashed arrow lines represent only progression.

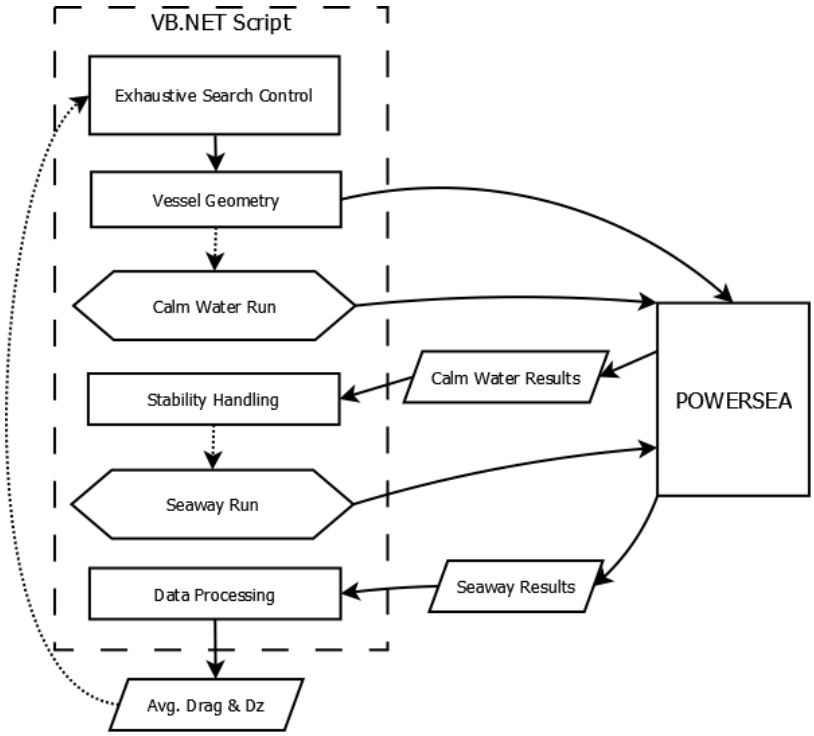

Figure 3.4: Process schematic for vessel designed without ACS.

creates in POWERSEA an ACS with a heave and pitch velocity feedback high-gain controller. The forces dictated by the 'Velocity-Feedback ACS', as shown in Eq. (3.3), have no drag penalties and the forces create pure moment on the vessel.

$$F_1 = \begin{bmatrix} -5 \cdot 10^4 & 7 \cdot 10^6 \end{bmatrix} \begin{bmatrix} \dot{\eta}_3 \\ \dot{\eta}_5 \end{bmatrix} \tag{3.3}$$

$$F_2 = -F_1$$

Since the 'Velocity-Feedback ACS' has only feedback on the state velocities, the vessel should reach its unforced equilibrium even when the vessel is open-loop unstable. Stability by this controller is not guaranteed and it was tuned so that an open-loop unstable vessel reached its steady state (closed-loop) at roughly 20 sec.[1]

[1]This procedure could be made more sophisticated by tuning the controller for each test case with the linear model using the equilibrium found with Savitsky (1964). However, the controller obtained

Next, the vessel is run in calm water until it reaches equilibrium (if it does not reach equilibrium, the run is classified as a "fail" and the process ends), and the steady calm-water running attitude is set as the initial conditions for the seaway simulation and also passed to the "Controller Design" module. The "Controller Design" module calls the MATLAB script "Linear Model Estimation" — whose equations are shown in Appendix A — where a state space model is created and passed to the "LQR Design" MATLAB script. The "LQR Design" module takes the state space model and the LQR parameters as described in Section 3.2.1.2, and uses MATLAB's `lqr` function to calculate the controller's gains. The controller gains are then passed to the "ACS Incorporation" module, where it then replaces the 'Stabilizing Velocity-Feedback' ACS with the ACS described in Section 3.2.1.2. Afterwards, the "Seaway Run" module is run, which passes the seaway parameters mentioned in Section 3.2.1.3, and simulates the vessel in POWERSEA. The results from the seaway simulation are then processed to obtain the performance metrics (average seaway drag and $D_z/t_m^{1/6}$). The whole process is then repeated for the next point in the design and control space.

When the vessel is designed with no ACS, the process will not have any of the ACS related steps as illustrated in Fig. 3.4. Since the vessel without ACS needs to be open-loop stable, the results from the calm water tests are used to check for stability. If the vessel is not stable, the test case is skipped; if it is stable, the process continues with the modules having the same function as previously described.

3.2.2.2 Pareto Fronts

The optimization problem formulations for the vessels following co-design and sequential design approaches are given in Tab. 3.5 and Tab. 3.6 respectively. The objective functions are defined as $J_1 = R_T^S$ (average seaway drag) and $J_2 = D_z/t_m^{1/6}$ (seakeeping metric) in both, while $\boldsymbol{x} = \begin{bmatrix} lcg/b & \beta & log(Q_{44}) \end{bmatrix}$ is the optimizing vari-

by tuning with a badly porpoising vessel ($\beta = 2°$, and $lcg/b = 0.10$) turns out to be sufficiently robust to avoid the added complexity — and subsequently required exception handling.

Table 3.5: Co-Design approach optimization

OLU		OLS	
$\min_{\boldsymbol{x}}$	$(J_1(\boldsymbol{x}), J_2(\boldsymbol{x})$|w/ ACS)	$\min_{\boldsymbol{x}}$	$(J_1(\boldsymbol{x}), J_2(\boldsymbol{x})$|w/ ACS)
s.t.	$0° < \tau^c < 15°$	s.t.	$0° < \tau^C < 15°$
	$\Delta\tau^C \geq 0.5°$|w/o ACS		$\Delta\tau^C < 0.5°$|w/o ACS
	$\Delta\tau^C < 0.5°$|w/ ACS		

Table 3.6: Sequential (or "Traditional") approach optimization

Step 1 (w/o ACS)		Step 2 (w/ ACS)	
$\min_{\hat{\boldsymbol{x}}}$	$(J_1(\hat{\boldsymbol{x}}), J_2(\hat{\boldsymbol{x}})$|w/o ACS)	$\min_{\check{x}}$	$(J_1(\hat{\boldsymbol{x}}, \check{x}), J_2(\hat{\boldsymbol{x}}, \check{x})$|w/ ACS)
s.t.	$0° < \tau^C < 15°$	s.t.	$0° < \tau^C < 15°$
	$\Delta\tau^C < 0.5°$|w/o ACS		$\Delta\tau^C < 0.5°$|w/o ACS
			$\Delta\tau^C < 0.5°$|w/ ACS

ables for the co-design problem, and $\hat{\boldsymbol{x}} = \begin{bmatrix} lcg/b & \beta \end{bmatrix}$ and $\check{x} = log(Q_{44})$ are the optimizing variables for the sequential design in Step 1 and 2 respectively. $\Delta\tau^C$ is the peak-to-peak amplitude of the calm-water trim angle (i.e., unacceptable porpoising is considered to be $\Delta\tau^C \geq 0.5°$).

In a multi-objective optimization, usually there is no unique optimum that optimizes both objectives. Instead, a family of optimal solutions that represents the trade-off among competing objectives can be obtained. This family of optimal solutions is called the Pareto set or Pareto frontier. We call a design Pareto optimal (part of the Pareto set) if its performance in one objective cannot be improved without degrading the performance on another objective.

The general approach to estimating the Pareto front from a series of runs is to find the non-dominated (ND) designs. For any x, if one cannot find any other point x' that dominates x, then x is called ND. It is usually easier to check for dominance. A simple approach for finding the Pareto front is to first find all the designs that are dominated, and then check for the designs there were not dominated (ND designs).

3.3 Results and Discussion

The naming convention used throughout this section is as follows. The Pareto fronts are:

- "Co-Design OLU": Pareto optimal vessels that are open-loop unstable and have ACS
- "Co-Design OLS": Pareto optimal vessels that are open-loop stable and have ACS
- "Sequential-1 (w/o ACS)": Pareto optimal vessels that are open-loop stable but without ACS

In addition, the performances of the Pareto fronts are named:

- "Co-Design OLS, w/o ACS": Pareto optimal designs of "Co-Design OLS" when ACS is removed
- "Sequential-2 (w/ ACS)": Pareto optimal designs of "Sequential-1 (w/o ACS)" with optimized ACS.

3.3.1 Pareto Optimality

In both tested sea states, SS 2 and SS 3, the Pareto optimal vessels co-designed with ACS and allowed to be open-loop unstable ("Co-Design OLU") dominate all other Pareto optimal designs, see Fig. 3.5. (i.e., there is a design in "Co-Design OLU" which outperforms both in seakeeping and drag any other possible design in the other classes.)

If the "Sequential-1 (w/o ACS)" vessels are then modified to have an ACS (which is optimized to perform well in seakeeping), we can see that the designs ("Sequential-2 (w/ACS)") are in general not the Pareto optimal designs obtained by co-designing both an open-loop stable vessel and its ACS ("Co-Design OLS"), see Fig. 3.6.

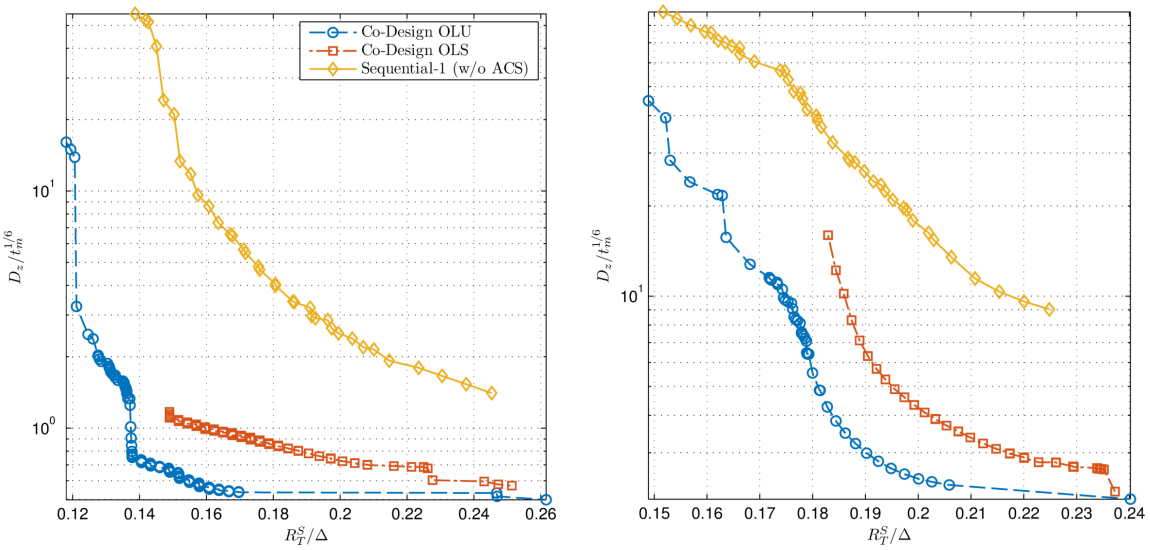

(a) SS 2 (b) SS 3

Figure 3.5: Pareto fronts assuming convexity from exhaustive search.

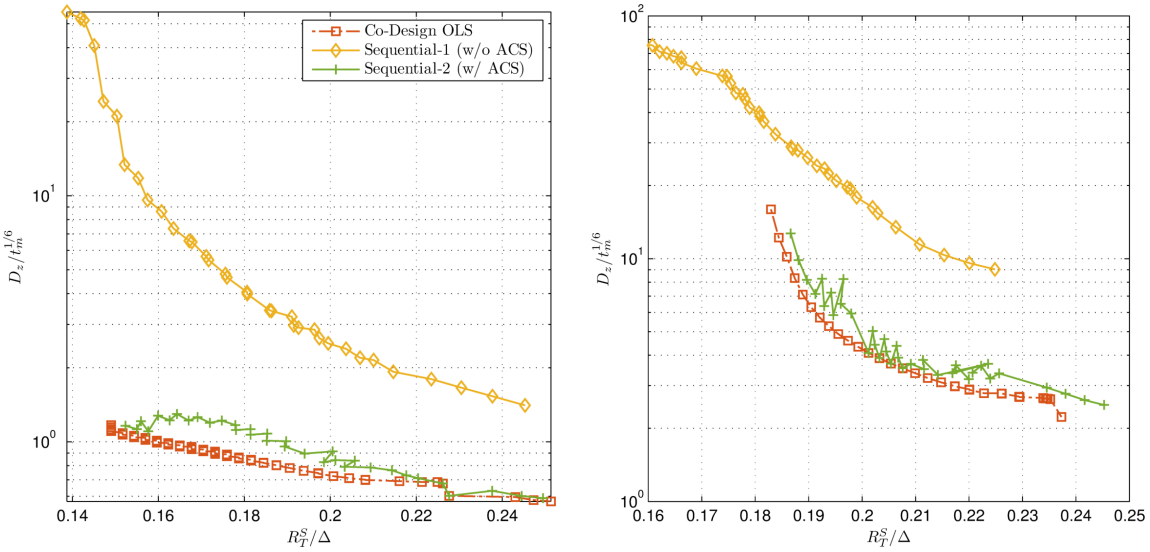

(a) SS 2 (b) SS 3

Figure 3.6: Effect of sequentially designing the vessel and the ACS ("Sequential-2 (w/ ACS)"), compared to the Pareto fronts with open-loop stable vessels.

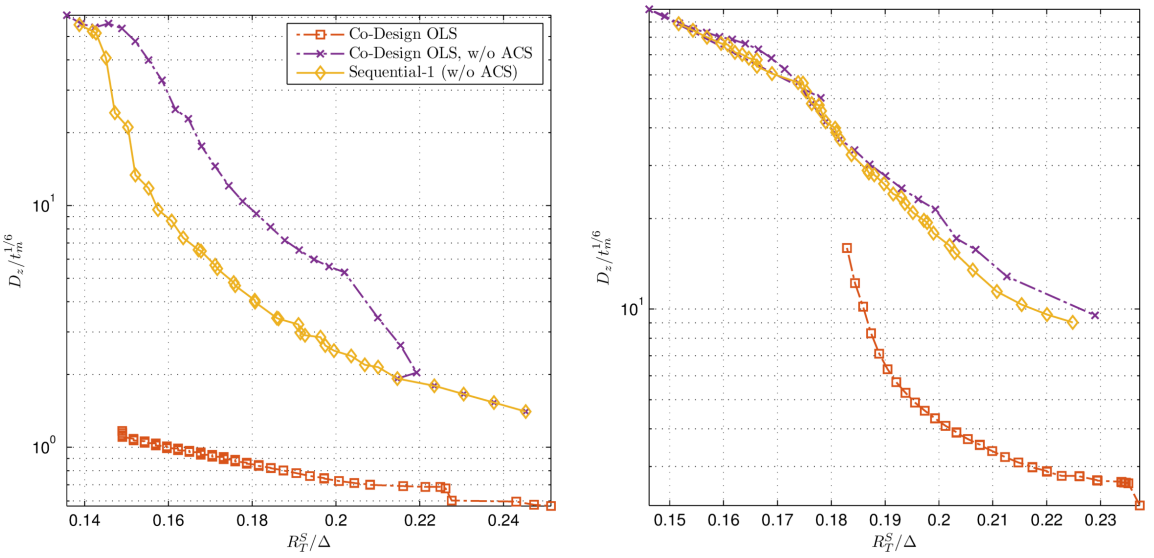

(a) SS 2 (b) SS 3

Figure 3.7: Open-loop performance of the "Co-Design OLS" vessels with respect to the Pareto fronts with open-loop stable vessels.

Moreover, a designer following the sequential design would quickly discard the vessels that have the greatest synergy with their ACS; since as the performance of "Co-Design OLS, w/o ACS" shows in Fig. 3.7, these vessels have in general a considerably inferior performance when compared to the "Sequential-1 (w/o ACS)" vessels.

3.3.1.1 Performance Evaluation

We can see from Fig. 3.5 and Fig. 3.6 that considerable improvement can be made if one follows the co-design methodology instead of the sequential — and this improvement is at its greatest when the stability constraint is relaxed and the vessels are allowed to be open loop unstable.

Some example changes in performance from the Pareto optimal "Sequential-2 (w/ ACS)" vessels to the vessels in "Co-Design OLU" and "Co-Design OLS" are shown in Tab. 3.7 and Tab. 3.8. These results were found by linear interpolation within the Pareto fronts.

Table 3.7: Percent decrease in seaway drag for fixed seakeeping metric from "Sequential-2 (w/ ACS)" to "Co-Design" Pareto fronts.

SS	$D_z/t_m^{1/6}$	OLS	OLU
2	1	22%	28%
2	0.6	5%	37%
3	10	2%	7%
3	3	6%	17%

Table 3.8: Percent decrease in seakeeping metric for fixed seaway drag from "Sequential-2 (w/ ACS)" to "Co-Design" Pareto fronts.

SS	R_T^S/Δ	OLS	OLU
2	0.24	4%	14%
2	0.15	12%	42%
3	0.23	15%	31%
3	0.185	25%	70%

In short, for the tested speed coefficient and sea state conditions, the co-designed vessels outperformed the sequentially designed vessels in both seakeeping and drag by considerable margins for essentially all combinations of seaway drag or seakeeping constraints.

3.3.2 Optimal Design Parameters

The geometry design variables of the SS 2 Pareto fronts' designs are plotted in Fig. 3.8a, and for SS 3 in Fig. 3.8b. The results show that, in general, when there is an OLS constraint the Pareto-optimal designs are as close to being OLU as possible. However, the designs obtained by the sequential optimization, tells a different story; in SS 2, the designs try to keep the lowest running trim angle as possible (as expected from traditional vessel design), while in SS 3 the "optimal" sequential vessels appear to be those that are right in the middle of the OLS lcg/b range – which is likely due to the fact that the vessel has a finite length, therefore making very low trim angles

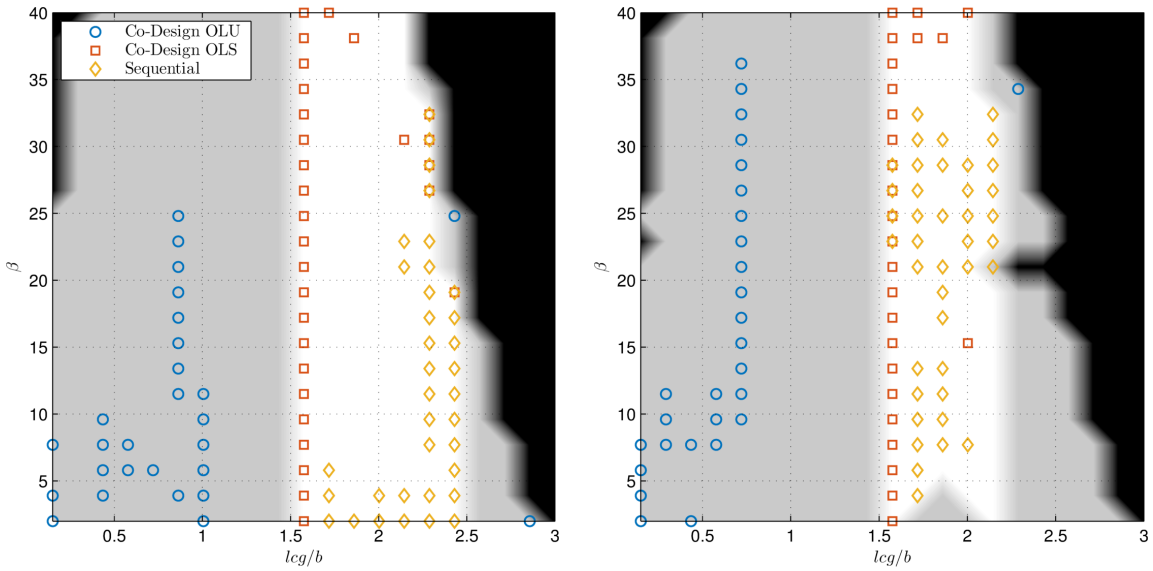

(a) SS 2. (b) SS 3.

Figure 3.8: Design variables lcg/b and β of Pareto optimal designs. The white area represents the OLS region, the gray areas represent the OLU regions, and the black area represent regions where the vessel failed to complete the 180 sec simulation run (the vessel bow-dived or had excessive trim).

in a bad seaway dangerous for bow-diving.

3.3.3 Effect of Average Seaway Trim

Fig. 3.9a and Fig. 3.9b show how R_T^S and D_z change with respect to the average seaway trim angle (which is changed by lcg/b) — the deadrise is fixed, and the controller variable that minimizes the seakeeping metric is selected for each point. The R_T^S results show that the seaway transport efficiency is improved as the vessel is allowed to be open loop unstable, which supports the preliminary results presented in Chapter II. A surprising result is that the seakeeping does not necessarily worsen monotonically with increasing trim angle, as the example in Fig. 3.9b shows; this goes against what it is commonly known from past research of vessels without ACS (Savitsky and Brown, 1976), and the fundamental reasons of why this behavior occurs when an ACS is present are unknown. However, since the co-designed vessel can go towards higher trim angles to improve both the seakeeping and transport efficiency, it

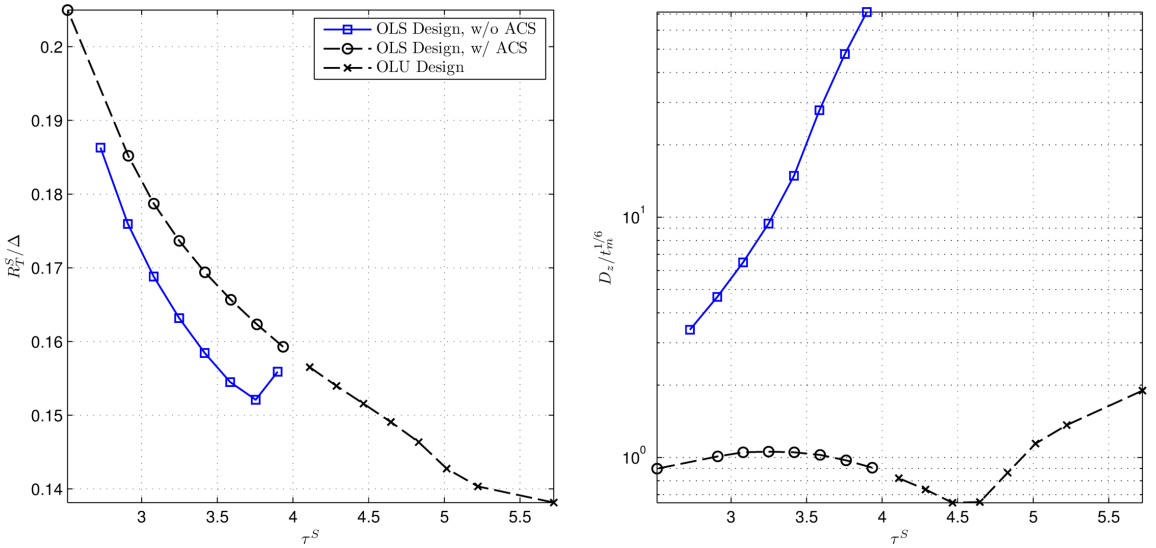

(a) Seaway drag, with $\log(Q_{44})$ optimized for drag metric

(b) Seakeeping metric, with $\log(Q_{44})$ optimized for seakeeping metric

Figure 3.9: Objective values as a function of average seaway trim angle with $\beta = 11.5°$ and SS 2.

is comprehensible how the co-designed vessels outperform the traditionally designed vessels in these two metrics.

3.3.4 General Design Observations

When designing a planing craft which will have an ACS, the designer should keep in mind the following observations:

- The overall optimal vessels are not obtained by following a sequential design.
- For the vessels investigated, the Co-Design OLS vessels are on the edge of being OLU, indicating that the OLS constraint is active.
- Having an ACS might create optimal seakeeping trim angles — which goes against the common rule-of-thumb that a planing craft's seakeeping will improve monotonically as the trim angle is reduced, an observation generally obtained for vessels without ACS.

3.4 Conclusion

Design optimization of a planing hull in both geometry space and control space is explored in this chapter through a case study. The results show a clear advantage of co-designing a planing craft with ACS over the traditional approach of sequentially designing one then followed by another; co-designed vessels show superior seakeeping and efficiency over the sequentially designed vessels.

Moreover, the co-designed Pareto optimal vessels are not the sequentially designed Pareto optimal vessels, even when the co-designed vessels are restricted to be OLS. In addition, the vessels obtained by sequential design have limited synergy with their ACS when compared to the co-designed vessels.

This investigation supports the hypothesis that because the ACS affects the relationship between seakeeping and the vessel's geometry, the conventional empirically based seakeeping guidelines are not appropriate for vessels with ACS.

In short, if a planing boat is expected to have an ACS, it is best if it is co-designed with the vessel's geometry in order to exploit the synergy between them.

CHAPTER IV

Search Techniques for Optimal Vessels

4.1 Overview

The results in Chapter III conclusively showed that the benefit from co-designing a vessel and its ACS can be significant. However, only two vessel geometry variables (lcg and β) and one ACS variable were explored — when in reality a designer has much more design freedom/responsibility. Moreover, the benefits of co-designing might vary depending on unexplored design variables. Hence an obvious progression is to expand the design space; but doing so with an exhaustive search will be exponentially expensive. Therefore, the work in this chapter has two purposes: (i) present tools a designer can use to co-design a planing craft with its ACS, and (ii) use these tools to expand the design space and further explore the potential of co-design.

The co-design tools available to a designer are highlighted in Section 4.1.1. Frequently, a designer does not have access to large computational resources for developing the initial concept design. Because of this, a Pareto estimating method, the Adaptive Weighted Sum (AWS), was modified to (i) reduce the number of optimizations required to estimate roughly evenly spaced Pareto points, and (ii) allow the use of constrained single-objective optimization methods which require valid initial guesses. The method is referred to as the Modified-AWS (MAWS), and it is presented in Section 4.2.

MAWS's performance is compared with Chapter III's results in Section 4.3, and it proved to accurately estimate the Pareto front. Next, MAWS is applied to a 5-variable optimization — three geometry variables (lcg, β, b) and two ACS variables (heave velocity and pitch velocity gains) — in Section 4.4. The 5-variable optimization showed that the benefits from co-design are less as the vessel's L/b is allowed to increase; but for realistic monohull L/b's ($L/b < 5.5$), co-designing continues to yield superior results. Moreover, the 5-variable results suggest that catamarans are the Pareto optimal vessels for high-speed operation in rough seas.

4.1.1 Background

Optimizations in applied sciences rarely, if ever, have a true single objective. However, the rich knowledge on algorithms for single-objective optimization frequently compels a designer to reformulate their multi-objective optimization (MOO) into a single-objective one — and explore the multi-objective problem in this fashion.

In MOO, a designer must choose a design which is evaluated on multiple criteria. These problems are usually formulated as in Eq. (4.1).

$$\begin{aligned} \min_{\boldsymbol{x}} \quad & \boldsymbol{J}(\boldsymbol{x}) \\ \text{s.t.} \quad & \boldsymbol{h}(\boldsymbol{x}) = 0 \\ & \boldsymbol{g}(\boldsymbol{x}) \leq 0 \\ \text{where} \quad & \boldsymbol{J} = [J_1(\boldsymbol{x}), J_2(\boldsymbol{x}), \cdots, J_k(\boldsymbol{x})]^T \\ & \boldsymbol{h} = [h_1(\boldsymbol{x}), h_2(\boldsymbol{x}), \cdots, h_l(\boldsymbol{x})]^T \\ & \boldsymbol{g} = [g_1(\boldsymbol{x}), g_2(\boldsymbol{x}), \cdots, g_j(\boldsymbol{x})]^T \\ & \boldsymbol{x} \in \mathbb{R}^n \end{aligned} \tag{4.1}$$

In this research we are concerned with a bi-objective optimization, namely $k = 2$.

There are different ways to classify the MOO approaches to optimizing Eq. (4.1),

and one of the most general ways is to class them by the way the designer, or human "decision maker" (DM), arrives at a design. In Hwang and Masud (1979), four different DM preference approaches are defined: (i) no articulation, (ii) 'a priori' articulation, (iii) progressive articulation (interactive), and (iv) 'a posteriori' articulation. In (i) no articulation of preference, the optimization itself makes assumptions on what is a desirable design (with no input from the DM). While in (ii) 'a priori' articulation of preference, the DM defines what are the "ideal" values and/or rank for the objectives and the optimization tries to get the "best" design. In (iii) progressive articulation of preference, the DM actively decides what are desirable results based on information that is made available while the MOO is underway. Then in (iv) 'a posteriori' articulation, the optimization's goal is to find the Pareto front of the problem, so that the DM can then make a decision. For further discussion of these methods, the reader is referred to Hwang and Masud (1979); Miettinen (1998).

This research is interested in comparing the seakeeping and drag performance of vessels that are co-designed with ACS and sequentially designed with ACS. The most general way to do this is to compare the Pareto fronts. Therefore, this research uses the 'a posteriori' method.

Similarly, there are different ways to class these 'a posteriori' methods. But the two general techniques for finding the Pareto front of a multi-objective problem are: scalarization and metaheuristic multi-objective procedures (for a more in-depth categorization, see Deb (2001)).

Metaheuristic multi-objective procedures search the design space in a blanket fashion, and they use the test points' objective values to decide, based on heuristics, the next search. Some of the most popular methods are based on evolutionary algorithms, such as the Non-dominated Sorting Genetic Algorithm-II (NSGA-II) (Deb et al., 2002) and Strength Pareto Evolutionary Algorithm-II (SPEA-2) (Zitzler et al., 2001); although other metaheuristics methods such as simulated annealing (Czyzzak

and Jaszkiewicz, 1998) are used. The field of metaheuristic optimization is constantly evolving, and a survey of the techniques used for multi-objective optimization can be found in Zhou et al. (2011). In general, metaheuristic approaches are computationally expensive but they capitalize from straightforward parallelization. However, because of technical difficulties with parallelizing the software used in this study, these methods where not explored — and scalarization was used instead.

In scalarization, the multi-objective problem is converted into a single-objective problem, and the Pareto front is reconstructed from multiple single-objective optimizations. Note that one can use any single-objective optimization method with scalarization (including metaheuristic single-objective methods). In general, the multi-objective to single-objective transformation is done by combining the objective functions into a scalar function, and/or by placing some objective functions as constraints. The traditional methods for these two techniques are the weighted-sum (WS) method (Zadeh, 1963) and the ϵ-constraint method (Marglin, 1967), respectively. The main drawback of the standard WS method is that it does not find equally spaced solutions in the Pareto, and it cannot find solutions in concave Pareto regions (as illustrated in Fig. 4.1a). One could argue that the techniques used to choose the weights in the scalar function and the desired constraints are heuristic in nature, therefore there are multiple modifications to these methods as well. Some popular methods are the Adaptive Weighted-Sum (AWS) (Kim and de Weck, 2005) and the Normal Boundary Intersection (NBI) (Das and Dennis, 1998). A survey of the methods used can be found in Marler and Arora (2004).

4.2 Modified Adaptive Weighted-Sum Method (MAWS)

The AWS method (Kim and de Weck, 2005) was originally selected for this investigation because of its simplicity and effectiveness; the general concept of the AWS can be seen in Fig. 4.1. However, implementation of this method quickly revealed two

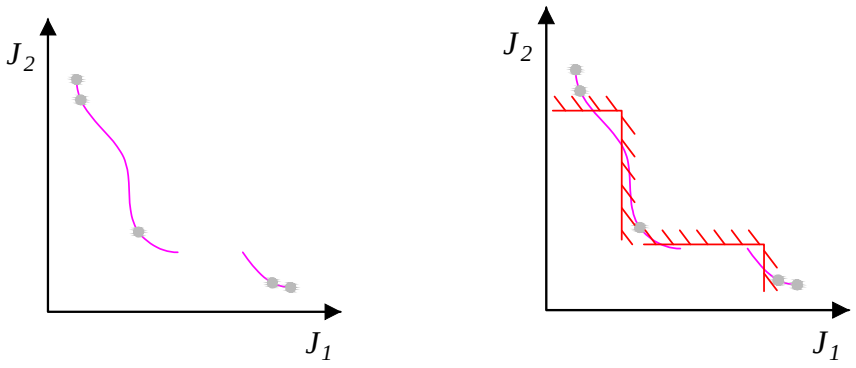

(a) Perform optimizations with parameterized weights (figure of final WS result and initial AWS)

(b) Impose AWS constraints, and repeat Fig. 4.1a in each segment

Figure 4.1: Concept of the AWS method.

drawbacks which were serious for this research's case; (i) nearly overlapping Pareto points are possible, in which case the computational effort in the optimization is wasted; and (ii) there is no systematic way to find valid initial guesses for the single-objective optimization without resorting to a random initialization. One can foresee these two drawbacks in Fig. 4.1.

These drawbacks motivated modifications to the AWS, resulting in what is coined as the Modified Adaptive Weighed Sum (MAWS). The modifications for preventing this work's problems with AWS are as follows.

The first drawback, risk of overlapping Pareto points, is prevented in the Modified Adaptive Weighted Sum (MAWS) by performing only one optimization per MAWS iteration. This increases the computational cost of the MAWS method itself when compared to AWS. Nonetheless, the computer wall-times for evaluating the objective functions in this research are in the order of minutes — making objective function evaluations the main computational cost.

The second drawback, no methodology to find valid initial guesses, is resolved by modifying the constraints set in AWS so that they are parallel to each other. Assuming that the objective functions are continuous, this allows finding an initial

valid point by performing a line search with the Pareto points. Note however that this solution only holds valid if the objective functions are continuous. While it is not possible to prove that the objective functions are continuous everywhere in this research's case, the exhaustive results from Chapter III suggest that the behavior of the objective functions is generally continuous. On the other hand, there are discontinuities in the search space caused by vessel designs which are unstable; these are heuristically handled by taking random step sizes in the line search any time a discontinuity is found.

In contrast with AWS which does not find solutions in non-Pareto optimal regions, the parallel constraints in MAWS means that non-Pareto optimal points are in the feasible space of the single-objective optimizations. As a result, a Pareto filter is required in MAWS, which further increases the complexity of MAWS. Nonetheless, in cases where local-optimum solutions are possible for the single-objective optimizations (as it is in this research), a Pareto filter is required to remove local-optimum solutions which are dominated by other better solutions. In other words, a Pareto filter would have been required for AWS as well if it would have been used in this work.

4.2.1 MAWS Procedures

This section describes the detailed procedure for implementing the modified adaptive weighted-sum method for the bi-objective case.

Step 1: Find the overall nadir and utopia points by performing two optimizations, namely

$$\begin{aligned} \min_{\boldsymbol{x}} \quad & J_i(\boldsymbol{x}) \\ \text{s.t.} \quad & \boldsymbol{h}(\boldsymbol{x}) = 0 \\ & \boldsymbol{g}(\boldsymbol{x}) \leq 0, \end{aligned}$$

for $i = 1, 2$. Defining $\boldsymbol{x_1^*} = \arg\min(J_1)$ and $\boldsymbol{x_2^*} = \arg\min(J_2)$, we have $\boldsymbol{J}(\boldsymbol{x_1^*}) = (J_1^u, J_2^n)$ and $\boldsymbol{J}(\boldsymbol{x_2^*}) = (J_1^n, J_2^u)$, where the n and u subscripts denote the overall

nadir and utopia values (see Fig. 4.2a).

Step 2: Compute the lengths of the segments in the Pareto front, and select a segment whose length is larger than a user-defined value. The top-left value of the segment is defined as $\boldsymbol{J}\left(\boldsymbol{x}_{\boldsymbol{u}}^{*}\right)$ and the bottom-right value as $\boldsymbol{J}\left(\boldsymbol{x}_{\boldsymbol{l}}^{*}\right)$. The length could be either normalized by user-defined max/min values or by dynamically normalizing to $\boldsymbol{J}\left(\boldsymbol{x}_{\mathbf{1}}^{*}\right)$ and $\boldsymbol{J}\left(\boldsymbol{x}_{\mathbf{2}}^{*}\right)$. If the algorithm is in its first iteration, the only segment is the line connecting $\boldsymbol{J}\left(\boldsymbol{x}_{\boldsymbol{u}}^{*}\right) = \boldsymbol{J}\left(\boldsymbol{x}_{\mathbf{1}}^{*}\right)$ and $\boldsymbol{J}\left(\boldsymbol{x}_{\boldsymbol{l}}^{*}\right) = \boldsymbol{J}\left(\boldsymbol{x}_{\mathbf{2}}^{*}\right)$.

Step 3: Normalize the objective functions to the segment's nadir and utopia values (denoted by subscripts n' and u', respectively),

$$\bar{J}_i = \frac{J_i - J_i^{u'}}{J_i^{n'} - J_i^{u'}},\ i = 1, 2.$$

Note that in the first MAWS iteration, $J_i^{n'} = J_i^n$ and $J_i^{u'} = J_i^u$ for $i = 1, 2$.

Step 4: Set constraints that are perpendicular to the selected segment when the Pareto is normalized with the overall utopia and nadir values, (J_1^u, J_2^u) and (J_1^n, J_2^n) respectively (see Fig. 4.2b). Eq. (4.2–4.4) are the constraint's slope (a), upper (b_u) and lower (b_l) intercept in unnormalized space.

$$a = \left(\frac{J_1^{u'} - J_1^{n'}}{J_2^{u'} - J_2^{n'}}\right)\left(\frac{J_2^n - J_2^u}{J_1^n - J_1^u}\right)^2 \tag{4.2}$$

$$b_u = J_2^{n'}(1-\beta) + J_2^{u'}\beta - a\left(J_1^{u'}(1-\beta) + J_1^{n'}\beta\right) \tag{4.3}$$

$$b_l = J_2^{n'}\beta + J_2^{u'}(1-\beta) - a\left(J_1^{u'}\beta + J_1^{n'}(1-\beta)\right) \tag{4.4}$$

For convenience, the constraint's slope and intercepts normalized to the segment's min/max values, $\left(J_1^{u'}, J_2^{u'}\right)$ and $\left(J_1^{n'}, J_2^{n'}\right)$ respectively, can be seen in

Eq. (4.5–4.7). See Fig. 4.2f for an illustration of the nomenclature used.

$$\bar{a} = a\frac{J_1^{n'} - J_1^{u'}}{J_2^{n'} - J_2^{u'}} \tag{4.5}$$

$$\bar{b}_u = \frac{aJ_1^{u'} - J_2^{u'} + b_u}{J_2^{n'} - J_2^{u'}} \tag{4.6}$$

$$\bar{b}_l = \frac{aJ_1^{u'} - J_2^{u'} + b_l}{J_2^{n'} - J_2^{u'}} \tag{4.7}$$

The constraints in the following optimization problem are then defined as in Eq. (4.8–4.9).

$$g_u(\bar{J}_1, \bar{J}_2) = \bar{J}_2 - \bar{a}\bar{J}_1 - \bar{b}_u \tag{4.8}$$

$$g_l(\bar{J}_1, \bar{J}_2) = \bar{a}\bar{J}_1 - \bar{J}_2 + \bar{b}_l \tag{4.9}$$

Step 5: If a valid initial guess is desired in the optimization, perform a line search (using the bisection method for example) with $\boldsymbol{x_0}(\lambda) = \boldsymbol{x_u^*}\lambda + \boldsymbol{x_l^*}(1-\lambda)$ (see Fig. 4.2c). Assuming that $\bar{J}_1(\boldsymbol{x})$ and $\bar{J}_2(\boldsymbol{x})$ are continuous functions, one can easily show that the linear combination of them is also continuous; therefore it directly follows that there are λ's which satisfy $g_u(\bar{J}_1(\boldsymbol{x_0}(\lambda)), \bar{J}_2(\boldsymbol{x_0}(\lambda))) \leq 0$ and $g_l(\bar{J}_1(\boldsymbol{x_0}(\lambda)), \bar{J}_2(\boldsymbol{x_0}(\lambda))) \leq 0$.

Step 6: Perform the optimization

$$\begin{aligned} \min_{\boldsymbol{x}} \quad & \bar{J}_1(\boldsymbol{x})\alpha + \bar{J}_2(\boldsymbol{x})(1-\alpha) \\ \text{s.t.} \quad & \boldsymbol{h}(\boldsymbol{x}) = 0 \\ & \boldsymbol{g}(\boldsymbol{x}) \leq 0, \end{aligned}$$

where $\alpha = 0.5$, and $\boldsymbol{g}$ includes Eq. (4.8–4.9).

Step 7: Check the result from step 6 for Pareto optimality. Some special cases that

might occur are the following.

- If the value is not Pareto optimal, attempt to find a Pareto point on the constraints Eq. (4.8–4.9) by setting $\alpha = 1$ and 0 in step 6, respectively, and optimizing. If neither optimizations result in a valid Pareto point, this segment is no longer refined.
- If the value dominates either of the current utopia/nadiar points, (J_1^u, J_2^n) or (J_1^n, J_2^u), then perform an optimization with either $\alpha = 1$ or $\alpha = 0$ accordingly, with *no* constraints and with the result of step 6 as an initial guess.

Step 8: Iterate from step 2, until all segments (not including those with failed optimizations from step 7) reach an user-defined size.

4.2.2 Implementation to the Design Framework

The design framework presented in Section 3.2.2.1 was further developed to incorporate the developed MAWS with the open-source optimization package PyOpt (Perez et al., 2012) as the optimizing engine. Since PyOpt is a Python programming language package, the MAWS method was written in Python. The extended general framework is illustrated in Fig. 4.3.

Using an optimization package allowed the testing of both gradient-based and gradient-free optimization methods. After preliminary tests, the simplex-based optimization algorithm named COBYLA (Powell, 1994) was selected for this research, since it proved to be more robust than the gradient-based optimizations in avoiding local-minimums.

In the following sections, MAWS is first tested with the 3-variable optimization presented in Chapter III, and then it is applied to a 5-variable optimization case by relaxing the vessel's b and ACS's Q_{33} (heave velocity) gain.

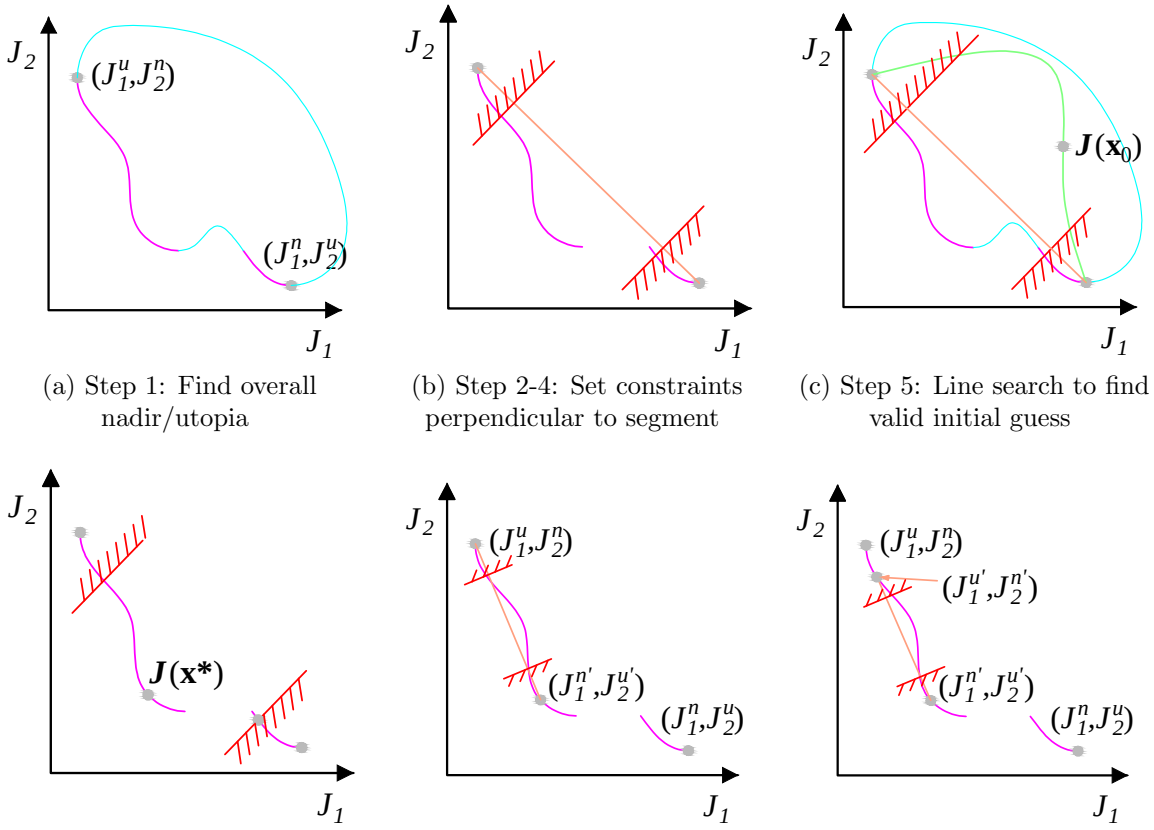

(a) Step 1: Find overall nadir/utopia

(b) Step 2-4: Set constraints perpendicular to segment

(c) Step 5: Line search to find valid initial guess

(d) Step 6-7: Perform optimization, and check for Pareto optimality

(e) Step 8: Find segment for refinement, and repeat from Fig. 4.2b

(f) Next iteration, showing all nomenclature

Figure 4.2: Modified adaptive weighted-sum method step illustrations.

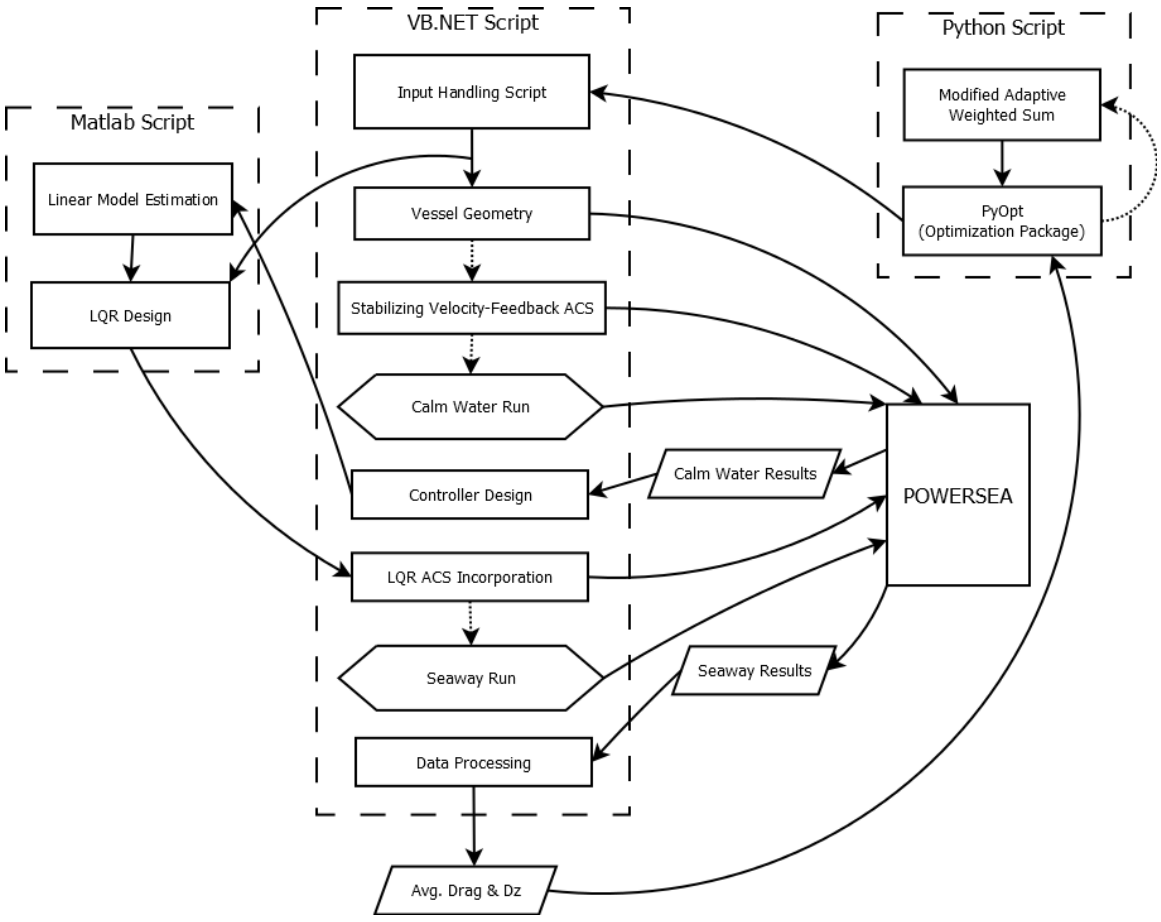

Figure 4.3: Process schematic for incorporating MAWS into the design framework.

4.3 MAWS Validation: 3-Variable Vessel Optimization

The optimizations from Section 3.2.2.2 are performed with the MAWS in order to compare with the results from Chapter III and validate the use of MAWS. The only change made to the optimization problem is the seakeeping metric, where it is modified in order to take into account both vertical and horizontal accelerations, and for its value to serve as a basis for operator safety recommendations as presented in ISO Standard 2631-5 (2004).

4.3.1 Problem Formulation

4.3.1.1 Optimization

The MAWS Step 6 optimization problem formulations for the co-design and sequential design approaches are given in Tab. 4.1 and Tab. 4.2 respectively. The objective function is defined as $J_1 = R_T^S$ (average seaway drag) and $J_2 = S_{ed}$ (seakeeping metric, Section 4.3.1.2) in both, while

$$\boldsymbol{x} = \begin{bmatrix} lcg/b & \beta & \log(Q_{44}) \end{bmatrix}$$

is the optimizing variables for the co-design problem,

$$\hat{\boldsymbol{x}} = \begin{bmatrix} lcg/b & \beta \end{bmatrix}, \check{\boldsymbol{x}} = \begin{bmatrix} \log(Q_{44}) \end{bmatrix}$$

are the optimizing variables for the sequential design in Sequential-1 and Sequential-2 respectively, and

$$\hat{\boldsymbol{x}}^* = \arg\min_{\hat{\boldsymbol{x}}} \left(\text{Sequential-1}\right).$$

$\Delta\tau^C$ is the peak-to-peak amplitude of the calm-water trim angle (i.e., unacceptable porpoising is considered to be $\Delta\tau^C \geq 0.5°$). In addition, the variables were normalized from 0 to 1 with the lower and upper values tabulated in Tab. 4.3.

Table 4.1: Co-Design approach optimization

$\min_{\boldsymbol{x}}$	$\left(\bar{J}_1(\boldsymbol{x})\alpha + \bar{J}_2(\boldsymbol{x})\left(1-\alpha\right)\right.$ |w/ ACS$\left.\right)$
s.t.	$1^\circ \leq \tau^C(\boldsymbol{x}) \leq 15^\circ$
	$\Delta\tau^C(\boldsymbol{x}) \leq 0.5^\circ$|w/ ACS
	$2.0 \leq \beta \leq 40.0$

Table 4.2: Sequential (or "Traditional") approach optimization

Sequential-1 (w/o ACS)		Sequential-2 (w/ ACS)	
$\min_{\hat{\boldsymbol{x}}}$	$\left(\bar{J}_1(\boldsymbol{x})\alpha + \bar{J}_2(\boldsymbol{x})\left(1-\alpha\right)\right.$ |w/o ACS$\left.\right)$	$\min_{\check{x}}$	$(J_2(\hat{\boldsymbol{x}}, \check{x})$|w/ ACS$)$
s.t.	$1^\circ < \tau^C < 15^\circ$	s.t.	$1^\circ < \tau^C < 15^\circ$
	$\Delta\tau^C < 0.5^\circ$|w/o ACS		$\Delta\tau^C < 0.5^\circ$|w/o ACS
	$2.0 \leq \beta \leq 40.0$		$\Delta\tau^C < 0.5^\circ$|w/ ACS

Table 4.3: Variable normalization for 3 and 5-variable case

	Lower	Upper
L/b	4	6
lcg/b	0.15	3
β	2	40
$\log(Q_{33})$	-1	7
$\log(Q_{44})$	-1	7

4.3.1.2 Seakeeping Metric

In this work, we follow the recommendations by ISO 2631-5 for the "daily equivalent static compression dose" S_{ed} (ISO Standard 2631-5, 2004). A shortcoming of this metric is that it is not accurate for impacts larger than 4 g's. As a result, the appropriateness of S_{ed} as a metric for qualitative safety guidelines is unknown for when the vessel experiences frequent > 4 g's impacts.

The S_{ed} is calculated based on estimated accelerations acting at the spine of the occupant. In the vessel, the accelerations are composed of vertical and horizontal components — and the most violent movements usually occur at the bow (Savitsky and Brown, 1976). In order to be conservative, the S_{ed} in this work is calculated with the bow accelerations; and the exposure is normalized to 8 hours following Peterson et al. (2004).

An advantage of the S_{ed} metric is that it can be used to give safety recommendations for the vessels. To illustrate, following ISO Standard 2631-5 (2004) we plot in Fig. 4.4 the maximum number of days per year that an operator can be exposed to an S_{ed} event in order to maintain a low probability of injury, assuming they are expected to work in these environments for 5, 10, or 20 years.

4.3.2 Results and Discussion

The MAWS results are shown in Fig. 4.5, along with Chapter III exhaustive search results. One can see in Fig. 4.5a that the MAWS method was able to closely capture the Pareto front, with the exceptions of the overall utopia points. The reason for this is because these overall utopia points are disjointed from the mostly continuous optimization variables as Fig. 4.5b shows. However, this is an unavoidable consequence from using single-objective optimizations which can only guarantee local-minimums.

The implementation of a Pareto filter in MAWS makes it capable of "escaping" local minimums that were previously classified as Pareto optimal. An example of

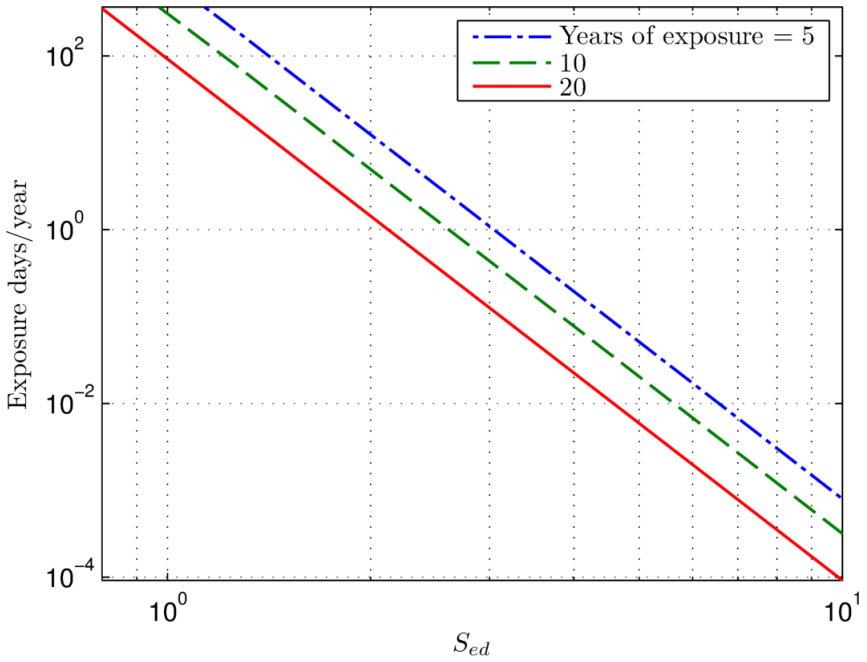

Figure 4.4: Maximum number of days of exposure per year for maintaining low probability of adverse health effect, if exposure starts at age 20 (following ISO Standard 2631-5 (2004)).

this is shown in Fig. 4.6. Since the MAWS algorithm performs initial guesses by performing a line search between neighboring Pareto points, the Pareto might follow a local minimum through the iterations.

The wall times for the MAWS Pareto approximations on a 2.67 GHz personal computer, along with the exhaustive search (including runs with and without ACS), are shown in Tab. 4.4. Note that MAWS was used to find the Pareto fronts of the Sequential-1 design, and Co-Design with and without a stability constraint. Pareto estimation for each design in Sequential-2 was not performed in this work.

The reason for the Co-Design OLS being more than twice as fast as the Co-Design OLU is that MAWS really takes advantage of the initial guess line search for the Co-Design OLS as one can infer from Fig. 4.5b.

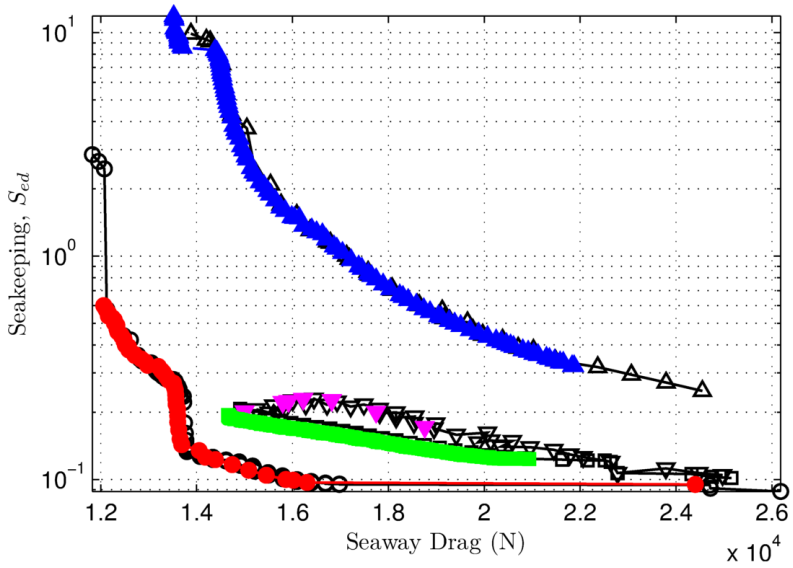

(a) Pareto fronts for MAWS's Sequential-1 (blue), Co-Design OLS (green), Co-Design OLU (red), and the filtered exhastive search (black markers)

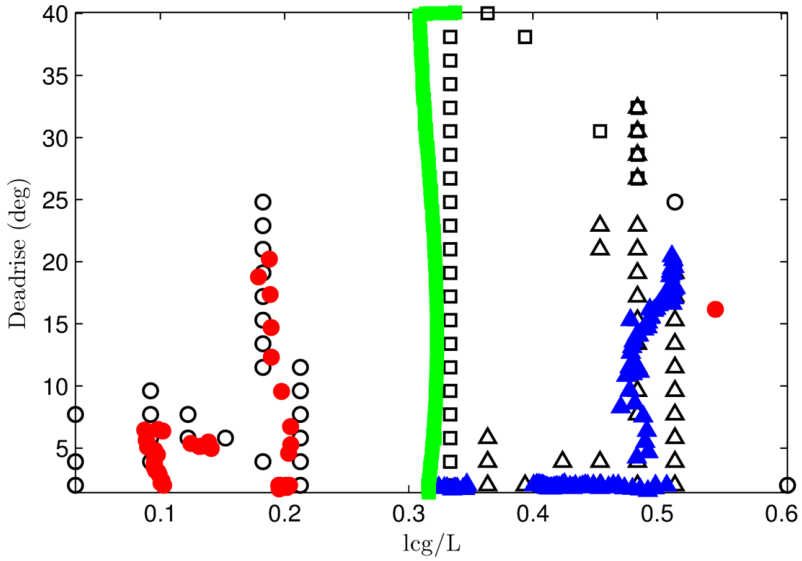

(b) Geometry variables

Figure 4.5: Comparison of the MAWS Pareto front (filled markers) with the exhaustive search results Pareto (black hollow markers) for the 3-variable design space and SS 2.

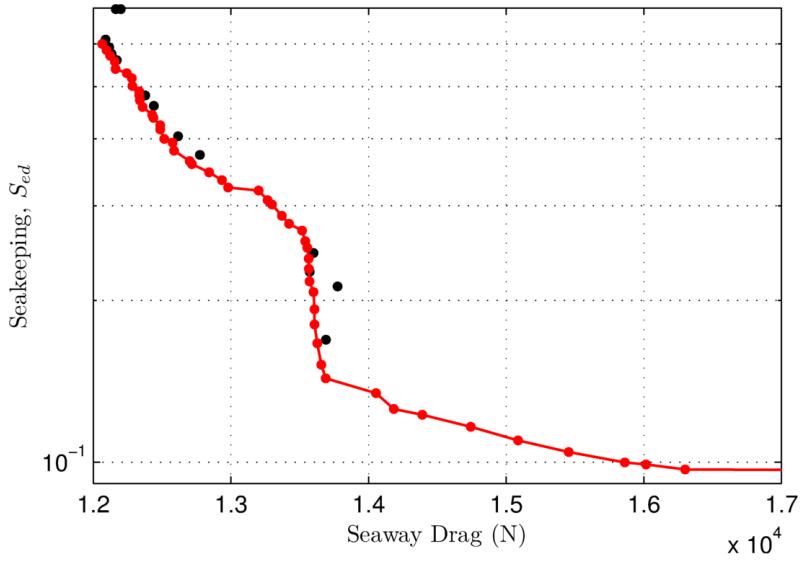

Figure 4.6: Co-Design OLU MAWS results with local minimums found in the MAWS iterations.

Table 4.4: 3-Variable MAWS Pareto approximation time comparison

	Avg. Time (hr)	Iterations	Points	Wall Time (days)
Seq-1	1.03	115	102	4.9
Co-Design OLS	1.64	114	51	7.8
Co-Design	3.45	65	102	9.3
Exhaustive	—	—	9705	27

Table 4.5: Fixed vessel particulars for 5-variable optimization

Fixed Variable	Value
LOA (m)	12.0
U (knot)	44.6
Δ (tonne)	10.20
vcg/b	0.294
R_g/b	1.25
Depth at Bow*	$5b/8$
Length of Bow*	b

*These are the values of Fridsma (1969) normalized with the beam.

4.4 MAWS Investigation: 5-Variable Vessel Optimization

In the 5-variable case, the vessel geometry and ACS were modified from those presented in Chapter III. The vessel geometry is now a function of the beam, which in turn changes the bow length and depth; and the ACS max/min force magnitudes are now constrained.

4.4.1 Problem Formulation

4.4.1.1 Geometry

The geometry of the vessels are prismatic (as shown in Fig. 3.1), with the bow shape following that of Fridsma (1969). The optimized geometry variables are the b, lcg and β. The vessel particulars that are fixed in the optimization are tabulated in Tab. 4.5.

4.4.1.2 ACS

The ACS is modeled as presented in Section 3.2.1.2, which consists of two point forces controlled by a Linear Quadratic Regulator (LQR), but with the addition of a force magnitude saturation constraint of 75 kN. This constraint was based on the

Table 4.6: Hydrofoil particulars for a 75 kN lift force with a 10deg Angle of attack at 44.6 knot

Property	Value
Span (m)	1.2
Chord (m)	0.3
Thickness (mm)	15
Depth(m)	1.0
Profile Curvature	0.025

maximum static force, following Matveev and Duncan (2005), that a hydrofoil of dimensions shown in Tab. 4.6 would have at an angle of attack of 10 deg. Note however that the hydrofoil hydrodynamics were not simulated in the time-domain — i.e., the ACS controller directly specified forces. The hydrofoil dimensions are simply used as a basis for the saturation force magnitude.

In addition, the time-domain ACS forces have a lift-to-drag penalty of 10. No appendage drag was taken into account.

The previous work in Chapter III optimized in the ACS space by tuning the gain responsible for the pitch velocity feedback (Q_{44}). In this work, we add to the optimization the gain responsible for the heave velocity feedback (Q_{33}).

4.4.1.3 Optimization formulation

The MAWS Step 6 optimization for the 5-variable case is as shown in Section 4.3.1.1, with the difference that

$$\boldsymbol{x} = \begin{bmatrix} L/b & lcg/b & \beta & log(Q_{33}) & log(Q_{44}) \end{bmatrix}$$

is the optimizing variables for the co-design problem,

$$\hat{\boldsymbol{x}} = \begin{bmatrix} L/b & lcg/b & \beta \end{bmatrix}, \check{\boldsymbol{x}} = \begin{bmatrix} log(Q_{33}) & log(Q_{44}) \end{bmatrix}$$

are the optimizing variables for the sequential design in Sequential-1 and Sequential-2 respectively, and

$$\hat{\boldsymbol{x}}^{*} = \arg\min_{\hat{\boldsymbol{x}}} \left(\text{Sequential-1}\right).$$

In addition, a constraint in L/b is set in the optimizations. First, in Section 4.4.2.1, the constraint is $3 \leq L/b \leq 10$, and later in Section 4.4.2.2 the constraint is $3 \leq L/b \leq 5.5$. Throughout the work, only the upper bound of the L/b will sometimes be mentioned since in neither of the optimizations the lower bound was ever active.

4.4.2 Results and Discussion

The first optimization was performed with a constraint of $L/b \leq 10$. A surprising result was that there seems to be no benefit from Co-Designing if the vessels are required to be $L/b \leq 10$. However, these results are in contradiction by the recommendations obtained from Chapters II and III, where Co-Design was found to be superior to the Sequential design.

Nonetheless, the vessels that appear to have no benefit from co-design have $L/b \approx 10$ — which is an unrealistic L/b for a monohull vessel. As a result, another investigation was conducted with an intermediary constraint: $3 \leq L/b \leq 5.5$. The value of $L/b = 5.5$ is representative of the maximum L/b present in 12 m production planing crafts[1].

4.4.2.1 $L/b \leq 10$ Vessels

As one could have predicted, the 5-variable design space contains much more local minimums than the 3-variable design space. The MAWS capability to "escape" local minimums was put to the test, and it was sometimes unsuccessful. Consequently, in order to have more confidence in the Pareto estimation, four independent MAWS runs were done, the final answers were stitched together, and then a final MAWS

[1]For reference, a 39' and 42' Cigarette racing boat is $L/b \approx 4.8$ and $L/b \approx 5.2$ accordingly

initialized with the stitched results was performed. The Pareto results are presented in Fig. 4.7 and the geometry variables in Fig. 4.8. In addition, the final overall count of MAWS iterations is shown in Tab. 4.7.

These results suggest that there is no real benefit from co-designing the vessels if the designer is allowed to reach a $L/b = 10$. The performance of the co-designed vessels is essentially identical to those from the sequentially designed crafts as Fig. 4.7 shows (with the exception of the extremes), and in Fig. 4.8 it is apparent that the geometry of the vessels are practically identical (again, with the exception of the vessels at the extremities). While co-designing did find utopia points which the sequential design could not match, these designs are in the extremes of the performance metrics and so they do not have any apparent practical interest.

Since the optimizations stated that they converged successfully, there is no indication that the equal results between the sequential and co-design optimizations are numerical artifacts. A possible explanations for equal vessel geometry design between the sequential and co-design results is the effective decoupling of the ACS and vessel geometry for vessels with large L/b ($L/b = 10$ in this case).

These results are novel in that they suggest that the "best" vessels for operating in rough seas at high speeds are catamarans. In other words, if the original design specifications are in fact twice of the investigated vessel displacement ($2\Delta = 20.4$ tonne), then these results preliminarily[2] show that the "best" vessels are catamarans. Indeed, if one looks into what is generally regarded as a pinnacle of offshore powerboat racing, the UIM Class 1 World Powerboat Championship, all the vessels are catamarans — and the individual hulls are actually $L/b \approx 10$. Nonetheless, these vessels are around 5 tonne which is much lighter than 20.4 tonne; but it is a possibility that throughout humans' history of powerboat engineering (which is essentially a metaheuristic multi-objective optimization), the same conclusion was reached for

[2]Preliminarily, since catamarans' seakeeping is also influenced by their centerline hull design and cross-deck slamming, which is not captured in these results.

Table 4.7: 5-Variable MAWS Pareto approximation time comparison for $L/b \leq 10$

	Avg. Time (hr)	Iterations	Points	Wall Time (days)
Seq-1	2.25	481	83	45
Co-Design	6.71	149	50	42

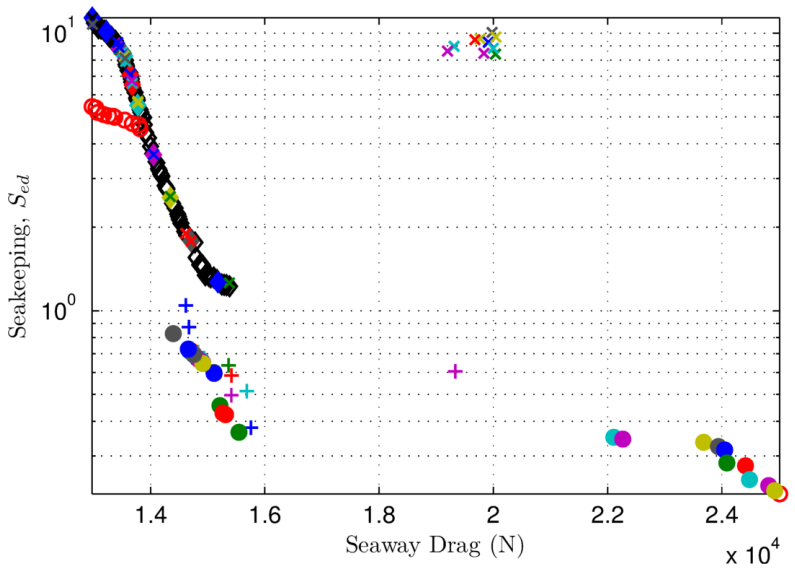

Figure 4.7: MAWS results for $3 \leq L/b \leq 10$, where $\circ$ is Co-Design, filled $\circ$ are OLS designs, $\times$ are the Co-Design OLS w/o ACS, $\diamond$ are the Sequential-1 (w/o ACS), filled $\diamond$ are the designs with a Sequential-2, and $+$ are the Sequential-2 (w/ACS) with $\alpha = 0$.

these lighter boats — that catamarans are the Pareto optimal vessels for high-speed, rough water operation.

4.4.2.2 $L/b \leq 5.5$ Vessels

In the MAWS runs performed in Section 4.4.2.1, many optimizations were found to be $L/b < 5.5$ (which were filtered out in subsequent MAWS iterations). Consequently, a "warm start" MAWS was done by starting with a Pareto approximation based on the new constraint and all the history of optimization results from the $3 \leq L/b \leq 10$ case.

The Pareto results are presented in Fig. 4.9 and the geometry variables in Fig. 4.10.

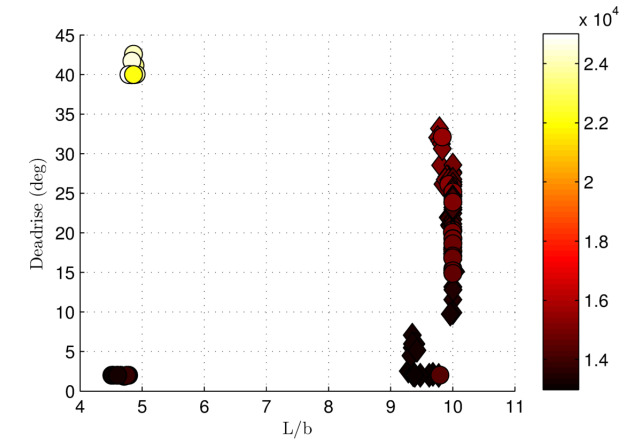

(a)

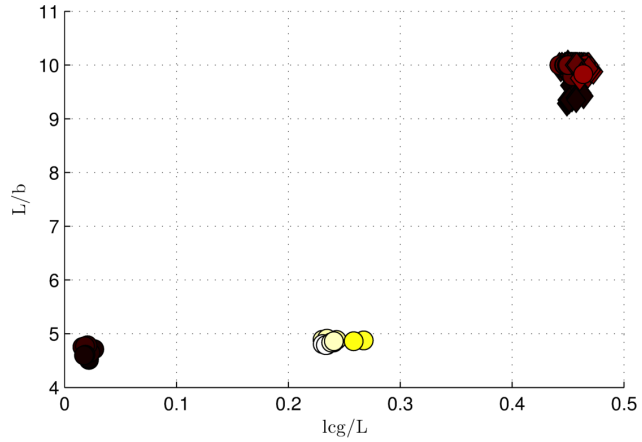

(b)

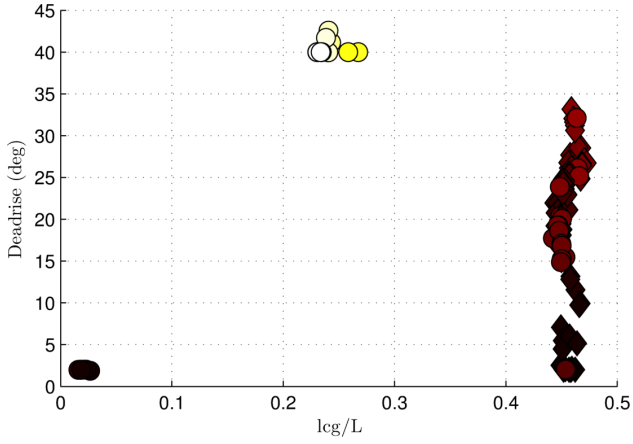

(c)

Figure 4.8: Geometry variables from MAWS results for $3 \leq L/b \leq 10$, where $\circ$ is Co-Design, $\diamond$ are the Sequential designs, and the color scale is the seaway average drag.

Table 4.8: 5-Variable MAWS Pareto approximation time comparison for $L/b \leq 5.5$, counting after "warm start"

	Avg. Time (hr)	Iterations	Points	Wall Time (days)
Seq-1	1.15	96	49	4.6
Co-Design	8.81	56	38	21

In addition, the final count of MAWS iterations after the "warm start" is shown in Tab. 4.8. The average time differences in Tab. 4.8 when compared to those in Tab. 4.8 are due to the "warm start" and the distribution of the Pareto points in the design variables' space; for the co-design, the variables are spaced out with discontinuities, and in the sequential design the design variables are for the most part neighboring each other without discontinuities.

Pareto Optimality

The results for when vessels are constrained to $3 \leq L/b \leq 5.5$ show a similar story to that from Chapter III. The Pareto optimal vessels which are co-designed dominate all other Pareto optimal designs as Fig. 4.9 shows. Moreover, the Sequential-2 vessels are not the OLS vessels from the co-design results. Once again, the implementation of an ACS to the Sequential-1 vessels drastically reduced the seakeeping metric, ranging from 70%-90% reductions in S_{ed}. But the vessels with the greatest synergy between the geometry and ACS were not obtained with a sequential design. Examples on the change in performance from the Sequential-2 designs to the co-designed vessels are tabulated in Tab. 4.9 and Tab. 4.10.

Moreover, in contrast with the results from Section 4.4.2.1, there are a number of Co-Design OLU vessels, as Fig. 4.9 shows.

In summary, the co-designed vessels are again superior to the sequentially designed vessels for all combinations of seaway drag or seakeeping constraints.

Table 4.9: Percent decrease in seaway drag for fixed seakeeping metric from "Sequential-2" to "Co-Design" Pareto front

S_{ed}	Percent Decrease
0.98	3.2%
0.48	11%

Table 4.10: Percent decrease in seakeeping metric for fixed seaway drag from "Sequential-2" to "Co-Design" Pareto front

$R_T^S/10^4$	Percent Decrease
1.85	26%
1.95	37%

Optimal Design Parameters

From the optimal geometry variables, shown in Fig. 4.10, we can see that the most significant difference between the co-designed and sequentially designed vessels is the *lcg* location; this is clearly illustrated in Fig. 4.10a, where the *lcg* axis is collapsed. A side effect of this is that many co-designed vessels are OLU, with the OLS designs falling inside $lcg/L > 0.17$.

4.5 Conclusion

The results from the 5-variable investigations present interesting implications. If the vessels are allowed to reach an $L/b = 10$, then all the Pareto optimal vessels are $L/b > 9$, OLS and their *lcg*'s around midships. Possibly suggesting that catamarans are the Pareto optimal vessels for high-speed, rough water operation. In addition, there appears to be no difference between the co-design and sequential designs of interest.

However, if the vessels are only allowed a maximum $L/b = 5.5$ (a realistic slender monohull), then the co-designed vessels revert back to OLU designs for when the

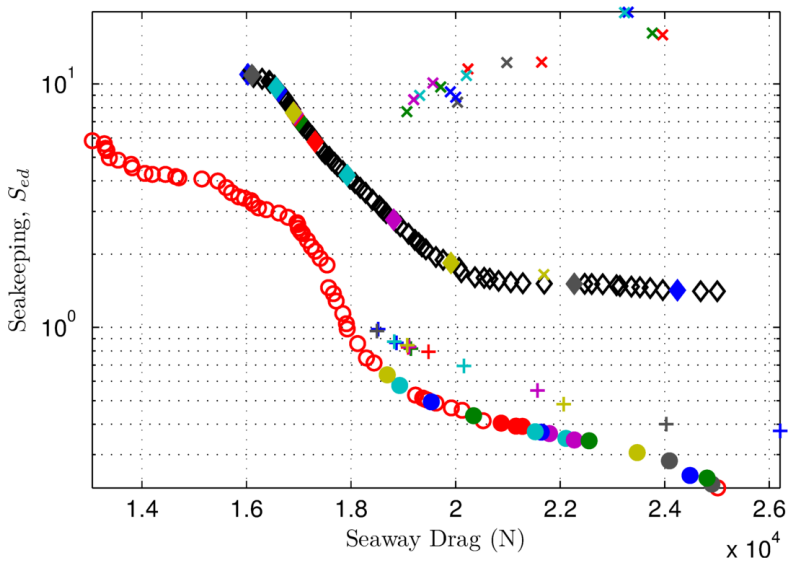

Figure 4.9: MAWS results for $3 \leq L/b \leq 5.5$, where $\circ$ is Co-Design, filled $\circ$ are OLS designs, $\times$ are the Co-Design OLS w/o ACS, $\diamond$ are the Sequential-1 (w/o ACS), filled $\diamond$ are the designs with a Sequential-2, and $+$ are the Sequential-2 (w/ACS) with $\alpha = 0$.

seaway drag is heavily minimized, but to OLS vessels when the seakeeping is heavily minimized — with both OLS and OLU vessels having *lcg*'s far aft. While the sequential designs maintain *lcg*'s just aft of midships.

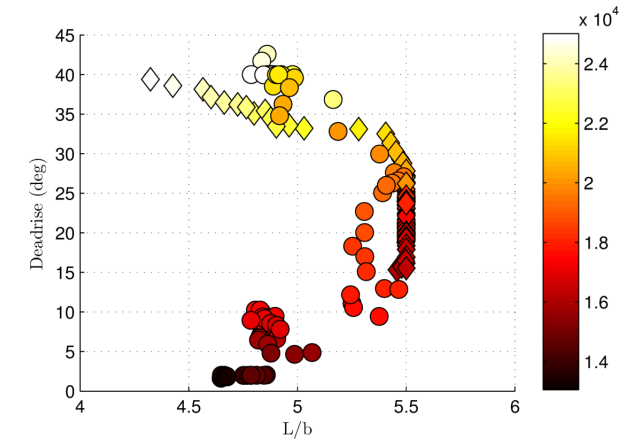

(a)

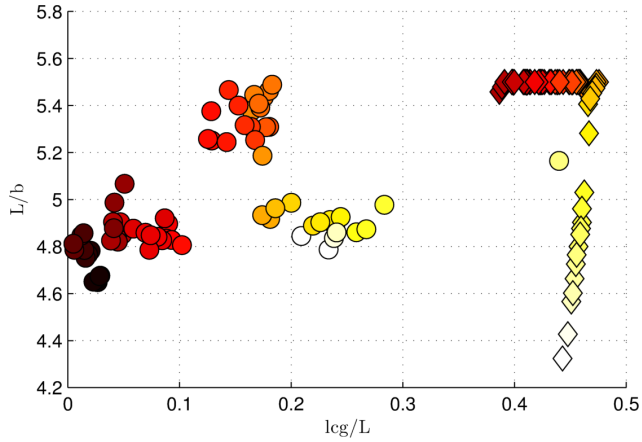

(b)

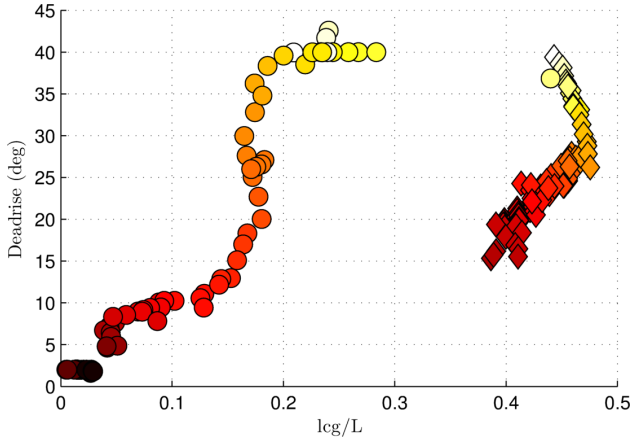

(c)

Figure 4.10: Geometry variables from MAWS results for $3 \leq L/b \leq 5.5$, where $\circ$ is Co-Design, $\diamond$ are the Sequential designs, and the color scale is the seaway average drag.

CHAPTER V

Case Study

5.1 Overview

Chapters III and IV suggest that superior seakeeping and drag performance is achievable if the vessel is co-designed with its ACS. But these co-designed vessels have different geometry which might present design challenges — such as the unnaturally aft center of gravity required in the co-designed vessels. Therefore, this case study investigates the feasibility of having a planing craft with ACS designed to the 5-variable co-design results found in Chapter IV for the $L/b \leq 5.5$ case (Section 4.4.2.2), and compares it to a traditionally designed vessel.

To the best of the author's knowledge, this work presents the first case study on a planing craft that is co-designed with its ACS.

This case study's main research question is, is it feasible to build a co-designed vessel as presented in previous chapters? In other words, can we design the vessel's structure, propulsor and payload so that it matches the optimized results?

In Section 5.2, the vessel optimization and design specifics are discussed. Then in Section 5.3, the optimizations results are presented, along with possible propulsor selections and the vessel's weight and hydrostatic results.

5.2 Design Methodology

The concept design for the case study follows the following steps:

1. A seakeeping constraint is set to the results in Section 4.4.2.2, and the "optimal" geometry (b, β and lcg) and ACS parameters (Q_{33} and Q_{44}) for the co-design and sequential design case are selected.

2. The vessel performance in calm water and sea states (SS) 1 and 2 are estimated.

3. The structure is designed by following a scantling rule.

4. The engines and fuel weight are selected based on a 322 km range at the design speed of 44.6 knot at SS 3.

5. The vessels' structure and fuel/engine location and overall dimensions are arranged with 3D modeling (using the Rhino software).

   (a) The fuel's lcg is placed at the design lcg, and its tanks are designed so that they do not go above the zero-trim waterline (WL).

6. The hydrostatics and weight are estimated with Rhino's plug-in Orca3D using the densities from the scantling rules.

7. The weight savings, payload, and hydrostatics are compared between the vessels.

The case study particulars come from the results of Chapter IV, by specifying a seakeeping constraint (see Section 5.2.1) and selecting the vessels with optimal seaway drag. Note that this work uses the Pareto results and not independent constrained optimizations. Consequently, the selected co-design and sequentially designed vessels are likely the very best that a designer could choose using these two approaches.

The vessels, which were optimized for sea state (SS) 3 are simulated in the time-domain program POWERSEA (Akers, 1999) to find their corresponding performance in SS 0, 1, 2.

As in the previous chapters, the seaway is assumed to be in the North Atlantic with the particulars defined in Tab. 3.2, and is simulated by using the ISSC sea spectrum with 100 wave components. For additional information on the virtual test bed, the reader is referred to Section 4.2.2.

5.2.1 Seakeeping Constraint

Following the ISO Standard 2631-5 (2004) recommendations, assuming the occupants to be operating the vessel 230 days a year, for 20 years starting at an age of 20 years, the maximum recommended S_{ed} is 0.86. To calculate the vessel's S_{ed} based on the simulations, the accelerations results were normalized to 8 hours as in Section 4.3.1.2. Example calculations for S_{ed} can be seen in Appendix B. The parameters chosen are very conservative; given that the ISO metric has not been validated for use in high-speed crafts, it is therefore wise to be on the conservative side of the recommendations.

5.2.2 Structure

The scantling rule followed in this paper to estimate the structural weight is the one presented in Gerr (1999) with the following specifics, additions and modifications:

1. The structure design follows the basic solid-glass hull shell, and fiberglass structure scantling rules.

2. Only the general hull and structure are estimated and the recommended fiberglass thicknesses are not modified to reflect the specific number of standard mat layers that would be used.

3. No deck superstructure/helm was designed. This allows for the paper results to be relevant for different vessel types (e.g., unmanned surface vessels, center

console vessels, and full cabin vessels); the resulting vessel payload only needs to be modified to reflect the desired deck structure design/configuration.

4. The cores used in the design was balsa (160 kg/m^3).

5. The deck has four longitudinal stringers.

6. The bulkheads are made out of 12.7mm marine plywood (601 kg/m^3).

7. There is a bulkhead placed right at the intersection of the bow/prismatic region of the vessel, and the remainder bulkheads are equally spaced throughout the vessel's prismatic length.

8. Both designs have four floors (transverse structure on the hull bottom), and each floor is placed in the middle of two bulkheads, starting forward.

The ACS hydrofoil was assumed to be made out of solid fiberglass, and it is connected to the vessel by two support structures on each hydrofoil (making a U-shape). The connecting structures' cross section is elliptical with dimensions 0.3 m x 0.1 m, and thickness of 11 mm. These dimensions are meant for calculating a rough weight estimate, and they are not optimized.

5.3 Results and Discussion

The selected vessels from the Pareto front of Section 4.4.2.2 results can be seen in Tab. 5.1. An interesting result is that the even though the co-design vessel was optimized for SS 3, the improvements above the sequential vessel are more noticeable for the other investigated SS's as Tab. 5.2 shows. Because the vessels are unlikely to be operating always in SS 3, the effective seakeeping improvement of the co-design is greater than 3.8%. While there are significant improvements in the co-design seakeeping metrics for SS 1 and 2, both the sequential and co-design results are well

Table 5.1: Case study objective and variable selection

Name	Sequential-1	Sequential-2	Co-Design
R_T^S (kN)	16.62	18.83	18.12
S_{ed} (MPa)	9.36	0.86	0.86
b (m)	2.182	2.182	2.257
lcg from Stern (m)	4.770	4.770	1.901
β (deg)	19.3	19.3	15.1
$\log Q_{33}$	—	-3.391	-2.462
$\log Q_{44}$	—	6.750	7.305

Table 5.2: Vessel performance in different sea-states

Metric	Name	SS 0	SS 1	SS 2	SS 3 (Design)
R_T^S (kN)	Sequential-2	16.08	16.26	16.96	18.83
	Co-Design	14.40	14.63	15.74	18.12
	% Diff.	10.4%	10.0%	7.1%	3.8%
S_{ed} (MPa)	Sequential-2	—	0.042	0.17	0.86
	Co-Design	—	0.027	0.096	0.86
	% Diff.	—	35.4%	43.6%	0.0%

inside the safety recommendations of $S_{ed} \leq 0.86$ — nonetheless, they do suggest that the co-design would have a smoother ride.

The sequential vessel is one that would be logical for a designer; the vessel has the highest L/b allowed (5.5) and a lcg just aft of midships (LOA/$lcg = 0.40$). Moreover, the ACS optimized variables support the results in Savitsky (2003); Wang (1985), which state that the ACS should rely on pitch velocity feedback control and not on the heave velocity.

Nonetheless, a designer might have had trouble finding this sequential vessel in the first place, since the vessel's seakeeping performance without ACS is one of the worst found in the sequential-1 Pareto front, $S_{ed} = 9.36$ (see Fig. 4.9). As a result, in a real-world design, this vessel might have been discarded due to its poor seakeeping performance without ACS. Thus assuming that the vessel performance with ACS is

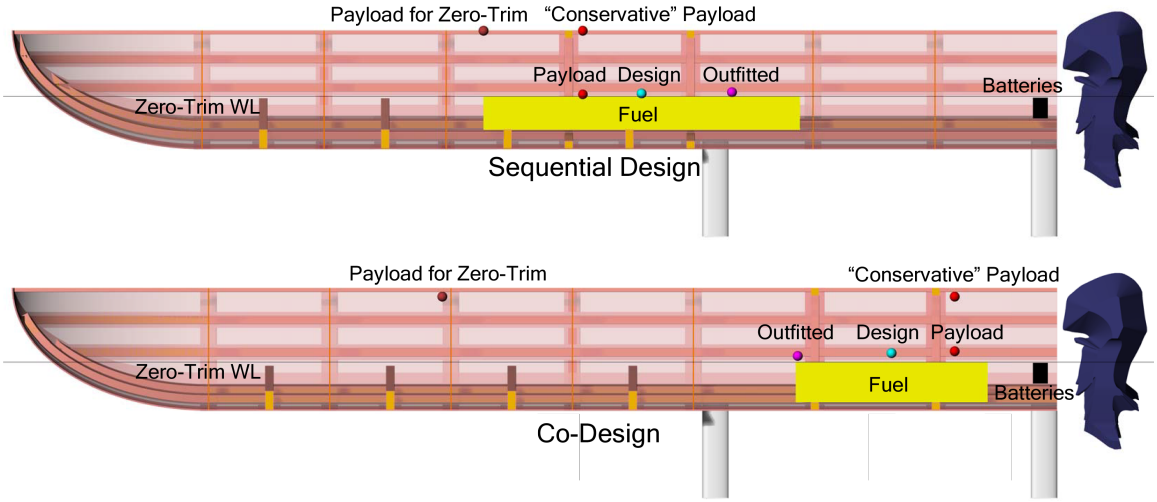

Figure 5.1: Crossection view of the sequentially designed vessel (top) and co-designed vessel (bottom).

the primary objective, the sequential design in this work shows a "smarter" approach to performing a sequential design: not discarding Pareto vessels with poor seakeeping performance in sequential-1.

The co-design beam and deadrise are very similar to the sequential vessel, however it has slightly larger beam and lower deadrise — two changes which a designer might conventionally think would make seakeeping worse according to empirical estimations (Savitsky and Brown, 1976). On the other hand, the lcg of the vessel is far aft (LOA/$lcg = 0.19$) — which is the most significant difference between the sequential and co-design results.

A perspective view of a longitudinal cross-section of the resulting vessels can be seen in Fig. 5.1. Fig. 5.1 clearly shows the importance of co-designing the vessel early in the concept phase, since the two would require very different internal arrangements. Moreover, the co-design vessel has additional design challenges which need to be addressed: payload location and hydrostatics. These two design challenges are further discussed in Section 5.3.2 and 5.3.3, accordingly.

5.3.1 Propulsion

The propulsion particulars are tabulated in Tab. 5.3. Because the required power in SS 3 between the two vessels is only 3.8% apart, the engine selection is identical for the two vessels. Because the vessels are narrow, it is not possible to install inboard engines side-by-side while leaving space for maintenance. Consequently, inboard engines would have to be staggered. But staggering the engines would move the *lcg* forward — which would go against the desired co-design *lcg*. As a result, outboard engines were selected to maintain the *lcg* aft.

A good engine candidate is a 223.7 kW (300 hp) outboard engine, such as the Yamaha F300, where a quad-engine configuration is used to meet the required power. Two of the engines would have a "short" shaft (at the sides), and the other two a "long" shaft (at the centerline). These engines use regular unleaded fuel, and the weight and cost savings are approximately the same as the power savings. As previously mentioned, even though at the design SS 3 the savings are 3.8%, the real effective savings are more if the vessel is operated at lower SS's.

5.3.2 Vessel Weight

The weight results summary is tabulated in Tab. 5.4. Based on the scantling rules of Gerr (1999), the co-design vessel's structure would be 6.8% heavier than the sequential design; the reason being that the co-design vessel has a larger beam. Nonetheless, after considering the fuel weight savings of the co-design, the co-design vessel is only 1.8% heavier and with 1.2% less available payload. In short, the payload difference between the designs is negligible.

The significant difference of the payload between the two designs is its location, as Fig. 5.1 illustrates. For the sequential vessel, the payload should be located just aft of midships (LOA/$lcg = 0.45$), something that can be easily accomplished since with the ACS, the entire deck is safe for the location of personnel (recall that the seakeeping

Table 5.3: Propulsion particulars

Name	Sequential Design	Co-Design
Design Margin	24%	
Est. Propulsion Efficiency	60%	
Required Power (kW)	894	860
Power Savings	—	3.8%
Engine	Yamaha F300 Outboard (×4)	
Power (skW)	$4 \times 223.7 = 894.8$	
Dry Weight (kg)	$2 \times 255 + 2 \times 259 = 1028$	
Overall Length (mm)	958	
Overall Width (mm)	634	
Fuel Type	Regular Unleaded	
Density (kg/m^3)	760	
Est. Fuel Consumption (L/hr)	$4 \times 98.4 = 394$	$4 \times 94.7 = 379$
Design Operation Time (hr)	3.9	
Required Fuel Volume (L)	1537	1478
Required Fuel Weight (kg)	1168	1123
Volume/Weight Savings (%)	—	3.8%

metric was calculated at the bow of the ship, where the most violent motions are encountered).

On the other hand, the co-design vessel requires that the payload be located completely aft (LOA/$lcg = 0.10$) — even more aft than the design lcg (LOA/$lcg = 0.16$), due to the outfitted lcg resting forward of the design lcg (see Fig. 5.1). This aft payload might be possible if the vessel's deck is extended so that payload can be placed aft of the transom; in other words, having an overhang on the transom which does not contact the water during operation. Another possibility would be to provide an equivalent upward trimming moment by using the ACS, but this would cause a steady drag component and make the ACS saturate at different times — changing the results. Consequently, using a steady ACS moment component to replicate an aft lcg requires further investigation and is recommend research. Other possible solutions to this problem are presented in Section 5.4. Nevertheless, this result strongly suggests

Table 5.4: Vessel weight results excerpt

Name	Sequential Design	Co-Design
Structural Weight (kg)	1727	1844
Structural Weight Savings (%)	—	-6.8%
Structural *lcg* (m)	5.814	5.779
Structural *vcg* (m)	0.659	0.655
Outfitted Weight* (kg)	4024	4097
Outfitted Weight Savings (%)	—	-1.8%
Outfitted *lcg* (m)	3.733	2.980
Outfitted *vcg* (m)	0.657	0.631
Available Payload (kg)	6178	6106
Available Payload Increase (%)	—	-1.2%
Desired Payload *lcg* (m)	5.446	1.176
Desired Payload *vcg* (m)	0.631	0.685
"Conservative" Payload *vcg* (m)	1.359	1.309
"Conservative" Full Load *vcg* (m)	1.082	1.037
Payload *lcg* Shift for Zero-Trim (m)	1.140	5.882

*Includes the fuel, engines and batteries

that the co-design approach needs further research for it to be implementable in practice.

5.3.3 Hydrostatics

The close to midship *lcg* of the sequential vessel creates a vessel which has a good static attitude, as it can be seen in Tab. 5.5. Moreover, in order to investigate the hydrostatics for an "conservative" payload *vcg*, the payload was placed 0.75 m above the zero-trim waterline. In this location, the vessel is still transversely stable (as the GMt ¿ 0 shows).

In contrast, the far aft *lcg* of the co-design vessel produces a vessel with unacceptable hydrostatics. With payload at the design location, the vessel would rest statically with a 20 deg trim (see Tab. 5.5). Moreover, if the payload is placed conservatively, the vessel is statically unstable. While a direct solution is to actively shift the *lcg* of the vessel (e.g., ballast tanks, active payload and/or fuel shifting), this result sug-

Table 5.5: Vessel hydrostatics excerpt

	Sequential Design		Co-Design	
	Design *vcg*	"Conservative" *vcg*	Design *vcg*	"Conservative" *vcg*
Trim (deg)	1.6	1.6	19.63	Capsized
Draft (m)	0.760	0.763	1.909	
GMt (m)	0.699	0.258	0.346	
BMt (m)	0.942	0.942	0.339	

gest that additional investigation is needed for a proper co-design implementation in practice.

5.4 Conclusion

This case study shows that while the studied co-designed vessel is technically feasible, it would require unconventional deck superstructure to accommodate the aft payload, and active management of the *lcg* for stable static/low-speed operation. Some immediate solutions to this problem are:

- Actively shifting the *lcg* by means of ballast tanks, or moving payload or fuel.
- Design an overhand/hull step in which the hull surface aft of the step does not make contact with the water during operation; and when static or low speeds the step does provide buoyancy so that the trim angle is acceptable.
- Re-design the forward section of the vessel to drastically reduce the structural weight — for example only making the structure a planing surface, like a water ski.

Additional investigations that have potential to present a better co-design vessel without these problems are modifying the optimization to:

- Set a constraint on the hydrostatic trim angle.

- Allow the vessel to have variable beam and deadrise (so that if the *lcg* is still aft in the co-design vessels, the vessels can resort to slender/high-deadrise bows for lowering the hydrostatic trim angle).

- Investigate the use of the ACS's reference trim angle as an optimization variable (possibly removing the *lcg* as the optimization variable).

These results, on one hand, support the conventional wisdom that planing craft design is mature (since a conventional design and arrangement is obtained for the sequentially designed vessel) — but this is only true for the sequentially designed vessel. On the other hand, we see that a co-designed vessel is far from mature in its design. Hence, additional investigation is needed to fully exploit the potential of co-designing a planing craft with its ACS.

CHAPTER VI

Conclusions

6.1 Conclusions

The study was set out to explore the potential of co-designing planing crafts with ACS and has combined tools in the disciplines of naval architecture, control systems, and optimization in a novel way to show the possible co-design performance improvements in calm-water drag, seaway drag, and seakeeping performance — and therefore presents motivation to shift the design of planing crafts with ACS from the conventional sequential design to co-design.

In other words, the study was set out to answer: should the co-design of a planing craft with its ACS be recommended over the conventional sequential design method? Below follows a synthesis of the findings addressing this question:

- **Calm-water drag improvements:** Co-designing a planing craft with its ACS allows the designer to consider designs which would be otherwise discarded in a sequential design because they have open-loop instabilities. The co-design results in vessels which can operate more efficiently, some reaching 20% drag reduction estimates as shown in Chapter II.

- **Seaway drag and seakeeping improvements:** Co-designing assures that the true Pareto optimal designs are in the feasible space of the optimization.

Improvements over sequential design ranged from negligible in SS 3, as it was the case for when vessel designs were allowed to reach $L/b = 10$ in Chapter IV, to 30% in SS 2 and 10% in SS 3 for seaway drag, and 20% in SS 2 and 50% in SS 3 for seakeeping metrics when $L/b = 4.72$ in Chapter III.

- **Design efficiency:** As it was made apparent in Chapter IV, co-designing avoids the unexplored problem of how to choose a design in the first step of a sequential optimization based on requirements for the second step, thereby avoiding the time consuming iterations between the hardware design and ACS design.

This work complements recent research in the use of ACS in planing craft for improving the safety of mission-driven operators, since it supports their findings of improved seaway performance in a sequential design (Wang, 1985; Savitsky, 2003; Shimozono and Kays, 2011; Engle et al., 2011; Rijkens, 2013). However, because of the clear advantages in co-designing a planing craft with its ACS, future design of planing craft with ACS should, if possible, adopt a co-design procedure.

Given that the work on the co-design of planing craft with ACS is new, the study has a number of shortcomings and limitations which need to be considered. Firstly, a valid question which is not answered in this work is if the results are simply an artifact of the modeling techniques. For instance, POWERSEA has only had some validation in a regular seaway, and its behavior is influenced by tuning parameters which their accuracy is unknown for an irregular seaway (Akers, 1999). Moreover, planing crafts have nonlinear dynamics which an LQR is naive to. Also, while there were precautions to avoid local minimums, there is no way to guarantee with the methods used that the Pareto estimations in Chapter IV are in fact the true Pareto fronts. In addition, even though the results are presented in non-dimensional form, caution must be taken when applying these results to vessels which have different properties from those fixed in this study; this includes the fact that the ACS used in this work was two point forces at specific locations.

To support the co-design framework for planing boats with an ACS, future research should be carried out to develop effecitve tools to facilitate the streamlined design process. More specifically,

1. Investigate if the co-design improvements found in this study still hold when using higher fidelity modeling — as first steps, testing specific case studies.

2. If the computational resources are available, verify the Pareto estimations from Chapter IV with "global optimization" methods such as genetic algorithms and swarm optimization; this could be done by either scalarization or metaheuristic multi-objective procedures.

3. Investigate the use of ACS to change the operational trim angle instead of changing the lcg.

4. Explore the use of nonlinear controllers in the design to further exploit the co-design.

5. Further generalize the vessel geometry and estimate the Pareto fronts by using whichever tool was found to be effective from future work's item 2.

6. Investigate different ACS configurations, such as only one point force and actively controlled thrust vectors, and optimal ACS locations.

7. Include as a design objective the vessel's maneuverability.

8. Investigate the effect of ACS on hull bottom pressures, since vessels with ACS will undoubtedly require different hull structure guidelines.

9. Research the influence of time-simulations' length, and explore possible ways to exploit it for expediting optimization convergence.

To the best of the author's knowledge, co-designing a planing craft and its ACS has never been performed in practice — thus the proposed framework offers an opportunity of designing planing craft that are more efficient and have better seakeeping than conventionally designed planing craft.

APPENDICES

APPENDIX A

Planing Boat Reduced Order Model

In this section, the equations used to find the linearized values of the system – for using 'Faltinsen Method' – will be presented in a programmatic fashion, i.e., the equations are presented in a sequence which can be sequentially calculated. No derivations or explanations will be presented; for the interested reader, the derivations can be found in Faltinsen (2005) unless otherwise stated.

The added mass coefficients are "based on a high-frequency free-surface condition and strip theory" (Faltinsen, 2005). For the damping coefficients B_{33} and B_{55}, a quasi-steady approach is used using the hydrodynamic lift forces estimated by Savitsky's equations (Savitsky, 1964); and for B_{35} and B_{53} a rough estimation is done by using the Euler beam equation applied to high-frequency rigid-body oscillations (Faltinsen, 2005). And the restoring coefficients are the linearizations of Savitsky's equations rewritten following A. W. Troesch's procedure (Troesch, 1992).

Note that these equations could be defined as a function of any of the used variables. For the purpose of making the linearized model used in this paper, the equations are made functions of η_3 and η_5.

A.1 Reduced-Order Model Equations

Keel wetted length:

$$L_K = lcg + \frac{vcg}{\tan(\tau + \eta_5)} - \frac{(z_{wl} + \eta_3)}{\sin(\tau + \eta_5)}$$

Note: If $L_K < 0$, the vessel is out of the water and so it should be set to $L_K = 0$.

Distance from keel/water-line intersection to start of wetted chine:

$$x_s = \frac{0.5b\tan(\beta)}{\left(1 + \frac{z_{max}}{Ut}\right)(\tau_{rad} + \eta_5)}$$

where $\frac{z_{max}}{Ut}$ is the coefficient of maximum pressure coordinate, which can be interpolated from Tab. A.1.

Chine wetted length:

$$L_C = \begin{cases} L_K - x_s & \text{if } L_K > x_s \\ 0 & \text{otherwise} \end{cases}$$

Note: If $L_C = 0$, the vessel is running "chines-dry".

Mean wetted length-beam ratio:

$$\lambda_W = \frac{L_K + L_C}{2b}$$

Adjusted distance from keel/water-line intersection to start of wetted chine:

$$\tilde{x}_s = \begin{cases} x_s & \text{if } L_C > 0 \\ L_K & \text{otherwise} \end{cases} \tag{A.1}$$

Note: Equation A.1 is an adjustment made to Faltinsen (2005).

Table A.1: Coefficient of maximum pressure coordinate (Faltinsen, 2005).

β	$\frac{z_{max}}{Ut}$	β	$\frac{z_{max}}{Ut}$
4°	0.5695	20°	0.5087
7.5°	0.5623	25°	0.4709
10°	0.5556	30°	0.4243
15°	0.5361	40°	0.2866

Distance of CG from keel-WL intersection:

$$x_G = L_K - lcg$$

K constant Faltinsen (2005):

$$K = \cot(\beta)\left[\frac{\pi}{\sin(\beta)}\frac{\Gamma(1.5-\beta_{rad}/\pi)}{\Gamma^2(1-\beta_{rad}/\pi)\,\Gamma(0.5+\beta_{rad}/\pi)} - 1\right]$$

where Γ is the gamma function.

Added mass coefficients for dry chine region:

$$\kappa = (1+z_{max})(\tau_{rad}+\eta_5)$$

$$A_{33}^{(1)} = \tfrac{1}{3}\rho\kappa^2 K\tilde{x}_s^3$$

$$A_{35}^{(1)} = A_{53}^{(1)} = A_{33}^{(1)}\left(x_G - \tfrac{3}{4}\tilde{x}_s\right)$$

$$A_{55}^{(1)} = A_{33}^{(1)}\left(x_G^2 - \tfrac{3}{2}x_G x_s + \tfrac{3}{5}\tilde{x}_s^2\right)$$

where ρ is the water density.

Added mass coefficients for wetted chine region; thus if $L_C = 0$ then $A_{jk}^{(2)} = 0$, else

$$\begin{aligned}
C_1 = &\quad \tfrac{2\tan^2(\beta)}{\pi} K \\
A_{33}^{(2)} = &\quad \rho b^3 C_1 \tfrac{\pi}{8} \tfrac{L_C}{b} \\
A_{35}^{(2)} = A_{53}^{(2)} = &\quad -\rho b^4 C_1 \tfrac{\pi}{16} \left[\left(\tfrac{L_K}{b}\right)^2 - \left(\tfrac{\tilde{x}_s}{b}\right)^2 \right] + x_G A_{33}^{(2)} \\
A_{55}^{(2)} = &\quad \rho b^5 C_1 \tfrac{\pi}{24} \left[\left(\tfrac{L_K}{b}\right)^3 - \left(\tfrac{\tilde{x}_s}{b}\right)^3 \right] \\
&\quad -\rho b^4 C_1 \tfrac{\pi}{8} x_G \left[\left(\tfrac{L_K}{b}\right)^2 - \left(\tfrac{\tilde{x}_s}{b}\right)^2 \right] + x_G^2 A_{33}^{(2)}
\end{aligned}$$

Total added mass coefficients:

$$A_{jk} = A_{jk}^{(1)} + A_{jk}^{(2)}$$

Draft from the spray root:

$$d = \begin{cases} 0.5b \tan(\beta) & \text{if } L_C > 0 \\ \left(1 + \frac{z_{max}}{Ut}\right)(\tau_{rad} + \eta_5) L_K & \text{otherwise} \end{cases}$$

Two-dimensional added mass coefficient in heave for a wedge (Faltinsen 2000):

$$a_{33} = \rho K d^2$$

Hydrodynamic lifting force coefficient for $\beta = 0°$:

$$C_{L0} = \left(\frac{180}{\pi}\right)^{1.1} 0.012 \left(\tau_{rad}^{1.1} + \eta_5\right) \lambda_W^{0.5}$$

Hydrodynamic lift coefficient for $\beta > 0$:

$$C_{L\beta} = C_{L0} - 0.0065 \beta_{deg} C_{L0}^{0.60}$$

Derivatives of the hydrodynamic lift coefficients:

$$\frac{\partial C_{L0}}{\partial \tau} = \left(\frac{180}{\pi}\right)^{1.1} 0.0132 \left(\tau_{rad} + \eta_5\right)^{0.1} \lambda_W^{0.5}$$

$$\frac{\partial C_{L\beta}}{\partial \tau} = \frac{\partial C_{L0}}{\partial \tau} \left(1 - 0.0039 \beta_{deg} C_{L0}^{-0.4}\right)$$

Damping coefficients:

$$B_{33} = \frac{\rho}{2} V b^2 \frac{\partial C_{L\beta}}{\partial \tau}$$

$$B_{35} = -V \left(A_{33} + a_{33} lcg\right)$$

$$B_{53} = B_{33} \left(0.75 \lambda_W b - lcg\right)$$

$$B_{55} = V a_{33} lcg^2$$

Wetted surface area for dry chine region:

$$S^{(1)} = \frac{\tilde{x}_s b}{2 \cos\left(\beta\right)}$$

Wetted surface area for wetted chine region:

$$S^{(2)} = \frac{b L_C}{\cos\left(\beta\right)}$$

Total wetted surface area:

$$S = S^{(1)} + S^{(2)}$$

Average bottom velocity, from Hadler (1966):

$$V_m = V \sqrt{1 - \frac{0.0120 \sqrt{\lambda_W} \tau_{rad}^{1.1} - 0.0065 \beta_{rad} \left(0.0120 \sqrt{\lambda_W} \tau_{rad}^{1.1}\right)^{0.6}}{\lambda_W \cos\left(\tau\right)}}$$

Reynold's number based on the average bottom velocity

$$R_n = \frac{V_m \lambda_W b}{\nu}$$

where ν is the fluid's viscosity.

ITTC 1957 friction drag coefficient:

$$C_f = \frac{0.075}{\left(\log_{10}\left(R_n\right) - 2\right)^2}$$

Friction drag coefficient correction for hull roughness, from Bowden and Davidson (1974):

$$10^3 \Delta C_f = 44 \left[\left(\mathrm{AHR} / \left(\lambda_W b \right) \right)^{1/3} - 10 R_n^{-1/3} \right] + 0.125$$

where AHS is the average hull roughness, and a value of $\mathrm{AHR} = 150 \times 10^{-6}$ was used.

Friction drag:

$$R_f = \frac{1}{2} \rho \left(C_f + \Delta C_f \right) S V^2$$

Hydrodynamic lift:

$$F_{L\beta} = \frac{1}{2} C_{L\beta} \rho V^2 b^2$$

Total drag force (horizontal force w.r.t. calm water):

$$R_T = F_{L\beta} \tan\left(\tau\right) + R_f \cos\left(\tau\right)$$

Sum of forces along z (about η_3):

$$F_z = F_{L\beta} - R_f \sin\left(\tau + \eta_5\right)$$

Longitudinal position of the center of pressure:

$$l_p = \lambda_W b \left(0.75 - \frac{1}{5.21\left(C_v/\lambda_W\right)^2 + 2.39}\right)$$

Longitudinal position of the center of drag:

$$l_f = \frac{b\tan\left(\beta\right)\left(\frac{1}{6}S^{(1)} + \frac{1}{4}S^{(2)}\right)}{S^{(1)} + S^{(2)}} \tag{A.2}$$

Note: Equation A.2 is the geometric center of the wetted area.

Lift's normal force w.r.t. keel:

$$F_N = \frac{F_{L\beta}}{\cos\left(\tau + \eta_5\right)}$$

Moment about CG (about η_5):

$$M_{cg} = -F_N\left(lcg - l_p\right) + R_f\left(l_f - vcg\right)$$

where the coordinate system used follows that of Faltinsen (2005), with positive towards aft and up.

Linearized restoring coefficients in heave and pitch:

$$\begin{aligned} C_{3k} &= \frac{\partial F_3^{cg}}{\partial \eta_k} = \frac{\partial F_z}{\partial \eta_k} \\ C_{5k} &= \frac{\partial F_5^{cg}}{\partial \eta_k} = \frac{\partial M_{cg}}{\partial \eta_k} \end{aligned} \tag{A.3}$$

where the derivatives in Eqn. A.3 were found numerically by using the complex-step method Martins et al. (2003) – using this method, the accuracy of the derivatives can be found up to machine precision.

A.1.1 State-Space Representation

The vessel's unforced equation of motion can be written as

$$A_m\ddot{\eta} + B\dot{\eta} + C\eta + Du = 0$$

$$A_m = \begin{bmatrix} \frac{\Delta}{g} & 0 \\ 0 & \frac{\Delta r_g^2}{g} \end{bmatrix} + \begin{bmatrix} A_{33} & A_{35} \\ A_{53} & A_{55} \end{bmatrix} \quad B = \begin{bmatrix} B_{33} & B_{35} \\ B_{53} & B_{55} \end{bmatrix} \tag{A.4}$$

$$C = \begin{bmatrix} C_{33} & C_{35} \\ C_{53} & C_{55} \end{bmatrix} \quad D = \begin{bmatrix} 1 & 1 \\ lcg & lcg - LOA \end{bmatrix}$$

where $\eta = \begin{bmatrix} \eta_3 & \eta_5 \end{bmatrix}^T$, $u = \begin{bmatrix} f_{aft} & f_{fwd} \end{bmatrix}^T$, and the control inputs f_{aft} and f_{fwd} are the ACS forces at the stern and bow respectively. The right-hand side of Eqn. A.4 is zero only when τ and z_{wl} are chosen so that $F_z = 0$ and $M_{cg} = 0$ (vessel is in equilibrium – but not necessarily stable).

By using the state $\tilde{\eta} = \begin{bmatrix} \eta_3 & \eta_5 & \dot{\eta}_3 & \dot{\eta}_5 \end{bmatrix}^T$, we can rewrite Eqn. A.4 in state-space form as

$$\dot{\tilde{\eta}} = \tilde{A}\tilde{\eta} + \tilde{B}u$$

$$\tilde{A} = \begin{bmatrix} 0 & 1 \\ -A_m^{-1}C & -A_m^{-1}B \end{bmatrix} \tag{A.5}$$

$$\tilde{B} = \begin{bmatrix} 0 & 0 \\ 0 & 0 \end{bmatrix} \quad A_m^{-1} \begin{bmatrix} 1 & 1 \\ -lcg & LOA - lcg \end{bmatrix}$$

The local stability and controllability can now be easily investigated with Eqn. A.5.

A.2 Stability and Controllability

This appendix is only meant to be a concise and practical presentation of the tools used in this work to investigate local stability and local controllability, with no

proofs. For proofs and discussion on these techniques, the reader is referred to Khalil (2002).

For the following discussions, it is assumed that the nonlinear system has an equilibrium point at $x^* = 0$, i.e., $f(x^*) = f(0) = 0$. Moreover, we are considering the system

$$\dot{x} = f(x,u) \approx Ax + Bu$$

$$A = \frac{\partial f}{\partial x}(x,u)\Big|_{x=0,u=0} \qquad B = \frac{\partial f}{\partial u}(x,u)\Big|_{x=0,u=0}$$

Therefore, the following statements only apply if $f(x,u)$ is continuously differential within a neighborhood of the origin – which is not true when the vessel is operating precisely between $L_C = 0$ and $L_C > 0$.

A.2.1 Stability: Lyapunov's Indirect Method

Lyapunov's indirect method states that (i) the origin ($x^* = 0$) is asymptotically stable if $\mathrm{Re}\lambda_i < 0$ for all eigenvalues of A, (ii) and the origin is unstable if $\mathrm{Re}\lambda_i > 0$ for one or more of the eigenvalues of A Khalil (2002). This method is inconclusive if $\mathrm{Re}\lambda_i \leq 0$ for all eigenvalues of A.

A.2.2 Controllability

Following from Lyapunov's indirect method and linear systems theory, a nonlinear system can be locally controlled by linear feedback control if the controllability matrix W_c, Eqn. (A.6), is invertible.

$$W_c = \begin{pmatrix} B & AB & \cdots & A^{n-1}B \end{pmatrix} \tag{A.6}$$

APPENDIX B

ISO 2631-5 Excerpt

This appendix is meant to succinctly illustrate the ISO Standard 2631-5 (2004) metrics as used in this work. For a complete description of the equations presented and thorough instructions, the reader is referred to the original work, ISO Standard 2631-5 (2004). The symbols and subscrips used throught this appendix are shown in Table B.1.

B.1 Spinal Response and Exposure Metric

The x, y and z directions correspond to the longitudinal, transverse and vertical axes, with the positive directions forward, left (port) and up. Assume the vessel's accelerations, a_{vk}, are measured with a sampling frequency of f_k, where $k = x, y$ or z. The x and y direction sampling rate should be "appropriate to the analysis of an 80 Hz signal", and the z direction a sampling rate "that is a multiple of 160 samples per second is recommended" (ISO Standard 2631-5, 2004).

B.1.1 Spinal Response in Horizontal Directions ($k = x, y$)

ISO Standard 2631-5 (2004) uses a linear model represented by a single-degree-of-freedom (SDOF) lumped-parameter model with natural frequency $\omega_n = 13.35\ s^{-1}$

Table B.1: Symbols and subscripts (from ISO Standard 2631-5 (2004))

Symbols		Subscripts	
a	acceleration	d	daily, as in duration of daily exposure t_{d}
A	peak acceleration	e	equivalent, as in equivalent static compressive stress S_{e}
δ	constant	i, j	counter
D	acceleration dose	k	counter (x, y or z)
f	frequency	l	lumbar
m	dose coefficient	m	measured, as in measured period t_{m}
R	factor	n	natural, as in natural frequency f_{n}
s	displacement	v	vessel
S	compressive stress	u	ultimate, as in ultimate stress S_{u}
t	time	x, y, z	reference axis
u	model acceleration term		
w, W	model coefficients		
ζ	critical damping ratio		
ω	angular frequency		

and critical damping ratio $\zeta = 0.22$. Therefore, using a 1-D filter we can estimate the lumbar response by using the rational transfer function,

$$\mathcal{A}_{\mathrm{l}k}(z) = \frac{b_0 + b_1 z^{-1} + b_2 z^{-2}}{c_0 + c_1 z^{-1} + c_2 z^{-2}} \mathcal{A}_{\mathrm{v}k}(z)$$

where $\mathcal{A}_{\mathrm{l}k}(z)$ and $\mathcal{A}_{\mathrm{v}k}(z)$ are the $\mathcal{Z}$-transform of the lumbar and vessel accelerations, and

$$b = \begin{bmatrix} 1 - \frac{\sin(\beta)}{\beta} e^{-\alpha} & 2\frac{\sin(\beta)}{\beta} e^{-\alpha} - \cos(\beta) & e^{-2\alpha} - \frac{\sin(\beta)}{\beta} e^{-\alpha} \end{bmatrix}$$

$$c = \begin{bmatrix} 1 & -2\cos(\beta) e^{-\alpha} & e^{-2\alpha} \end{bmatrix}$$

$$\alpha = \frac{\omega_{\mathrm{n}}}{2Q f_k}$$

$$\beta = \frac{\omega_{\mathrm{n}}}{f_k} \sqrt{1 - \frac{1}{(2Q)^2}}$$

$$Q = \frac{1}{2\zeta}$$

In MATLAB, $a_{\mathrm{l}k}$ can be calculated with $a_{\mathrm{l}k}(t) = \texttt{filter}(b, c, a_{\mathrm{v}k}(t))$.

B.1.2 Spinal Response in the Vertical Direction ($k = z$)

ISO Standard 2631-5 (2004) uses a recurrent neural network to represent the spinal vertical response. The lumbar spine vertical acceleration, $a_{\mathrm{t}z}$, is predicted (in m/s^2) using Eq. B.1 and Eq. B.2 along with Table B.2 and Table B.3.

$$a_{\mathrm{l}z}(t) = \sum_{j=1}^{7} W_j u_j(t) + W_8 \tag{B.1}$$

$$u_j(t) = \tanh\left[\sum_{i=1}^{4} w_{ji} a_{\mathrm{l}z}(t-i) + \sum_{i=5}^{12} w_{ji} a_{\mathrm{v}z}(t-i+4) + w_{j13}\right] \tag{B.2}$$

The range of applicability for the z axis lumbar acceleration model is -20 m/s^2 to 40 m/s^2 and 0.5 Hz to 40 Hz (ISO Standard 2631-5, 2004).

Table B.2: z axis model coefficients for Eq. B.1 (from ISO Standard 2631-5 (2004))

W_1	W_2	W_3	W_4
57.96539	52.32773	49.78227	53.16885
W_5	W_6	W_7	W_8
56.02619	-27.79550	72.34446	21.51959

Table B.3: z axis model coefficients for Eq. B.2 (from ISO Standard 2631-5 (2004))

j	1	2	3	4	5	6	7
w_{j1}	0.00130	0.01841	-0.00336	0.01471	0.00174	0.00137	0.00145
w_{j2}	-0.00646	-0.00565	-0.00539	0.01544	-0.00542	0.00381	0.00497
w_{j3}	-0.00091	-0.02073	0.00708	-0.00091	0.00255	-0.00216	0.01001
w_{j4}	0.00898	-0.02626	0.00438	-0.00595	-0.00774	-0.00034	0.01283
w_{j5}	0.00201	0.00579	0.00330	-0.00065	-0.00459	-0.00417	-0.00468
w_{j6}	0.00158	0.00859	0.00166	0.00490	-0.00546	0.00057	-0.00797
w_{j7}	0.00361	0.00490	0.00452	0.00079	-0.00604	-0.00638	-0.00529
w_{j8}	0.00167	-0.00098	0.00743	0.00795	-0.01095	0.00627	-0.00341
w_{j9}	-0.00078	-0.00261	0.00771	0.00600	-0.00908	0.00504	0.00135
w_{j10}	-0.00405	-0.00210	0.00520	0.00176	-0.00465	-0.00198	0.00451
w_{j11}	-0.00563	0.00218	-0.00105	0.00195	0.00296	-0.00190	0.00306
w_{j12}	-0.00372	0.00037	-0.00045	-0.00197	0.00289	-0.00448	0.00216
w_{j13}	-0.31088	-0.95883	-0.67105	0.14423	0.04063	0.07029	1.03300

B.1.3 Calculation of the Acceleration Dose

ISO Standard 2631-5 (2004) defines the acceleration dose, D_k (in m/s^2), as shown in Eq. B.3,

$$D_k = \left(\sum_i A_{ik}^6 \right)^{1/6} \tag{B.3}$$

where A_{ik} is the i^{th} peak of the response acceleration $a_{1k}(t)$, and $k = x$, y or z. From ISO Standard 2631-5 (2004):

> A peak is defined here as the maximum absolute value of the response acceleration between two consecutive zero crossings. For the x and y directions, peaks in positive and negative directions shall be counted. For the z direction, only positive peaks shall be counted (compression of the spine is the primary interest for exposure severity).

The average daily dose, $D_{k\text{d}}$ (in m/s^2), a person will be exposed to is calculated with Eq. B.4,

$$D_{k\text{d}} = D_k \left(\frac{t_\text{d}}{t_\text{m}} \right)^{1/6} \tag{B.4}$$

where t_d is the duration of the daily exposure, t_m is the period over which D_k has been measured. $D_{k\text{d}}$ can be used for health assessments as presented in Section B.2 (ISO Standard 2631-5, 2004).

ISO Standard 2631-5 (2004) also includes the possibility of calculating $D_{k\text{d}}$ when the daily vibration exposure consists of multiple (n) periods of different magnitudes by using Eq. B.5,

$$D_{k\text{d}} = \left[\sum_{j=1}^{n} D_{kj}^6 \frac{t_{\text{d}j}}{t_{\text{m}j}} \right]^{1/6} \tag{B.5}$$

where $t_{\text{d}j}$ is the duration of the daily exposure to condition j, and $t_{\text{m}j}$ is the period over which D_{kj} has been measured. While this study used Eq. B.4, Eq. B.5 would be relevant if the reader desires to do scenario-based optimizations (e.g., the vessel operates daily for 1 hour at SS 1, 2 hours at SS 2, and 1 hour at SS 3).

B.2 Assessment of Health Effects

From ISO Standard 2631-5 (2004):

> By use of a biomechanical model, based on experimental data, it has been shown that there is a linear relationship between the part of compressive stress that is due to the input shocks and the peak acceleration response in the spine.

The first step for assessing health effects is to calculate thee daily equivalent static compression dose, S_{e} (in MPa),

$$S_{\mathrm{ed}} = \left[\sum_{k=x,y,z} \left(m_k D_{k\mathrm{d}} \right)^6 \right]^{1/6} \tag{B.6}$$

where the recommended values of m_x, m_y and m_z are 0.015, 0.035 and 0.032 MPa/(m/s^2), accordingly (ISO Standard 2631-5, 2004).

Afterwards, the factor R is used to assess adverse health effects related to the human response acceleration dose (ISO Standard 2631-5, 2004), and is defiend as,

$$R = \left[\sum_{i=1}^{n} \left(\frac{S_{\mathrm{ed}} N^{1/6}}{S_{\mathrm{u}i} - \delta} \right)^6 \right]^{1/6} \tag{B.7}$$

where N is the number of exposure days per year, i is the year counter, n is the number of years of exposure, δ is a constant representing the static stress due to gravitational force, $S_{\mathrm{u}i}$ is the ultimate strength of the lumber spine for a person of age $(b+i)$ years, and b is the age at which the exposure starts. Following ISO Standard 2631-5 (2004), $\delta = 0.25$ MPa can be used for a driving posture, and

$$S_{\mathrm{u}i} = 6.75 - 0.066(b+i)$$

From ISO Standard 2631-5 (2004):

There is a significant human variability and $R < 0.8$ indicates a low probability of an adverse health effect; $R > 1.2$ indicates a high probability of an adverse health effect.

BIBLIOGRAPHY

BIBLIOGRAPHY

AGARD (1974). Impact of active control technology on airplane design. Number 157. Advisory Group for Aerospace Research & Development.

Akers, R. H. (1999). Dynamic analysis of planing hulls in the vertical plane. In *Society of Naval Architects and Marine Engineers, New England Section*.

Alyaqout, S. (2006). *A Multi-System Optimization Approach to Coupling in Robust Design and Control*. PhD thesis, University of Michigan.

Ayob, A. F. M., Ray, T., and Smith, W. (2009). An optimization framework for the design of planing craft. In *International Conference on Computer Applications in Shipbuilding 2009 (ICCAS09)*.

Ayob, A. F. M., Ray, T., and Smith, W. (2010). Hydrodynamic design optimization of a hard chine planing craft for coastal surveillance. In *Pacific 2010 International Maritime Conference*.

Bibuli, M., Caccia, M., Lapierre, L., and Bruzzone, G. (2012). Guidance of unmanned surface vehicles: Experiments in vehicle following. *IEEE Robotics and Automation Magazine*, 19(3):92–102.

Blank, J. and Bishop, B. E. (2008). In-situ modeling of a high-speed autonomous surface vessel. In *IEEE's 40th Southeastern Symposium on System Theory*, pages 347–351.

Blount, D. L. and Condega, L. T. (1992). Dynamic stability of planing boats. *Marine Technology*, 29(1):4–12.

Bowden, B. and Davidson, N. (1974). Resistance increments due to hull rougness associated with form factor extrapolation methods. Technical Report Ship TM380, National Maritime Institute.

Charles L. Shuford, J. (1958). A theoretical and experimental study of planing surfaces including effects of cross section and plan form. Technical Report 1355, National Advisory Committee for Aeronautics.

Czyzzak, P. and Jaszkiewicz, A. (1998). Pareto simulated annealing — a metaheuristic technique for multiple-objective combinatorial optimization. *Journal of Multi-Criteria Decision Analysis*, 7(1):34–47.

Das, I. and Dennis, J. E. (1998). Normal-boundary intersection: A new method for generating the pareto surface in nonlinear multicriteria optimization problems. *SIAM Journal of Optimization*, 8(3):631–657.

Day, J. P. and Haag, R. J. (1952). Planing boat porpoising. Master's thesis, Webb Institute.

Deb, K. (2001). *Multi-Objective Optimization using Evolutionary Algorithms*. Wiley.

Deb, K., Pratp, A., Agarwal, S., and Meyarivan, T. (2002). A fast and elitist multiobjective genetic algorithm: Nsga-ii. *IEEE Transactions on Evolutionary Computation*, 6(2):182–197.

Doctors, L. J. (1985). Hydrodynamics of high-speed small craft. Technical report, University of Michigan.

Engle, A., Lien, V., and Hart, C. (2011). Seakeeping evaluation and loads determination of a high-speed hull form with and without a bow lifting body. In *11th International Conference on Fast Sea Transportation*. American Society of Naval Engineers.

Ensign, W., Hodgdon, J. A., Prusaczyk, W. K., Ahlers, S., Shapiro, D., and Lipton, M. (2000). A survey of self-reported injuries among special boat operators. Technical report, Naval Health Research Center.

Faltinsen, O. M. (2005). *Hydrodynamics of High-Speed Marine Vehicles*, chapter Planing Vessels, page 342. Cambridge University Press.

Fathy, H. (2003). *Combined PPlan and Control Optimization: Theory, Strategies and Applications*. PhD thesis, University of Michigan.

Fridsma, G. (1969). A systematic study of the rough-water performance of planing boats. Technical report, Stevens Institute of Technology.

Fridsma, G. (1971). A systematic study of the rough-water performance of planing boats (irregular waves - part ii). Technical report, Stevens Institute of Technology.

Friedland, B. (1975). Controllability index based on conditioning number. *Journal of Dynamic Systems, Measurement, and Control*, 97(4):444–445.

Gerr, D. (1999). *The Elements of Boat Strength for Builders, Designers and Owners*. McGraw-Hill.

Ghadimi, P., Dashtimanesh, A., and Maghrebi, Y. F. (2013). Initiating a mathematical model for prediction of 6-dof motion of planing crafts in regular waves. *International Journal of Engineering Mathematics*.

Hadler, J. B. (1966). The prediction of power performance on planing craft. *SNAME Transactions*, 74.

Hale, A., Lisowski, R., and Dahl, W. (1985). Optimal simultaneous structural and control design of maneuvering flexible spacecraft. *Journal of Guidance, Control, and Dynamics*, 8:86–93.

Hicks, J. D., Troesch, A. W., and Jiang, C. (1995). Simulation and nonlinear dynamics analysis of planing hulls. *Journal of Offshore Mechanics and Artic Engineering*, 117(1):38–45.

Hughes, M. and Weems, K. (2011). Time-domain seakeeping simulations for a high speed catamaran with an active ride control system. In *11th International Conference on Fast Sea Transportation*. American Society of Naval Engineers.

Hwang, C.-L. and Masud, A. S. M. (1979). *Multiple Objective Decision Making — Methods and Applications*. Springer-Verlag.

ISO Standard 2631-5 (2004). Mechanical vibration and shock — evaluation of human exposure to whole-body vibration — part 5: Method for evaluation of vibration containing multiple shocks.

ITTC (2002). The special committee on waves — final report and recommendations to the 23rd ittc. In *Proceedings of the 23rd ITTC*, volume 2, pages 505–736.

Kays, B. J., Rosenthal, B. J., Holcomb, R. S., and Peltzer, T. J. (2009). Implementation and full-scale testing of adaptive vs. pid control system algorithms for advanced marine vehicles. In *10th International Conference on Fast Sea Transportation*.

Khalil, H. K. (2002). *Nonlinear Systems*. Prentice Hall.

Kim, I. Y. and de Weck, O. L. (2005). Adaptive weighted-sum method for bi-objective optimization: Pareto front generation. *Structural Multidisciplinary Optimization*, 29:149–158.

Marglin, S. A. (1967). *Public Investment Criteria; Benefit-Cost Analysis for Planned Economic Growth*. M.I.T. Press.

Marler, R. T. and Arora, J. S. (2004). Survey of multi-objective optimization methods for engineering. *Structural Multidisciplinary Optimization*, 26:369–395.

Martins, J. R. R. A., Sturdza, P., and Alonso, J. J. (2003). The complex-step derivative approximation. *ACM Transactions on Mathematical Software*.

Matveev, K. and Duncan, R. (2005). Development of the tool for predicting hydrofoil system performance and simulating motion of hydrofoil-assisted boats. In *Symposium on High Speed / High Performance Ships and Craft*. ASNE.

Michel, W. H. (1999). Sea spectra revisited. *Marine Technology*, 36(4):211–227.

Miettinen, K. M. (1998). *Nonlinear Multiobjective Optimization*. Springer.

Naeem, W. and Sutton, R. (2008). An assessment of a modified optimal control strategy as applied to the control of an unmanned surface vehicle. In *United Kingdom Automatic Control Council International Control Conference*.

Nguyen, L. T., Ogburn, M. E., Gilbert, W. P., Kibler, K. S., Brown, P. W., and Deal, P. L. (1979). Simulator study of stall/post-stall characteristics of a fighter airplane with relaxed longitudinal static stability. Technical Report 1538, NASA.

Perez, R. E., Jansen, P. W., and Martins, J. R. R. A. (2012). pyOpt: A Python-based object-oriented framework for nonlinear constrained optimization. *Structures and Multidisciplinary Optimization*, 45(1):101–118.

Peters, D. L. (2010). *Coupling and Controllability in Optimal Design and Control*. PhD thesis, University of Michigan.

Peterson, R., Pierce, E., and Price, B. (2004). Shock mitigation for the human on high speed craft: Development of an impact injury design rule. Technical report, Naval Surface Warfare Center Panama City.

Powell, M. J. D. (1994). *A Direct Search Optimization Method that MModel the Objective and Constraint Functions by Linear Interpolation*, pages 51–67. Kluwer Academic.

Rijkens, A. A. K. (2013). Improving the sea keeping behaviour of fast ships using a proactive ride control system. In *12th International Conference on Fast Sea Transportation*.

Rijkens, A. A. K., Keuning, J. A., and Huijsmans, R. H. M. (2011). A computational tool for the design of ride control systems for fast planing vessels. *International Shipbuilding Progress*, 58:165–190.

Rosenthal, B. J., Milewski, W. M., Connell, B., Kring, D. C., and Peltzer, T. J. (2009). Extension of a nonlinear coupled hydro-mechanical simulation tool. In *10th International Conference on Fast Sea Transportation*.

Savitsky, D. (1964). Hydrodynamic design of planing hulls. *Marine Technology*, 1(1):71–94.

Savitsky, D. (1985). Planing craft. *Naval Engineers Journal*, 97(2):113–141.

Savitsky, D. (2003). On the subject of high-speed monohulls. In *Society of Naval Architects and Marine Engineers (SNAME) Section Papers*, Athens.

Savitsky, D. and Brown, P. W. (1976). Procedures for hydrodynamic evaluation of planing hulls in smooth and rough water. *Marine Technology*, 13(4):381–400.

Savitsky, D. and J. G. Koelbel, J. (1993). Seakeeping of hard chine planing hull. Technical report, Society of Naval Architects and Marine Engineers.

Shimozono, G. and Kays, B. (2011). Shock mitigation of planing craft using the ares aft lifting body system. In *11th International Conference on Fast Sea Transportation*. American Society of Naval Engineers.

Smith, W. F., Ayob, A. F. M., and Ray, T. (2012). The design of high speed planing craft using and optimization framework. In *ASME 2012 International Mechanical Engineering Congress & Exposition (IMECE 2012)*.

Sobieszczanski-Sobieski, J. and Hafka, R. T. (1997). Multidisciplinary aerospace design optimization: Survey of recent developments. *Structural Optimization*.

Sun, H. and Faltinsen, O. M. (2011). Predictions of porpoising inception for planing vessels. *Journal of Marine Science and Technology*, 16:270–282.

Troesch, A. W. (1992). On the hydrodynamics of vertially oscillating planing hulls. *Journal of Ship Research*, 36(4):317–331.

Veen, D. and Gourlay, T. (2012). A combined strip theory and smoothed particle hydrodynamics approach for estimating slamming loads on a ship in head seas. *Ocean Engineering*, 43:64–71.

Wang, L. W. (1985). A study on motions of high speed planing boats with controllable flaps in regular waves. *International Shipbuilding Progress*, 32:6–22.

Xi, H. and Sun, J. (2006). Feedback stabilization of high-speed planing vessels by a controllable transom flap. *IEEE Journal of Oceanic Engineering*, 31(6):421–431.

Zadeh, L. A. (1963). Optimizality and non-scalar-valued performance criteria. *IEEE Transactions on Automatic Control*.

Zarnick, E. E. (1979). A nonlinear mathematical model of motions of a planing boat in irregular waves. Technical report, David W. Taylor Naval Ship Research and Development Center.

Zhou, A., Qu, B.-Y., Li, H., Zhao, S.-Z., Suganthan, P. N., and Zhang, Q. (2011). Multiobjective evolutionary algorithms: A survey of the state of the art. *Swarm and Evolutionary Computation*, 1(1):32–49.

Zhou, K., Salomon, G., and Wu, E. (1999). Balanced realization and model reduction for unstable systems. *International Journal of Robust and Nonlinear Control*, 9:183–198.

Zitzler, E., Laumanns, M., and Thiele, L. (2001). Spea2: Improving the strength pareto evolutionary algorithm for multiobjective optimization. Technical report, Swiss Federal Institute of Technology.